Report Title: Enhanced High Temperature Corrosion Resistance in Advanced Fossil Energy Systems by Nano-Passive Layer Formation

Type of Report: Final Scientific / Technical Report

Reporting Period Start Date: 15 September 2004

Reporting Period End Date: 14 June 2007

Principal Author: Arnold R. Marder

Report Issue Date:

DOE award Number: DE-FG26-04NT42169

Submitting Organization: Lehigh University 27 Memorial Drive West Bethlehem, PA 18015

Abstract

Due to their excellent corrosion resistance, iron aluminum alloys are currently being considered for use as weld claddings in fossil fuel fired power plants. The susceptibility to hydrogen cracking of these alloys at higher aluminum concentrations has highlighted the need for research into the effect of chromium additions on the corrosion resistance of lower aluminum alloys. In the present work, three iron aluminum alloys were exposed to simulated coal combustion environments at 500°C and 700°C for both short (100 hours) and long (5,000 hours) isothermal durations. Scanning electron microscopy was used to analyze the corrosion products. All alloys exhibited excellent corrosion resistance in the short term tests. For longer exposures, increasing the aluminum concentration was beneficial to the corrosion resistance. The addition of chromium to the binary iron aluminum alloy prevented the formation iron sulfide and resulted in lower corrosion kinetics. A classification of the corrosion products that developed on these alloys is presented.

Scanning transmission electron microscopy (STEM) of the as-corroded coupons revealed that chromium was able to form chromium sulfides only on the higher aluminum alloy, thereby preventing the formation of deleterious iron sulfides. When the aluminum concentration was too low to permit selective oxidation of only aluminum (upon initial exposure to the corrosion environment), the formation of chromium oxide alongside the aluminum oxide led to depletion of chromium beneath the oxide layer. Upon penetration of sulfur through the oxide into this depletion layer, iron sulfides (rather than chromium sulfides) were found to form on the low aluminum alloy. Thus, it was found in this work that the role of chromium on alloy corrosion resistance was strongly effected by the aluminum concentration of the alloy. STEM analysis also revealed the encapsulation of external iron sulfide products with a thin layer of aluminum oxide, which may provide a secondary layer of a corrosion protection in these regions. In a separate set of experiments, *in-situ* oxidation performed in x-ray photoelectron spectroscopy (XPS) equipment showed that the formation of aluminum oxide in a pure oxygen environment at 500°C was slowed by the addition of chromium.

Table of Contents

Executive Summary

Iron aluminum alloys are currently being researched to determine their suitability for use as weld overlays in fossil fuel fired power plants. These alloys offer several advantages over the currently used nickel based overlays, such as alloy 622, including lower cost, lack of microsegregation and coefficient of thermal expansion similar to that of the waterwall tube. Most importantly, the ability to form a protective surface oxide in very low oxygen levels (like those encountered in coal combustion processes) provides these alloys with excellent corrosion resistance. One potential disadvantage of Fe-Al alloys, however, is the weldability limit due to hydrogen cracking that is encountered at aluminum concentrations around 10-15wt%. Additions of chromium have been shown to have beneficial effects on the corrosion resistance of Fe-Al alloys and such additions are currently being investigated as a method of improving corrosion behavior of low aluminum (weldable) Fe-Al alloys.

Three as-cast alloys were examined in this study: Fe-10Al-5Cr, Fe-12.5Al- and Fe-12.5Al-5Cr (all values wt%). Short term (100 hours) corrosion tests in simulated coal combustion environments were performed at both 500°C and 700°C. It was found that all three alloys exhibited excellent corrosion resistance after 100 hours in these environments. Longer term tests (up to 5,000 hours) were performed at 500°C in the most representative environment. All three alloys exhibited negligible weight gain after 500 hours; after 1,000 hours, the binary alloy developed a significant corrosion product on the surface, while the ternary alloys exhibited no weight gain. After 5,000 hours, the binary alloy was found to gain approximately the same amount of weight as in the 1,000 hours exposure, the Fe-10Al-5Cr alloy started to exhibit slight weight gain, and the Fe-12.5Al-5Cr alloy did not develop any appreciable corrosion.

Corrosion products from all long term corrosion exposures were examined using scanning electron microscopy (SEM). A wide range of corrosion product morphologies were observed on the alloy surfaces. Large alloy weight gain was associated with the development of large iron sulfide type corrosion products,; these were present as either sulfide plates, blocks, nodules or film, each one representing more severe attack than the previous. Such products were observed on the binary alloy at all exposure times, and on the Fe-10Al-5Cr alloy after 1,000 and 5,000 hours. The Fe-12.5Al-5Cr alloy exhibited flake like corrosion products that were found to be rich in Fe, Al, Cr, O and S; large iron sulfide products (as found on the Fe-12.5Al alloy) were not observed on this alloy at any exposure time. A classification scheme of the different corrosion products was developed for these alloys based on the SEM analysis.

Scanning transmission electron microscopy (STEM) was performed on cross sections from all three alloys after 500 and 5,000 hours of exposure to gain more information on the corrosion product development. The Fe-10Al-5Cr and Fe-12.5Al alloys were found to develop thick, multi-layered corrosion products, with the inner most layers being rich in iron, aluminum, oxygen and sulfur, and the external layer being mostly iron sulfide. The Fe-12.5Al-5Cr alloy, on the other hand developed a very thin (less than 200nm) corrosion scale that consisted of aluminum oxide and chromium sulfide. The ability of this alloy to develop chromium-rich rather than iron-rich sulfide was responsible for it's superior corrosion resistance and was attributed to the higher level of aluminum compared to the Fe-10Al-5Cr alloy. An encapsulation or outlining

of the external sulfur rich corrosion products with an aluminum and oxygen rich layer was observed on all three alloys at both 500 and 5,000 hours. This encapsulation is not often observed in the high temperature corrosion of Fe-Al alloys and several mechanisms for its formation were discussed. Regardless of the origin of this layer, its presence was deemed beneficial, as it would serve as an additional barrier to slow the diffusion of corroding species into the alloy.

In addition to the exposures in simulated coal combustion environments, *in-situ* oxidation of the Fe-12.5Al and Fe-12.5Al-5Cr alloys was performed in x-ray photoelectron spectroscopy (XPS) equipment in pure oxygen at 500°C. It was found that the addition of chromium slowed the formation of aluminum oxide on the alloy surface. The presence of the native oxide (that forms at room temperature after sample preparation) was also beneficial, as it appeared to slow or prevent the formation of iron oxide corrosion products after exposure times of 30 minutes.

The results presented in this work show that the addition of chromium to Fe-12.5Al is beneficial to alloy corrosion resistance in coal combustion environments at 500°C in that it prevents the formation of deleterious iron sulfides. Additionally, it was shown that the minimum aluminum concentration for adequate corrosion resistance in these environments was between 10wt% and 12.5wt%. These results represent a beneficial towards the commercial application of iron aluminum alloys for corrosion resistance in fossil fuel power systems.

1 EVALUATION OF THE CORROSION RESISTANCE OF FE-AL-CR ALLOYS IN SIMULATED LOW NOX ENVIRONMENTS: Part 1 – Corrosion Exposures And Scanning Electron Microscopy

1.1 Introduction

Iron aluminum alloys have long been utilized in high temperature corrosive environments due to the ability to form a thin protective layer of Al_2O_3 that acts as a permeation barrier. More recently, these alloys have also received considerable attention for use as weld overlays in fossil fuel power plants. Changes in combustion practices have altered the fireside environment, leading to accelerated corrosion of waterwall tubes[1,2,3]. Deposition of a more corrosion resistant alloy on existing tube wall surfaces is an efficient method of providing increased protection from gaseous and solid state corrosion. Iron aluminum alloys offer many advantages over the nickel based alloys currently used for this application, including decreased cost, lack of microsegregation[4,5], and excellent elevated temperature corrosion resistance due to the formation of a protective Al_2O_3 surface scale[6].

The stability of the Al_2O_3 layer and the ability to self-heal any cracks or defects improves with increasing aluminum concentration, but a hydrogen cracking problem has been observed for iron alloys with greater than 10 to 15wt% aluminum[7]. This concentration is also close to the critical composition required to form an external Al_2O_3 layer[8,9,10]. It has been shown that additions of chromium reduce this critical concentration of aluminum[11] in oxidizing conditions, but other researchers have reported detrimental effects of adding chromium to iron aluminum alloys[12] with respect to sulfidation resistance. The role of chromium in iron aluminum therefore requires

further investigation if it is to be used as a corrosion resistant weld overlay alloy. In the present study, three iron aluminum chromium alloys are exposed to simulated coal combustion environments and the resulting corrosion products are characterized and discussed.

1.2 Experimental Procedure

Alloys used in this study were prepared at Oak Ridge National Laboratory by arc-melting high purity components and drop casting into water cooled copper molds. Three alloys were produced: Fe-10Al-5Cr, Fe-12.5Al and Fe-12.5Al-5Cr (all values wt%). In order to preserve the as-cast microstructure, no heat treatment was performed after casting. Due to the similar grain structure between castings and weld overlays, and the ferritic solidification mode of these iron-based alloys (which would limit any microsegregation during solidification), the high temperature corrosion resistance of weld overlay alloys can be simulated using cast alloys[13]. Sections from the middle of each cast ingot were removed for chemical analysis (Table I); carbon and oxygen were determined by combustion-infrared absorbance, nitrogen by inert gas fusion-thermal conductivity, and all other elements by inductively coupled plasma analysis. Aluminum and chromium concentrations were also measured in sections removed from the top and bottom regions of the casting, in order to determine the variability of these elements in the ingot. It was found that the variation in concentration of aluminum and chromium was at most 0.1 wt% between the three sections within the ingot and that the concentration of all trace elements was minimal. Sections of the as cast ingots were prepared metallographically to compare grain structure and to check for the presence of voids or other defects in the castings. No casting defects were observed and grain structure was typical of as-cast materials.

Alloys were tested in two different simulated low NO_x environments, referred to as sulfidizing and mixed oxidizing / sulfidizing, based on their partial pressures of oxygen and sulfur, as shown in Table II. For all test environments, 2 volume percent water vapor was added to the corrosion gas in-situ using a syringe pump connected to quartz capillary inserted in the hot zone of the furnace. Partial pressures of oxygen and sulfur were calculated using HSC Chemistry for Windows software.

Coupons for corrosion tests were cut from the cast ingots and ground on all faces to 600 grit SiC, followed by polishing on 6μm diamond and 0.3μm alumina. The edges of the coupons were not rounded; all corners and edges were kept square. A 0.2mm hole was drilled near the top of the coupon for suspension in the furnace. Coupons for long term tests (500 to 5000 hours) received an extra grinding step in a specially designed jig to impart a 10° taper on the bottom half of the coupon, as shown in Figure 1 (the reason for this will be explained below). Following polishing, all coupons were cleaned ultrasonically in acetone and then weighed to the nearest tenth of a milligram on a digital balance.

Short term corrosion experiments (100hrs) at 500°C and 700°C were performed in both gases using a Netzsch STA 409 thermogravimetric analyzer (TGA). Long term corrosion experiments (500 to 5,000hrs) were performed in the mixed oxidizing / sulfidizing gas only at 500°C in Lindberg horizontal tube furnaces. For all corrosion tests, samples were inserted into a cold furnace, corrosion gas was flushed through the furnace for a minimum of 1 hour, and the sample was heated at 50°C/min to the desired temperature.

As-corroded coupons were analyzed using a Hitachi 4300LV field emission gun scanning electron microscope (SEM). Secondary electron imaging of unmounted, uncoated corrosion samples was performed at an accelerating voltage of 5kV; electron dispersive spectroscopy (EDS) analysis was performed at 15kV. Select corrosion coupons were also examined in cross section by dry cutting the sample three-quarters through thickness on a high speed diamond saw, immersing it in liquid nitrogen, and fracturing the coupon.

1.3 Results

1.3.1 Short Term Corrosion Exposures

Atmospheric conditions in the combustion zone of a fossil fuel power plant can differ significantly depending on a number of variables, including the type of coal and operating temperature of the boiler. To account for such variability, the short term corrosion tests (100 hours) were performed in both the sulfidizing and the mixed oxidizing / sulfidizing environments at 500°C and 700°C. Results from these tests are shown in Figure 2 and Figure 3. Corrosive attack for all alloys in both environments at 500°C and 700°C was negligible; no alloy exhibited a weight gain after 100 hours of greater than 0.2 mg/cm^2.

Given the minimal weight gain of these alloys and the detectability limit of the test equipment (estimated experimentally to be on the order of 0.05mg/cm^2), this data does not permit a ranking of alloy performance. Comparison of this weight gain data to that of other commercial alloys used for the same application, however, is useful. Several nickel based alloys, such as alloy 622, have been used as a weld overlay material in low NO_x boilers for many years. The weight gain after 100 hours of alloy 622, along with the data from the experimental FeAlCr alloys examined

in this study, is shown in Figure 4 for the same mixed gas at 500°C. From this figure, the superior corrosion resistance of all the FeAlCr compositions compared to the nickel based alloy is clearly evident.

1.3.2 Long Term Corrosion Exposures

Depletion of aluminum and/or chromium in iron and nickel based alloys by the formation and thickening of the reaction product(s) has been shown to lead to breakaway corrosion[14], where corrosion kinetics rapidly increase due to the formation of non-protective corrosion products. Determining when depletion occurs is useful for predicting lifetimes based on alloy consumption. In order to increase the likelihood of depletion occurring in these highly corrosion resistant alloys, a half-wedge shaped coupon (Figure 1) was used for long term experiments. The thinned bottom half of the coupon should decrease the amount of aluminum and chromium available to form protective corrosion products, while the thick top half ensures that the entire coupon is not consumed during the test. This sample geometry is similar to one utilized in studies by Al-Badairy and Tatlock[15,16], in which wedge shaped coupons were oxidized at temperatures up to 1350°C in laboratory air. In those experiments, it was found that breakaway corrosion eventually occurred in the thin region of the sample due to depletion of aluminum.

To ensure that this sample geometry did not cause any unexpected anomalies in the corrosion behavior of these alloys, baseline tests of two different alloy compositions (separate from the alloys used in the present investigation) were performed in the mixed sulfidizing / oxidizing gas and in laboratory air at 500°C for 100 hours. In these tests, one standard square shaped coupon was placed alongside two half-wedge coupons of the same composition. The weight change of

these six corrosion coupons are shown in Table III. The variation in weight gain between the three coupons for each test was minimal. As a further check, the coupons from the mixed oxidizing / sulfidizing test were prepared metallographically to compare the corrosion product morphology and thickness, as shown in Figure 5. In accordance with the weight gain data, the corrosion products that formed on the half-wedge and square coupons were very similar in thickness and morphology. It was determined from these tests that the half-wedge design did not have any undesirable effect on the corrosion performance of these alloys, and that this sample geometry was suitable for long term corrosion exposures.

Long term corrosion tests were carried out for durations of 500, 1000 and 5000 hours in the mixed oxidizing / sulfidizing environment; weight gain data from these tests are presented in Figure 6. The Fe-10Al-5Cr alloy exhibited negligible weight gain for both the 500 and 1000 hour exposure, but showed a significant increase in weight gain after 5000 hours. The binary alloy did not experience significant weight gain until 1000 hours; the magnitude of weight gain after 5000 hours was very similar to that of the 1000 hour exposure. The ternary Fe-12.5Al-5Cr alloy did not exhibit any significant weight gain for any exposure time.

1.3.3 SEM / EDS Analysis

Corrosion coupons from the 500 and 5000 hour exposure tests were analyzed using SEM and EDS to determine the difference in corrosion products among the alloys. No significant change in the corrosion product morphologies was observed between the thick and thinner wedge regions of the examined coupons for any alloy composition.

In general, very similar corrosion products were observed on both Fe-10Al-5Cr and Fe-12.5Al-5Cr at both 500 and 5000 hours, as shown in Figure 7. These products were generally flat and thin; thickness was estimated from SEM images to be less 0.5μm and the flakes were generally less than 5μm width. EDS analysis of these flake-like corrosion products detected iron, aluminum, oxygen and sulfur, but it is likely that x-rays were generated from both the corrosion product and underlying metal, given the size of the flakes.

Although the majority of the surface of the Fe-10Al-5Cr alloy tested at 500 hours was covered with these flakes, some isolated, larger plate-like products were observed, Figure 8. Compositional analysis of these plates and surrounding areas indicate that the plates are primarily iron sulfide. The amount of sulfide coverage was found to increase dramatically on this alloy for the 5000 hour exposure, Figure 9, consistent with the increase in mass gain (Figure 6). Large sulfide type products were found in large regions adjacent to the sample edge (Figure 10) and suspension hole. Areas not covered with the sulfide exhibited the same flake-like corrosion products observed at 500 hours (Figure 7 and Figure 10c).

The image in Figure 9a depicts an interesting anomaly observed in some regions on the Fe-10Al-5Cr alloy. The concentration of flake-like corrosion products was found to vary from grain to grain. The dashed lines shown in his figure indicate probable grain boundaries in the cast alloy, and it is evident that the amount of corrosion product coverage varies by grain. This phenomenon was only observed on this alloy in isolated regions, and was not thoroughly analyzed in the present work. It is possible that the adsorption of oxygen or sulfur is more favorable on certain grains do to their orientation. Graupner et al[17] observed a similar grain

boundary dependence in a study on the oxidation of low index FeAl. The authors report that the rate of oxygen uptake at 500°C in UHV varied with grain orientation, FeAl(110) being about 2 order of magnitude slower than that of FeAl(100). It is possible in the present work that a similar phenomenon is occurring and leading to the differing corrosion product coverage on this alloy.

As shown in Figure 11, the Fe-12.5Al alloy exhibited a number of different corrosion product morphologies after 500 hours of exposure. The majority of the coupon was covered in very small particle-like corrosion products with a random distribution of isolated, single plates, Figure 11b. EDS analysis from both the center of this plate and a region adjacent to it, Figure 12a and b, respectively, shows an increase in both iron and sulfur in the plate. The darker regions in the low magnification image for this alloy, Figure 11a, were found to be iron sulfide type blocks and nodules, as shown in Figure 11c and d and Figure 12c.

After 5000 hours of exposure, the amount of iron sulfide type corrosion products on the binary alloy increased dramatically, Figure 13a. Over 75% of the sample was covered with an iron sulfide type film, as shown in Figure 13b. Regions not covered by the film appeared similar to the binary alloy exposed for 500 hours, with small particles and isolated iron sulfide type plates, Figure 13c. The film thickness was estimated to be on the order of 20 to 25μm from the cracked cross section image shown in Figure 14; the faceted structure of this corrosion product is also evident in this image.

In contrast to Fe-10Al-5Cr and Fe-12.5Al, no iron sulfide-type plates, blocks or nodules were found on the Fe-12.5Al-5Cr alloy after 500 or 5000 hours of exposure. Only the flake type corrosion products shown in Figure 7 were observed on this alloy, indicating that these corrosion products acted as a sufficient barrier to the diffusion of iron and/or sulfur up to 5000 hours.

1.4 Discussion

The negligible weight gain observed in the 100 hour TG tests indicates that protective corrosion products formed on all alloys at short exposure times. Similar minimal weight gains for FeAlCr alloys in sulfur-bearing environments have been observed by other researchers. Banovic et al[10] exposed iron aluminum alloys to a 1%H_2S-Ar atmosphere at 700°C for up to 100 hours and found that alloys with more than 10wt% aluminum exhibited weight gains of less than 1mg/cm^2. Several studies by DeVan and Tortorelli[18,19,20] of iron aluminum alloys with and without chromium additions in H_2S-bearing gases have shown that alloys with greater than 10wt% aluminum experience weight gains on the order observed in the present study. Utilizing very similar gaseous environments as in the present work, Regina et al[21] found that Fe-10wt% Al alloys with Cr additions resulted in weight gains of less than 0.5 mg/cm^2 at 500°C.

In the study of Regina et al[20], the authors observed that corrosion of iron alloys containing 7.5wt% and 10wt% aluminum was more severe in the mixed oxidizing / sulfidizing environment than in the purely sulfidizing environment. The reported weight gain after 100 hours of the Fe-7.5Al-5Cr alloy increased from 0.0mg/cm^2 in the sulfidizing gas to greater than 4mg/cm^2 in the mixed gas. No such relationship was observed in the present study, most likely due to the higher concentration of aluminum and chromium in the alloys used here. In the Regina study[20], the

critical alloy content factors (the sum of the aluminum and chromium concentration in atomic percent) required to prevent significant corrosion after 100 hours were reported as approximately 19at% and 22at% for the sulfidizing and mixed gases, respectively. Alloys with content factors below these levels exhibited either high weight gain or significant formation of FeS nodules on the surface. The critical alloy content factors for the alloys in the present study range from 23at% to 27at%, indicating that the aluminum and chromium concentrations are high enough based on the Regina criteria to prevent excessive attack in both environments at these short times.

Longer term exposures and analysis of the resultant corrosion products indicated significant differences in alloy corrosion resistance in the mixed oxidizing / sulfidizing gas. The addition of 5 wt% chromium to the binary Fe-12.5Al alloy prevented the formation of the thick iron sulfide type film (Figure 13) and reduced the weight gain of this alloy after 5000 hours from greater than 2mg/cm^2 for the binary to less than 0.1mg/cm^2 for the ternary alloy.

Chromium additions to aluminum containing alloys have been found to have both beneficial and deleterious effects on corrosion resistance. In a study of iron aluminum intermetallics in H_2-H_2S-H_2O environments, DeVan[12] found that chromium additions above 2at% to Fe_3Al increased the corrosion kinetics at 800°C and changed the corrosion products from a thin Al_2O_3 layer for the binary alloy to a mixture on the ternary alloy of Cr_2S_3 plates and a thick film of Al_2S_3 and Al_2O_3. Velon and Yi[22] more recently observed a similar detrimental effect of 2at% and 4at% chromium additions to Fe_3Al oxidized at 500°C. The increase in oxide growth rate upon adding chromium was attributed to enhanced diffusion of Fe ions through the mixed $(Al,Cr)_2O_3$ film as

compared to the Al_2O_3 film that developed on the pure intermetallic. In contrast to these results, Tomaszewicz and Wallwork[11] noted decreased corrosion rates with chromium additions to low aluminum Fe-Al alloys in oxidizing environments at 800°C. For binary alloys in their study, aluminum concentrations of 7wt% were required to suppress formation of external iron oxide nodules. This critical concentration was reduced to 3-4wt% with the addition of 4-5wt% chromium. It was suggested that chromium acted as a secondary getter, wherein Cr_2O_3 filled defects that may have formed in the Al_2O_3 scale.

It is not possible from the SEM results shown here to elucidate the mechanistic role of the chromium addition on the corrosion resistance of the Fe-12.5Al alloy. Clearly, the addition of chromium was beneficial, but whether it was due to the formation of Cr_2O_3 or to the chromium affecting the formation of Al_2O_3, for example, could not be determined in the present work. A more detailed description and analysis of the role of chromium on the Fe-12.5Al alloy is presented in Part II of this work[23].

After 5000 hours of exposure, the Fe-10Al-5Cr alloy developed significant amounts of iron sulfide type products, as shown in Figure 10, resulting in measurable weight gain for this alloy. The higher aluminum alloy, Fe-12.5Al-5Cr, however, remained relatively free of any large iron sulfide type corrosion product, indicating that the scale on this alloy was more protective. The relationship of decreased corrosion rates with increased aluminum concentration has been well established for iron aluminum alloys[8,9,10,24-,26] and is generally attributed to the simultaneous increased likelihood of forming Al_2O_3 and suppression of other base metal corrosion products with increased Al concentration. The results presented here indicate that for an iron alloy with

5wt% chromium, a critical aluminum concentration of between 9.2wt% and 11.5wt% (the actual alloy compositions in this study) is required to suppress the formation of iron sulfide at 500°C in the mixed oxidizing / sulfidizing environment.

The absence of any increased sample weight gain for the Fe-12.5Al alloy between 1000 hours and 5000 hours was a surprising result. This alloy exhibited the highest amount of iron sulfide formation of all three alloys at both 500 and 5000 hours. The high deviation from stoichiometry of iron sulfide allows for rapid diffusion of sulfur or base metal ions through it at high temperatures[27] and the formation of this phase usually corresponds to rapid corrosion kinetics in iron aluminum alloys[28-32]. The fact that weight gain for this alloy was essentially the same at both 1000 and 5000 hours indicates that the corrosion products that formed at 1000 hours were protective enough to prevent further significant corrosion with prolonged exposure time. Considering the typical non-protective nature of iron sulfides on iron aluminum alloys, it is likely that a more protective corrosion product eventually formed underneath the iron sulfide film and acted as a sufficient diffusion barrier to inhibit the transport of either sulfur or iron ions through the scale. Further examination of the corrosion product development on this alloy is presented in Part II[23].

No difference in corrosion product morphology, composition or number density was observed between the thick and wedge region of the coupon for any alloy at any exposure time. This indicates that depletion of aluminum or chromium did not occur, even after 5,000 hours of exposure. It is possible that at the low temperature of these tests, the growth rates of the corrosion products were too low to cause significant bulk depletion. Development of protective

corrosion products that prevented any sufficiently fast diffusion of aluminum or chromium, or ingress of sulfur to react with these elements at the product-alloy interface, may also be responsible for the lack of depletion.

A generalized classification scheme for the different corrosion products observed on the alloys in this study based on size and morphological observation is shown in Figure 15. The mixed particles (Figure 15a) were the smallest product observed, ranging in size from a few hundred nanometers to a few microns. EDS analysis of this product yielded iron, aluminum, chromium, oxygen and sulfur. However, as stated earlier, the interaction volume of the electron beam was considerably larger than these particles and x-rays were likely generated from the underlying alloy as well as the corrosion product. The flake-like corrosion products (Figure 15b) were found only on the chromium-containing alloys, and EDS analysis for this product was very similar to that of the particles. Banovic[33] observed the formation of similar particle and flake type corrosion products on binary iron aluminum alloys in a sulfidizing environment at 500°C. EDS analysis in that study indicated only iron, aluminum and sulfur for the flakes, and aluminum and oxygen for the particles; the thickness of the particle product was on the order of 100 nm. Exposure of iron-aluminum-chromium weld overlays to a sulfidizing environment by Tortorelli[34] also resulted in flake type corrosion products on select samples. X-ray diffraction analysis of the corrosion product from that study revealed a mixture of iron, aluminum and chromium sulfides, in addition to a small amount of oxide.

Iron sulfide type plates (Figure 15c) were found on the Fe-10Al-5Cr and the Fe-12.5Al alloys at both 500 and 5000 hours. The dimensions of these plates varied significantly, with plate widths

ranging from 5μm to 50μm, and both isolated and clustered plates were observed. Iron sulfide blocks, nodules and continuous film (Figure 15d, e, and f, respectively) were found primarily on the binary alloy samples. These morphologies are similar to those reported previously in the literature[10,31,32,35,36,37].

The sequence of corrosion morphologies presented in Figure 15 does not necessarily represent a linear progression of one corrosion product developing into the next. This may be true only of the last three morphologies; it is likely that the continued growth and eventual coalescence of several sulfide blocks forms a nodule, and several nodules combine to form a film. A similar sulfide film formation mechanism was proposed by Patnaik and Smeltzer for iron aluminum alloys in a sulfidizing environment at 900°C[31].

The different morphologies from (a) to (f) can be said to represent the nature and degree of corrosive attack that has occurred. The long term exposure samples did not exhibit significant weight gain prior to the formation of significant amounts of the sulfide block, nodule and film products. The mixed particle and flake products were associated primarily with the minimal weight gains at 500 hours; iron sulfide formation became significant only at longer times. This is especially evident for the Fe-10Al-5Cr alloy; at 500 hours, there was no measurable increase in sample weight, and the majority of the coupon was covered with mixed particles and flakes. After 5000 hours of exposure, however, the majority of the coupon had developed iron sulfide nodules and film-like products, and there was a measurable amount of weight increase. The iron sulfide products that developed at this time overgrew the existing flakes, and regions of sulfide-free flakes were still visible between nodules, Figure 10b.

Although continuous kinetic measurements were not made during these long term tests, this delayed development of non-protective corrosion products and associated increase in sample weight could be described as two stage corrosion kinetics. The mixed particles and flakes were protective enough during early exposure times to prevent significant attack of the coupon, but this protection broke down with increased exposure time, resulting in the increased coupon weight gain observed at 5000 hours. Definitive compositional analysis of the particle and flake composition was not possible in this work due to their small size, but it is likely that their formation consumed some amount of aluminum at the alloy surface and led to a reduction in the partial pressure of oxygen in the local gaseous environment. This change in alloy and environmental composition would increase both the activity of iron and the partial pressure of sulfur, making it more thermodynamically stable for iron sulfide to form. This hypothesis was cited by Kai[26] in a study of the sulfidization of binary iron aluminum alloys. In that work, similar two stage corrosion kinetics were observed, with formation of iron sulfide occurring after an incubation time during which Al_2O_3 whiskers formed on the alloy surface. In the present work, the Fe-12.5Al-5Cr alloy did not form any iron sulfide products after 5000 hours, in contrast to the development of sulfide on the Fe-10Al-5Cr alloy. The increase in aluminum concentration between these two compositions could have been enough to ensure that even with consumption of some aluminum due to Al_2O_3 formation, the aluminum concentration at the alloy surface remained high enough to prevent iron sulfide from becoming thermodynamically favored.

1.5 Conclusions

Corrosion of Fe-10Al-5Cr, Fe-12.5Al and Fe-12.5Al-5Cr alloys was carried out in simulated coal combustion environments. The following conclusions can be drawn from this work:

- For short exposure times (less than 100 hours), all of the alloy compositions exhibited excellent corrosion resistance at 500°C and 700°C in both the sulfidizing and the mixed oxidizing / sulfidizing environment.

- At longer exposure times in the mixed oxidizing / sulfidizing environment, the binary alloy Fe-12.5Al alloy developed a thick iron sulfide film that resulted in weight gains considerably higher than either of the ternary alloys. Addition of 5wt% chromium to the Fe-12.5Al alloy was sufficient for suppressing the formation of any iron sulfide type corrosion products.

- In the long term tests, corrosion products on all alloys were similar in the thick and wedge region of the corrosion coupons, indicating that long-range depletion of alloy elements did not occur for these alloys at 500°C even after 5000 hours of exposure to the mixed oxidizing / sulfidizing environment.

- The development of iron sulfide on the Fe-10Al-5Cr alloy at the 5000 hours exposure indicates failure of the protective scale that formed on this alloy at shorter times. Increasing the aluminum concentration to 12.5wt% was sufficient to prevent the formation of iron sulfide up to 5000 hours.

- The corrosion products that developed on these alloys could be classified by size or morphology into one of six different categories. The small mixed particles and flakes were associated with minimal weight gain and were responsible for generally protective behavior; the formation of iron sulfide blocks, nodules and continuous films represented substantially increased reaction and non-protective behavior.

Table I - Composition of cast alloys. All values wt %; Al, and Cr averaged for top, middle and bottom samples.

Element	Fe-10Al-5Cr	Fe-12.5Al	Fe-12.5Al-5Cr
Fe	balance	balance	balance
Al	9.21 +/- 0.08	11.56 +/- 0.10	11.47 +/- 0.08
Cr	4.94 +/- 0.01	< 0.01	4.92 +/- 0.03
B	< 0.005	< 0.005	< 0.005
C	< 0.01	< 0.01	< 0.01
Cu	< 0.01	< 0.01	< 0.01
Mn	< 0.01	< 0.01	< 0.01
N	0.002	0.002	0.001
Ni	< 0.01	< 0.01	< 0.01
O	0.008	0.004	0.004
P	< 0.005	< 0.005	< 0.01
S	0.004	0.004	0.003
Si	0.02	0.02	0.02
Ti	< 0.01	< 0.01	< 0.01
Y	< 0.01	< 0.01	< 0.01
Zr	< 0.01	< 0.01	< 0.01

Table II - Composition of gases used in corrosion exposures.
Composition values in volume percent, partial pressure values in atmospheres.

	CO	CO_2	H_2	H_2O	H_2S	N_2	Log pO_2	Log pS_2
Sulfidizing	**15**	**-----**	**3**	**2**	**0.12**	**bal**	**-28**	**-6**
Mixed Oxidizing / Sulfidizing	**10**	**5**	**-----**	**2**	**0.12**	**bal**	**-19**	**-8**

Table III - Comparison of weight change (mg/cm^2) for wedge and square shaped coupons after 100 hours of exposure at 500°C.

Coupon Shape	Mixed Oxid. / Sulfid. Environment *(Fe-7.5Al-1Cr)*	Air *(Fe-7.5Al-5Cr)*
Wedge 1	0.0757	0.0115
Wedge 2	0.0843	0.0089
Square	0.0842	0.0096

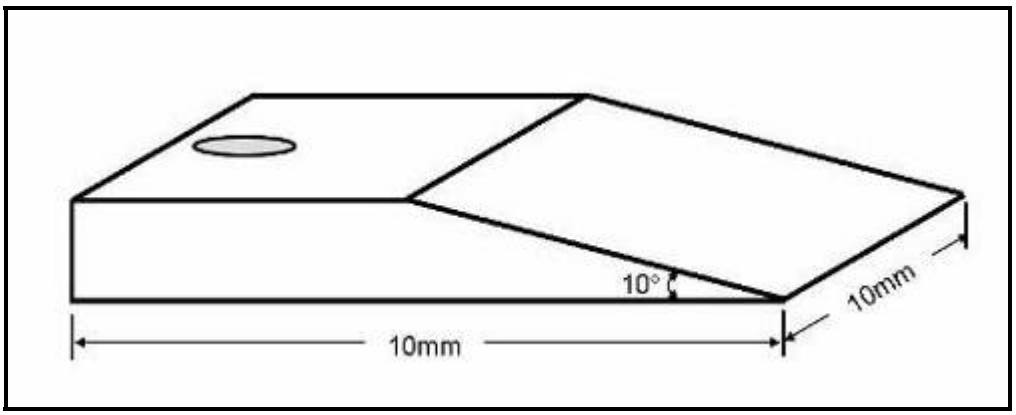

Figure 1 - Schematic diagram of wedge shaped coupons used in long term corrosion experiments.

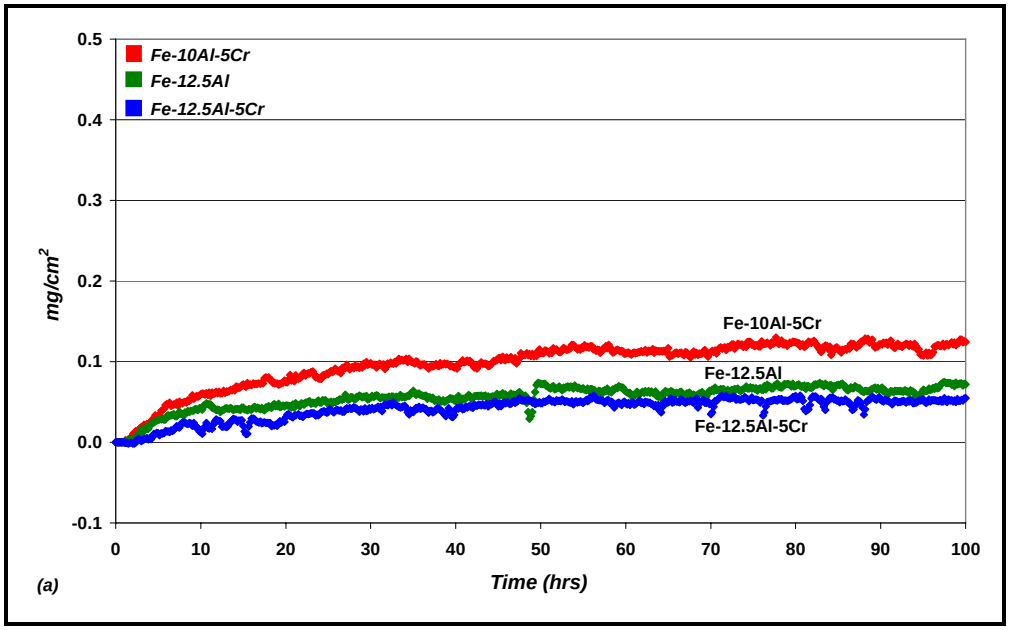

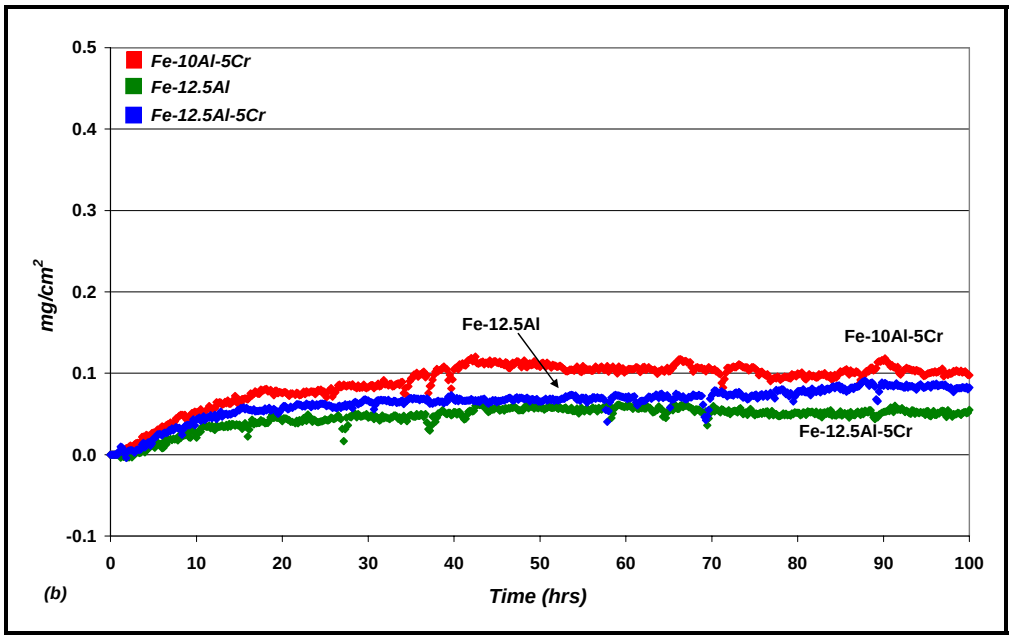

Figure 2 - Weight change for all three alloys in the sulfidizing environment at (a) 500°C and (b) 700°C, 100hrs.

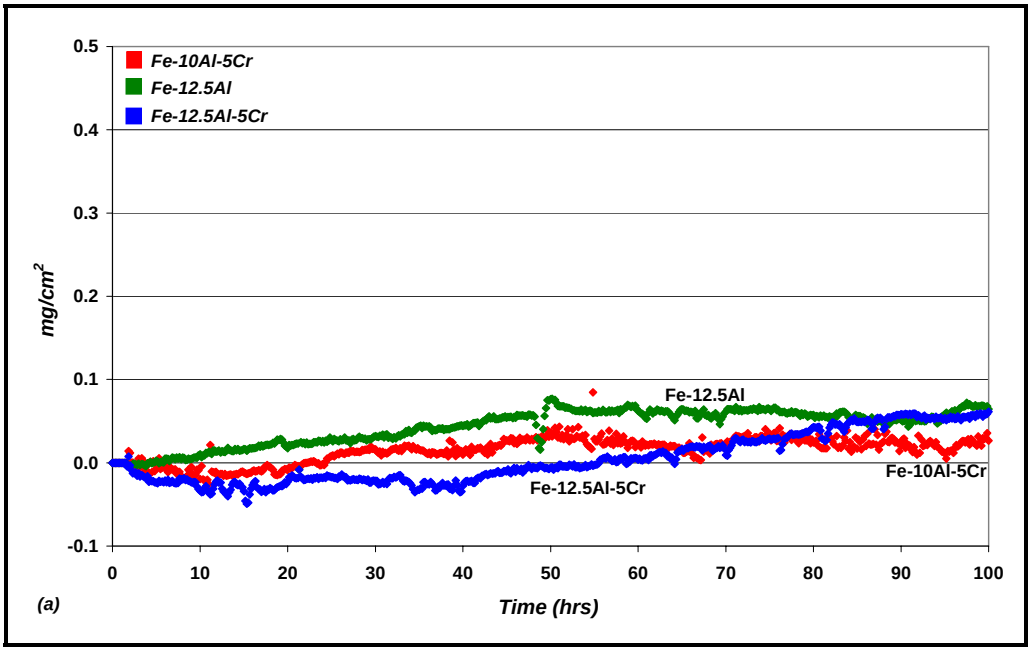

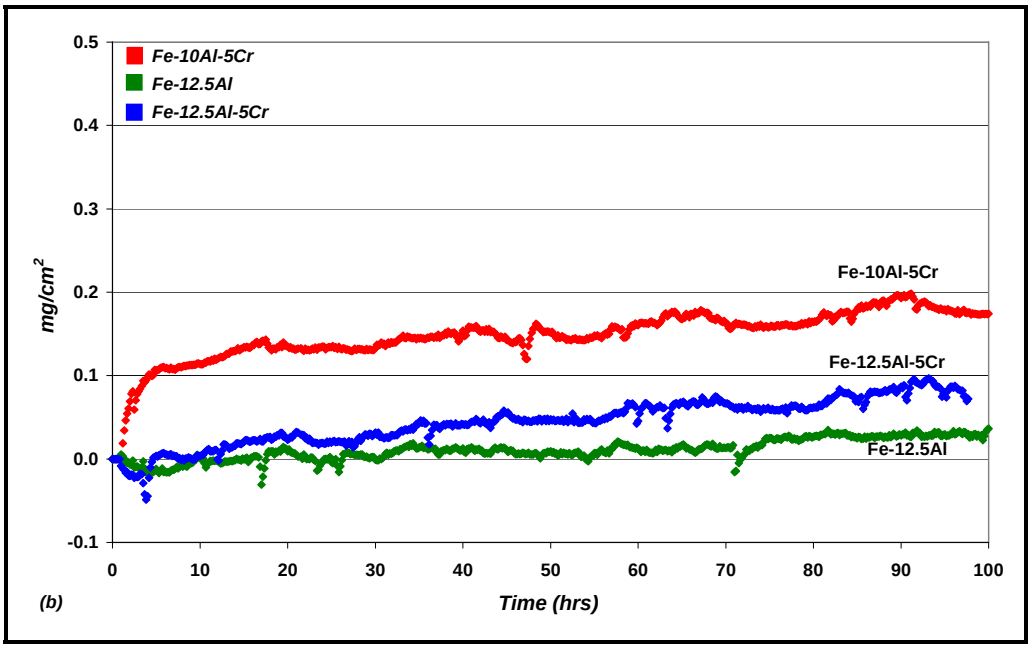

Figure 3 – Weight change for all three alloys in the mixed oxidizing / sulfidizing environment at (a) 500°C and (b) 700°C, 100hrs.

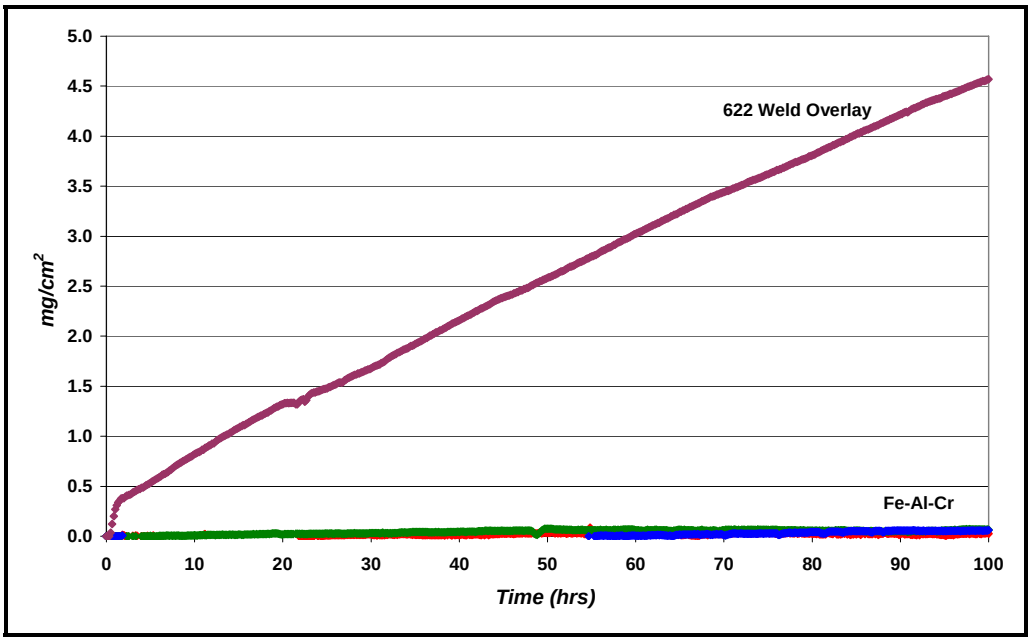

Figure 4 – Weight change for all FeAlCr alloys and alloy 622 weld overlay in mixed oxidizing / sulfidizing environment at 500°C, 100hrs.

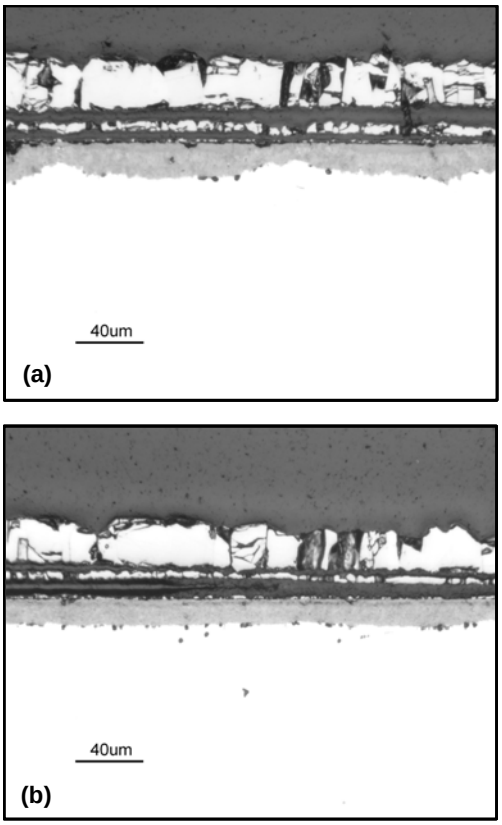

Figure 5 - Optical micrographs of cross sectioned (a) square and (b) wedge Fe-7.5Al-5Cr coupons exposed to the mixed oxidizing / sulfidizing environment at 500°C for 100 hours.

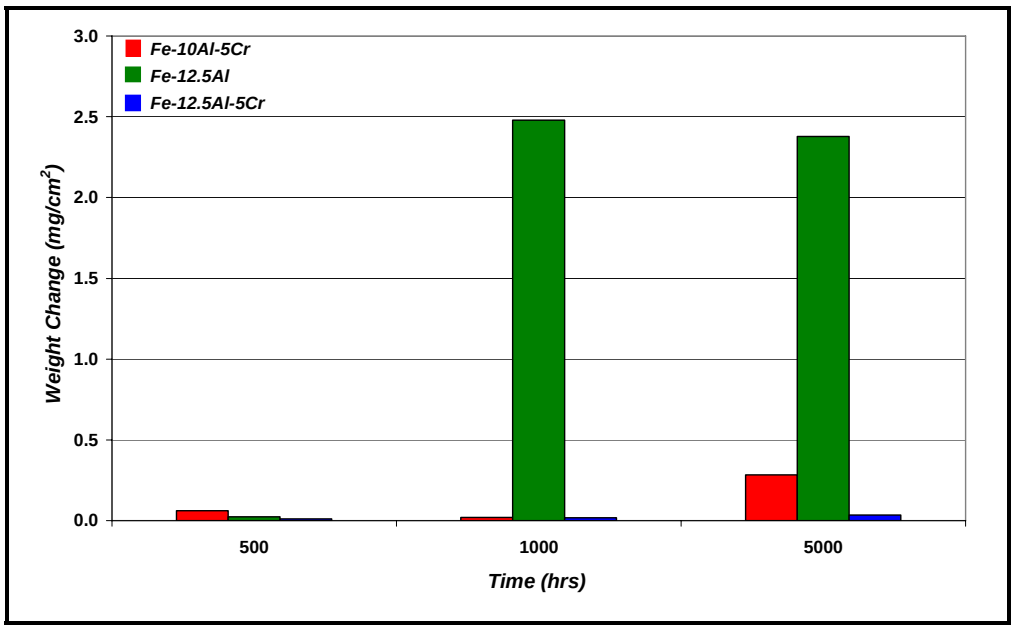

Figure 6 – Weight change for long term corrosion exposures in mixed oxidizing / sulfidizing environment at 500°C.

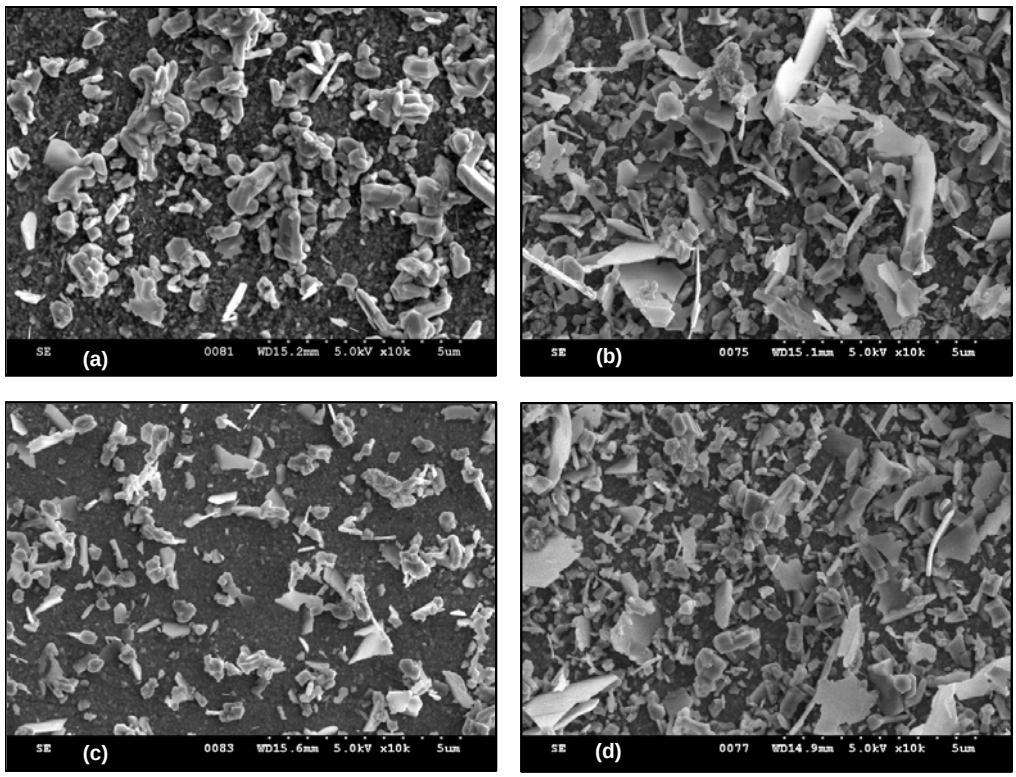

Figure 7 - Comparison of corrosion products formed on Fe-10Al-5Cr after (a) 500hrs and (b) 5000 hours, and Fe-12.5Al-5Cr after (c) 500hrs and (d) 5000hrs.

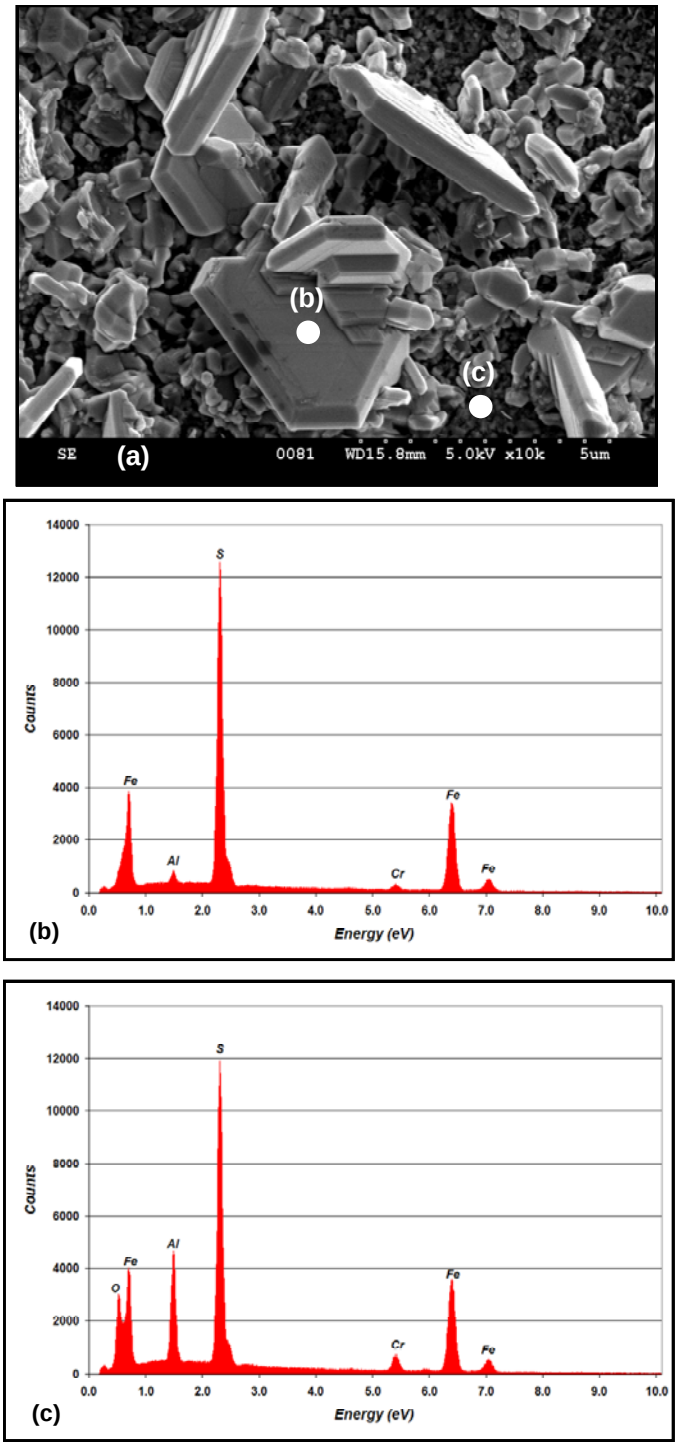

Figure 8 - Iron sulfide type plates (a) and EDS data (b) and (c) from Fe-10Al-5Cr alloy exposed for 500hrs.

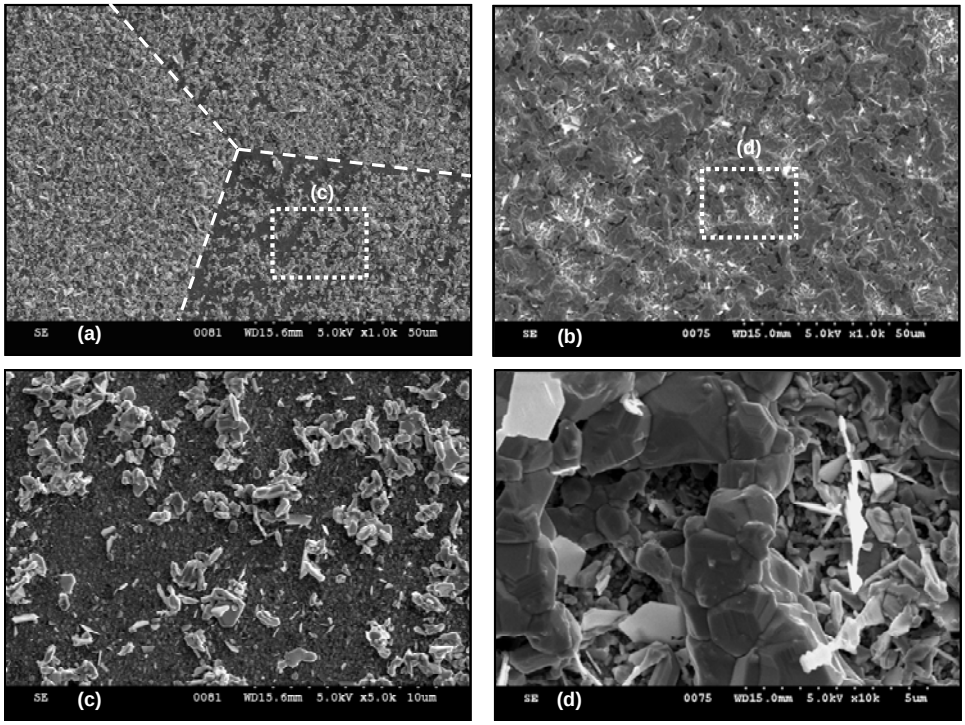

Figure 9 – Comparison of sulfide corrosion product coverage for Fe-10Al-5Cr at (a and c) 500 hours and (b and d) 5,000 hours. Dashed lines in (a) indicate probable location of cast alloy grain boundaries.

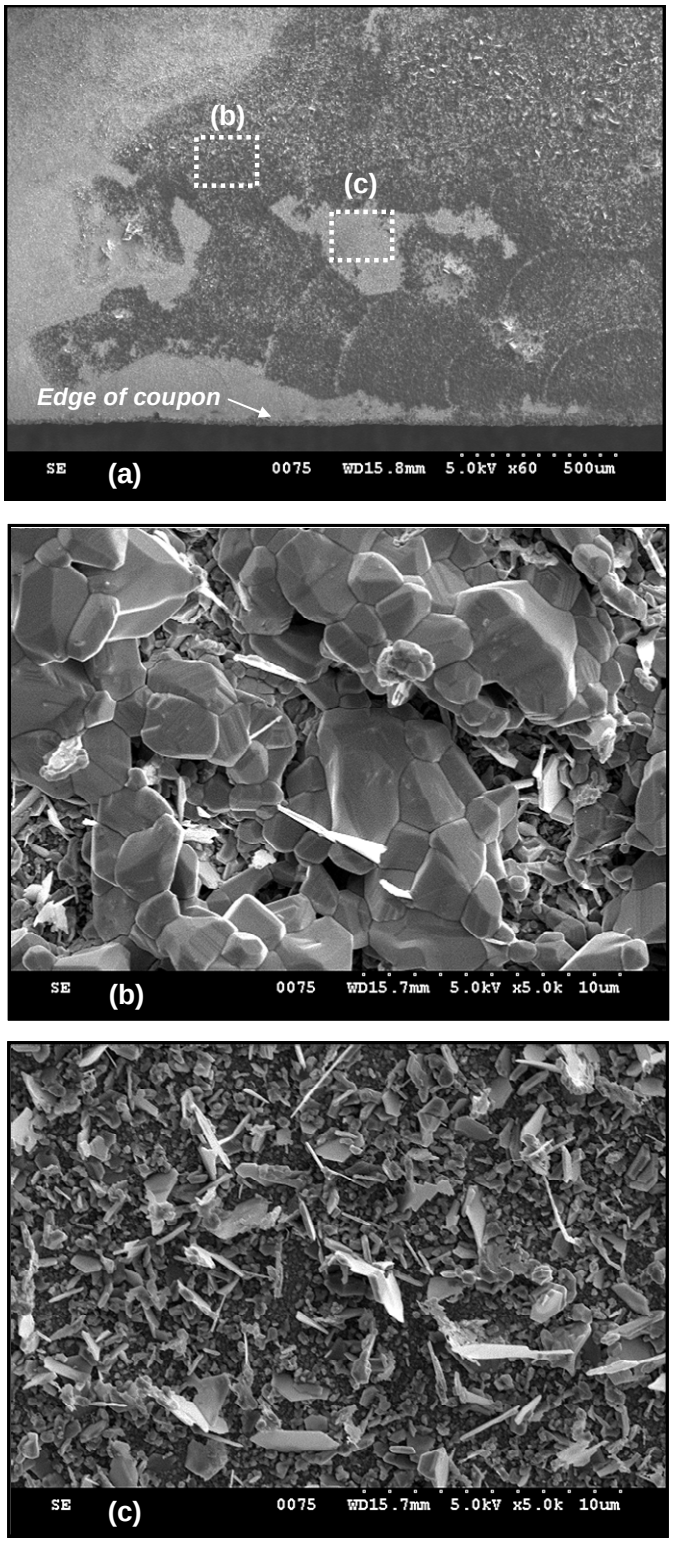

Figure 10 – Corrosion products observed at the coupon edge of Fe-10Al-5Cr alloy after 5000 hours exposure. Dark regions observed in (a) were found to be mostly iron sulfide, as shown in (b), while regions in between sulfides showed mixed flake products (c).

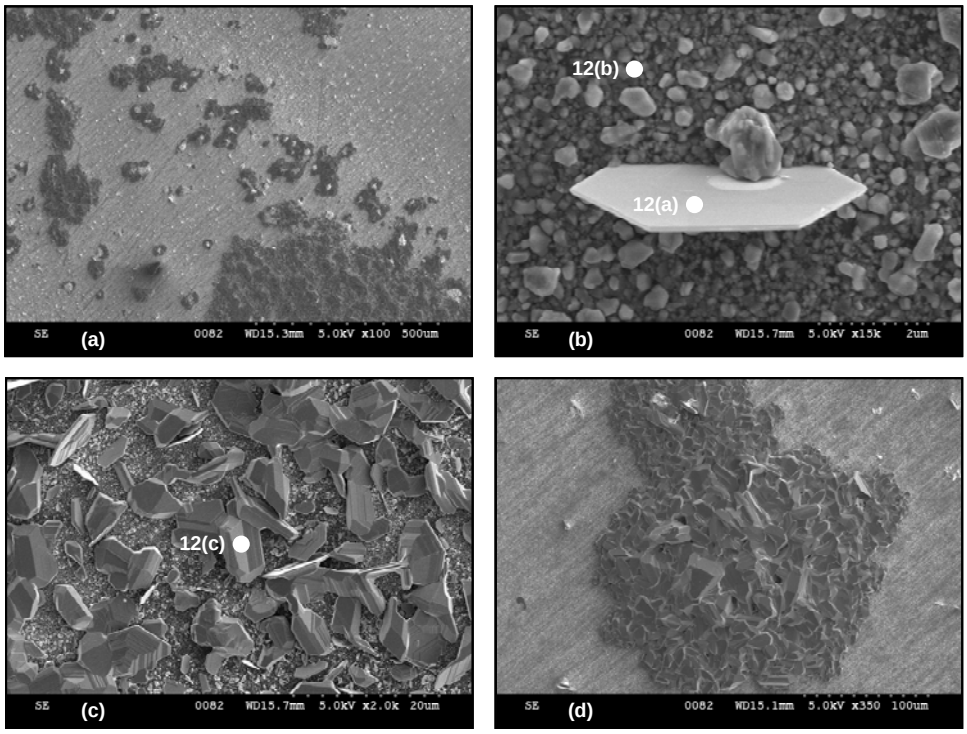

Figure 11 - Corrosion products observed on Fe-12.5Al alloy after 500hrs. White specks in low magnification image (a) are individual or small groups of plates (b). Note faceted morphology of isolated sulfide blocks (c) and larger sulfide nodules (d). White circles show location of EDS analyses presented in Figure 12.

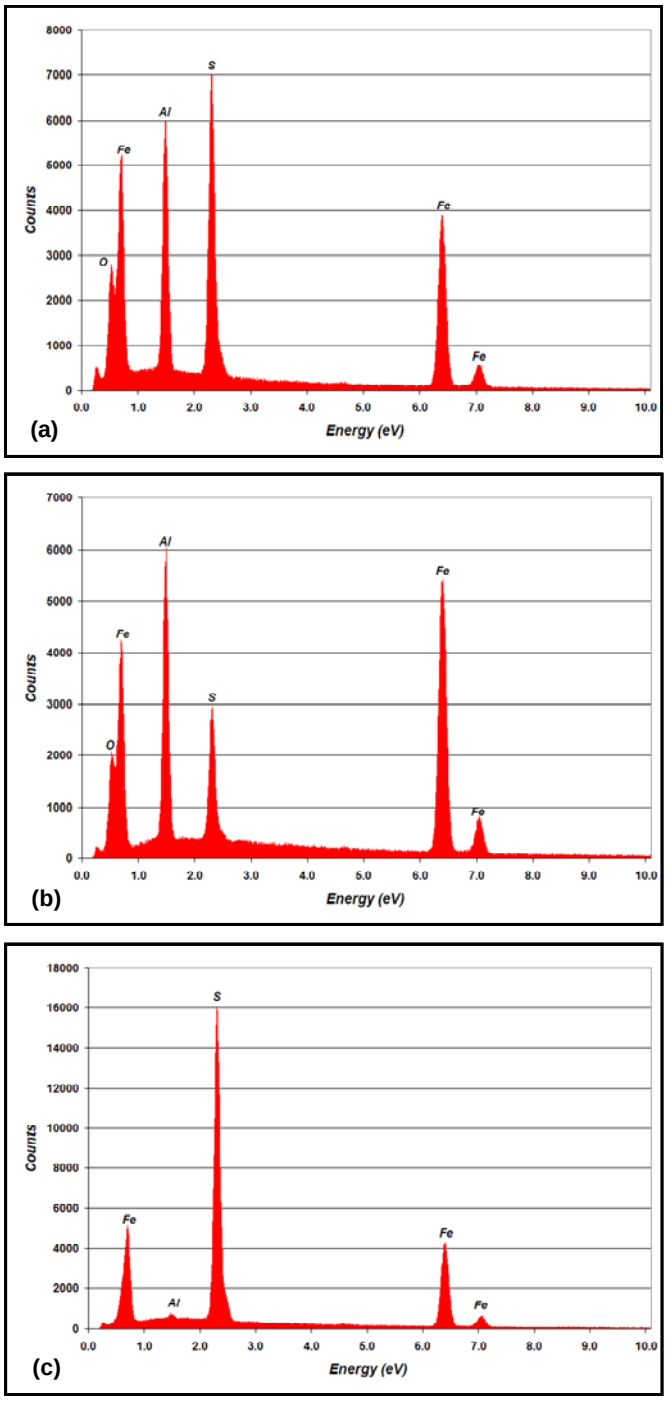

Figure 12 – EDS data from corrosion products shown in (a) Figure 11b center of plate, (b) Figure 11b, region adjacent to plate, and (c) Figure 11c, center of block. Location of EDS analyses shown in Figure 11.

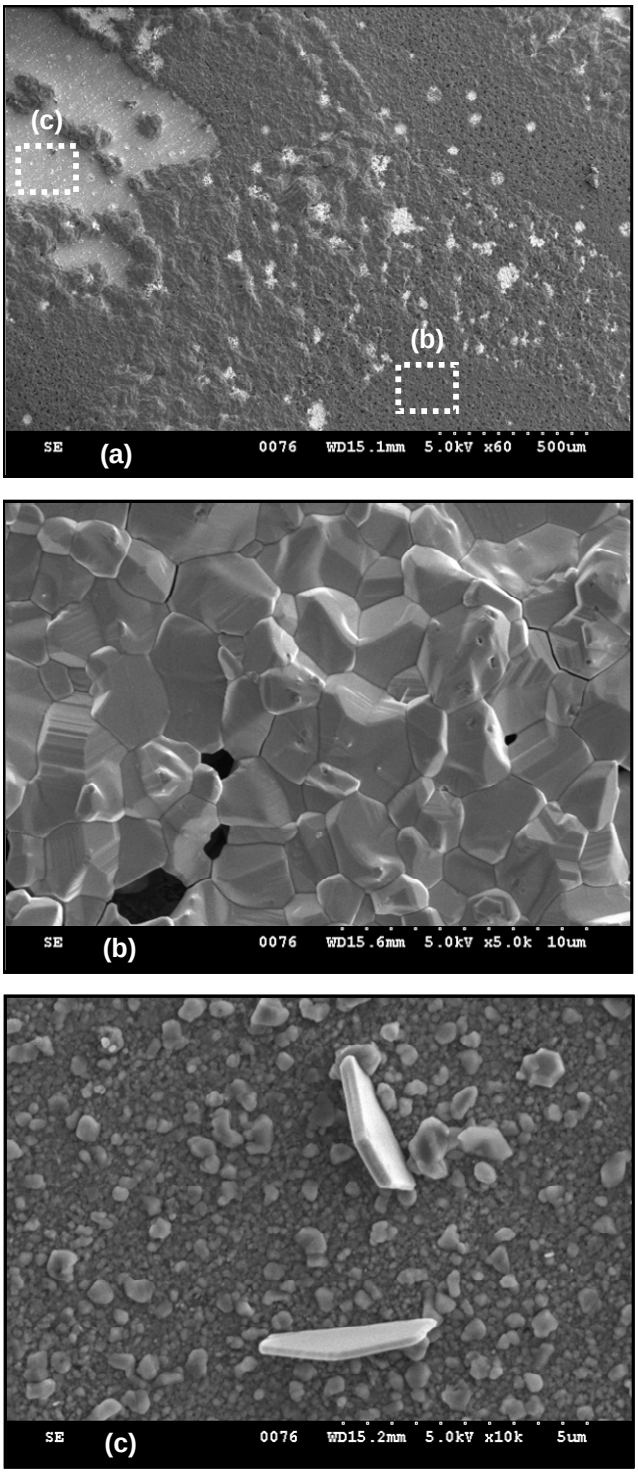

Figure 13 - Corrosion products observed on Fe-12.5Al alloy after 5000 hours of exposure. Low magnification image (a) shows coverage of sulfide film (b) and regions of isolated sulfide plates (c).

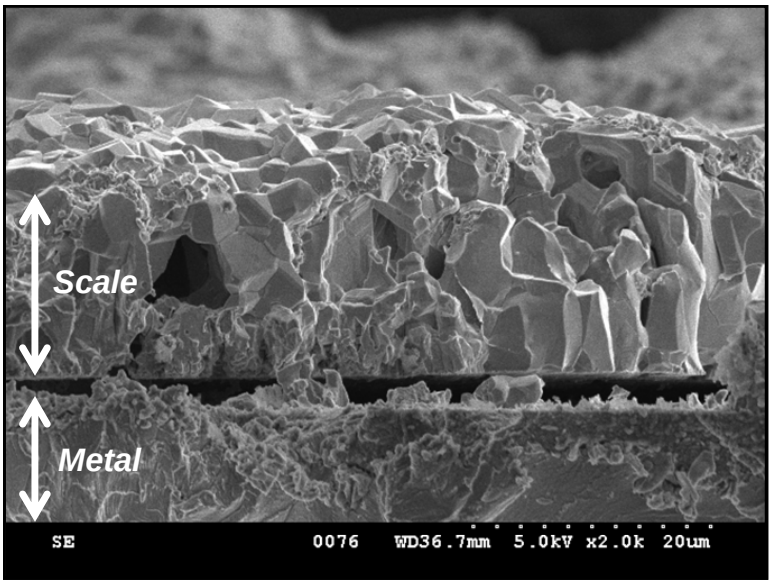

Figure 14 - Cracked cross section of Fe-12.5Al alloy after 5000hrs of exposure.

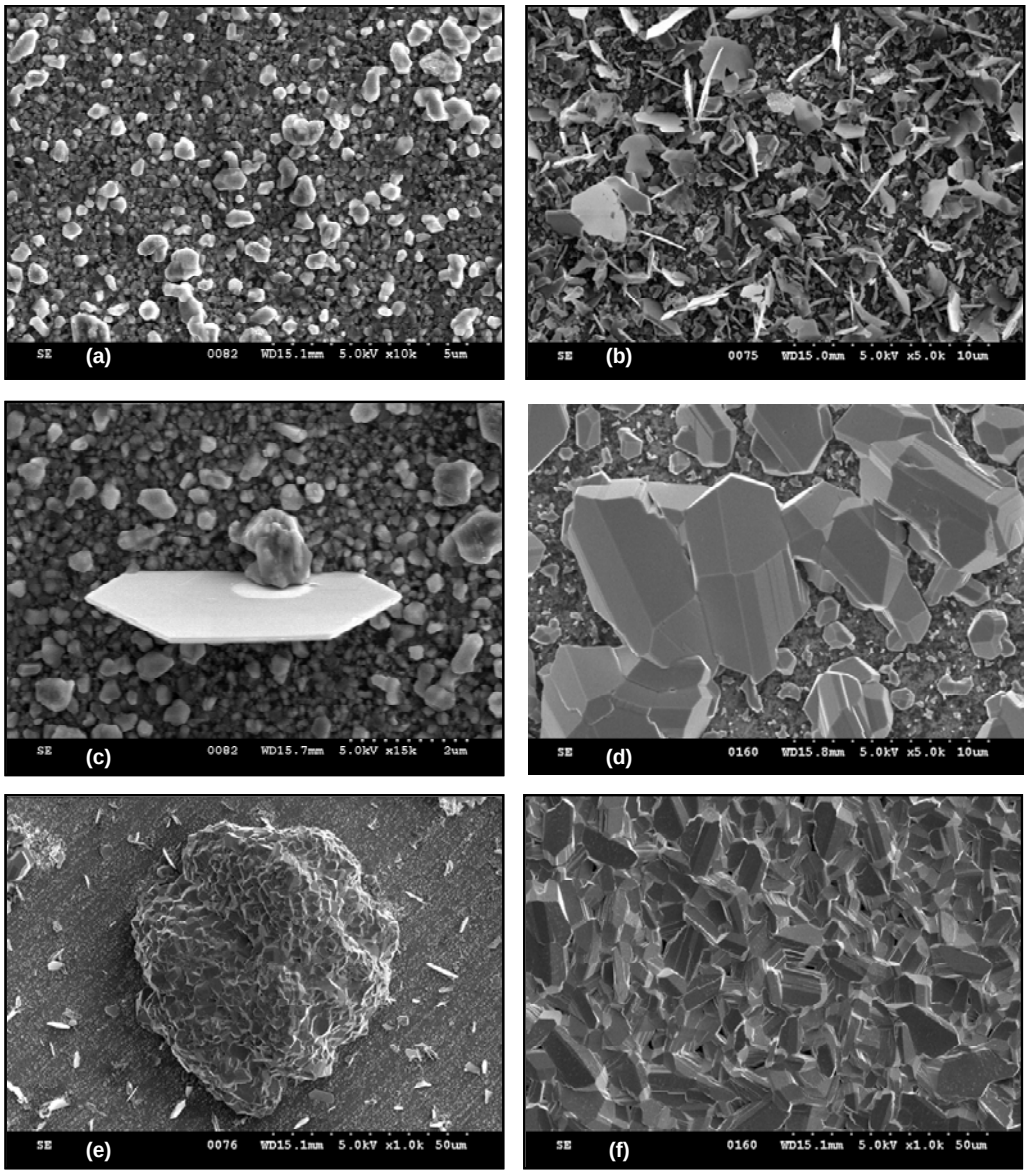

Figure 15 - Summary of corrosion products observed on long term exposure samples. (a) mixed particles, (b) mixed flakes, (c) sulfide plates, (d) sulfide blocks, (e) sulfide nodules and (f) sulfide film.

1.6 References

(1) Jones C. Maladies of Low-NO_x Firing Come Home to Roost. *Power* 1997, *January/February*, 54-60.

(2) Urich, J. A.; Kramer, E. Designing Solutions for Low NOx Related Waterwall Corrosion. *FACT (American Society of Mechanical Engineers)* 1996, *21*, 25-29.

(3) Kung, S. C.; Bakker, W. T. Furnace Wall Corrosion in Reducing-Sulfidizing Combustion Gas. *Materials at High Temperatures* 1997, *14*, 175-182.

(4) Luer, K.; DuPont, J.; Marder, A.; Skelonis, C. Corrosion Fatigue of Alloy 625 Weld Claddings in Combustion Environments. *Mater. High Temp.* 2001, *18*, 11-19.

(5) Banovic, S. W.; DuPont, J. N.; Marder, A. R. Dilution and Microsegregation in Dissimilar Metal Welds Between Super Austenitic Stainless Steel and Nickel Base Alloys. *Science and Technology of Welding and Joining* 2002, *7*, 374-383.

(6) Stott, F. H.; Wood, G. C.; Stringer, J. The Influence of Alloying Elements on the Development and Maintenance of Protective Scales. *Oxid. Met.* 1995, *44*, 113-145.

(7) Banovic, S. W.; DuPont, J. N.; Marder, A. R. Weldability and high temperature sulfidation behavior of iron-aluminum weld overlays. 1999. Trends Weld. Res., Proc. Int. Conf., 5th.

(8) Saegusa, F.; Lee, L. Oxidation of Iron-Aluminum Alloys in the Range of 500-1000°C *Corrosion* 1966, *22*, 168-177.

(9) Tomaszewicz, P.; Wallwork, G. R. Observations of Nodule Growth During the Oxidation of Pure Binary Iron-Aluminum Alloys. *Oxid. Met.* 1983, *19*, 165-185.

(10) Banovic, S. W.; DuPont, J. N.; Marder, A. R. The Effect of Aluminium Content on the Corrosion Behavior of Fe-Al Alloys in Reducing Environments at 700°C. *Metall. Mater. Trans. A* 2000, *31A*, 1805-1817.

(11) Tomaszewicz, P.; Wallwork, G. R. The Oxidation of High-Purity Iron-Chromium-Aluminum Alloys at 800°C *Oxid. Met.* 1983, *20*, 75-109.

(12) DeVan, J. H. Oxidation behavior of iron-aluminum (Fe_3Al) and derivative alloys. 1988. Oxid. High-Temp. Intermet., Proc. Workshop.

(13) Tortorelli, P. F.; Goodwin, G. M.; Howell, M.; DeVan, J. H. Weld-overlay iron-aluminide coating for use in high temperature oxidizing/sulfidizing environments. 1995. Heat-Resist. Mater. II, Conf. Proc. Int. Conf., 2nd.

(14) Wright, I. G.; Peraldi, R.; Pint, B. A. Influence of Aluminum Depletion Effects on the Calculation of the Oxidation Lifetimes of FeCrAl Alloys. *Materials Science Forum* 2004, *461-464*, 579-589.

(15) Al Badairy, H.; Tatlock, G. J.; Bennett, M. J. A Comparison of Breakaway Oxidation in Wedge-Shaped and Parallel Sided Coupons of Fe-Cr-Al Alloys. *Materials at High Temperatures* 2000, *17*, 101-107.

(16) Al Badairy, H.; Tatlock, G. J. The Application of a Wedge-Shaped Sample Technique for the Study of Breakaway Oxidation in Fe-20Cr-5Al Base Alloys. *Oxidation of Metals* 2000, *53*, 157-170.

(17) Graupner, H.; Hammer, L.; Heinz, K.; Zehner, D. M. Oxidation of Low-Index FeAl Surfaces. *Surface Science* 1997, *380*, 335-351.

(18) DeVan, J. H.; Tortorelli, P. F. Oxidation/Sulfidation of Iron-Aluminum Alloys. *Mater. High Temp.* 1993, *11*, 30-35.

(19) DeVan, J. H.; Tortorelli, P. F. The Oxidation-Sulfidation Behavior of Iron Alloys Containing 16-40 at% Aluminum. *Corros. Sci.* 1993, *35*, 1065-1071.

(20) Tortorelli, P. F.; DeVan, J. H. Behavior of Iron Aluminides in Oxidizing and Oxidizing/Sulfidizing Environments. *Mater. Sci. Eng. , A* 1992, *A153*, 573-577.

(21) Regina, J. R.; DuPont, J. N.; Marder, A. R. Gaseous Corrosion Resistance of Fe-Al-Based Alloys Containing Cr Additions. Part I - Kinetic Results. *Mater. Sci. Eng. , A* 2005, *A404*, 71-78.

(22) Velon, A.; Yi, D. Q. Influence of Cr on the Oxidation of Fe3Al and Ni3Al at 500°C. *Oxidation of Metals* 2002, *57*, 13-31.

(23) Deacon, R. M.; DuPont, J. N.; Kiely, C. J.; Marder, A. R. *submitted* 2007.

(24) Boggs, W. E. Oxidation of Iron-Aluminum Alloys From 450°C to 900°C. *J. Electrochem. Soc.* 1971, *118*, 906-913.

(25) Tomaszewicz, P.; Wallwork, G. R. Iron-Aluminum Alloys: a Review of Their Oxidation Behavior. *Rev. High-Temp. Mater.* 1978, *4*, 75-105.

(26) Kai, W.; Huang, R. T. The Corrosion Behavior of Fe-Al Alloys in $H_2/H_2S/H_2O$ Atmospheres at 700-900°C. *Oxidation of Metals* 1997, *48*, 59-86.

(27) Mrowec, S. Mechanism of High-Temperature Sulfide Corrosion of Metals and Alloys. *Werkstoffe und Korrosion* 1980, *31*, 371-386.

(28) Strafford, K. N.; Manifold, R. Scaling Behavior of an Iron-5% Aluminum Alloy in Sulfur Vapor. *Oxid. Metals* 1969, *1*, 221-240.

(29) Strafford, K. N.; Manifold, R. Effects of Aluminum Alloying Additions on the Sulfidation Behavior of Iron. *Oxid. Metals* 1972, *5*, 85-112.

(30) Mrowec, S.; Wedrychowska, M. Kinetics and Mechanism of High-Temperature Sulfur Corrosion of Iron-Chromium-Aluminum Alloys. *Oxid. Met.* 1979, *13,* 481-504.

(31) Patnaik, P. C.; Smeltzer, W. W. Sulfidation Properties of Iron-Aluminum Alloys at 1173 K in Hydrogen Sulfide-Hydrogen Atmospheres. *Oxidation of Metals* 1985, *23,* 53-75.

(32) Smith, P. J.; Jackson, P. R. S.; Smeltzer, W. W. The Sulfidation Behavior of an Iron-10 Atomic Percent Aluminum Alloy in Argon-Sulfur and Hydrogen-Hydrogen Sulfide Atmospheres at 1023 K. *J. Electrochem. Soc.* 1987, *134,* 1424-1431.

(33) Banovic, S. W.; DuPont, J. N.; Marder, A. R. Growth of Nodular Corrosion Products on Fe-Al Alloys in Various High-Temperature Gaseous Environments. *Oxid. Met.* 2000, *54,* 339-369.

(34) Tortorelli, P. F.; Wright, I. G.; Goodwin, G. M.; Howell, M. High-temperature oxidation/sulfidation resistance of iron-aluminide coatings. 1996. Elevated Temp. Coat.: Sci. Technol. II, Proc. Symp.

(35) Narita, T.; Przybylski, K.; Smeltzer, W. W. Sulfidation Properties of an Fe-23.4Cr-18.6Al Alloy at Temperatures 1073 and 1173 K in Hydrogen Sulfide-Hydrogen Atmospheres of Sulfur at Pressures 104-10-5 Pa. *Oxidation of Metals* 1984, *22,* 181-200.

(36) Smith, P. J.; Smeltzer, W. W. A Method for Long-Term Sulfidation of Metal at Low Sulfur Pressures and Its Application to Sulfidation of an Iron-20 at.% Aluminum Alloy at 1023 K. *Oxid. Met.* 1987, *28,* 291-308.

(37) Regina, J. R.; DuPont, J. N.; Marder, A. R. The Effect of Water Vapor on Passive-Layer Stability and Corrosion Behavior of Fe-Al-Cr Base Alloys. *Oxidation of Metals* 2004, *61,* 69-90.

2 EVALUATION OF THE CORROSION RESISTANCE OF FE-AL-CR ALLOYS IN SIMULATED LOW NOX ENVIRONMENTS: Part 2 – Electron Microprobe Analysis and Scanning Transmission Electron Microscopy Studies

2.1 Introduction

The corrosion resistance of iron aluminum alloys makes them ideal candidates for use as weld overlays in coal combustion environments. Corrosion resistance increases with aluminum concentration[1,2], but susceptibility to hydrogen cracking[3] limits the aluminum concentration to around 10-15wt%. Researchers are currently considering ternary additions to such alloys to improve corrosion resistance. Chromium additions have been reported to have both beneficial[4] and detrimental[5] effects on the alloy corrosion resistance; further analysis is required to determine the relative advantages and disadvantages of chromium additions. Additionally, much of the work on the corrosion resistance of these alloys has been performed at higher temperatures, where formation kinetics are faster and the slower growing α- alumina phase is stable. Considerably less research has been performed on the corrosion resistance of these alloys at lower temperatures (500°C-700°C).

In Part I of this paper[6], the corrosion resistance of three model iron-aluminum alloys was discussed in the context of analysis by scanning electron microscopy and thermogravimetric results. In the present analysis, scanning transmission electron microscopy and electron probe microanalysis is used to further analyze the corrosion products that form on these alloys in order to gain mechanistic insight into the factors controlling the reported results[6]. The differences in corrosion resistance are compared and contrasted in terms of alloy composition and the corrosion products that develop over long exposure times (up to 5000 hours).

2.2 Experimental Procedure

The three alloys used in this study[6] were prepared at Oak Ridge National Laboratory by drop casting high purity elements into copper cooled molds. The compositions of the alloys are presented in Table IV; aluminum concentrations were slightly lower than the nominal values, chromium was within experimental error, and all trace elements were below acceptable levels. Throughout this work, the alloys are referenced by their intended compositions (Fe-10Al-5Cr, Fe-12.5Al and Fe-12.5Al-5Cr). Corrosion exposures were performed at 500°C in horizontal tube furnaces in a mixed oxidizing / sulfidizing atmosphere for times up to 5000 hours; the gas composition is listed Table V. Addition of 2 volume percent water vapor to the corrosion gas was achieved with the use of a syringe pump connected to a quartz capillary inserted into the hot zone of the furnace. Details of the corrosion experiments and scanning electron microscopy analysis of the as-corroded coupons are presented in Part I of this paper[6]. Quantitative chemical analysis of metal compositions after corrosion testing was performed for select coupons using a JEOL 733 electron probe micro analyzer (EPMA) with wavelength dispersive spectrometers (WDS). K_α x-ray lines were analyzed for all elements at an accelerating voltage of 20kV and a probe current of 30nA. A φ (ρz) correction factor was used to convert data to weight percentages[7]. Samples for scanning transmission electron microscopy (STEM) were prepared from selected long term corrosion coupons using a FEI Strata 235 DB Focused Ion Beam (FIB). All STEM samples were prepared from the wedge region of the coupon, in areas that were representative of the corrosion products observed on the majority of the coupon. STEM analysis was performed on a VG HB603 analytical electron microscope (AEM) equipped with a Nion aberration corrector and operated at 300kV. Elemental maps were obtained using an

Oxford/Link windowless Si(Li) XEDS detector. Kα lines were analyzed for each element; peak energies are listed in Table VI. Measurements of inner corrosion product thickness were determined from the STEM images and ImageJ™ quantitative image analysis software.

2.3 Results

Analysis of both short and long term corrosion kinetics for these alloys was discussed in detail elsewhere in Part I[6]; further analysis of the corrosion products that formed on long term coupons is the focus of the present paper. The long term results can be summarized as follows. Weight change data for all three alloys is presented in Figure 16. Fe-10Al-5Cr was found to be protective at short times, but exhibited considerable weight gain and formation of thick iron sulfide type products after 5000 hours. Iron sulfide products were found on the surface of the binary Fe-12.5Al alloy at all exposure times, with near complete coverage of the entire coupon surface with product at 5000 hours. Fe-12.5Al-5Cr did not experience significant weight gain for any exposure time, and no iron sulfide type corrosion products were found by SEM analysis of this alloy.

In order to assess the susceptibility of these alloys to failure by depletion, wedge shaped coupons were used in the long term tests[6]. Electron probe microanalysis was performed on the Fe-12.5Al alloy after 5000 hours due to the fact that this coupon experienced the highest weight gain for all tested alloys. It was therefore expected that this coupon would exhibit the largest amount of alloy depletion. Line scans were performed on the polished cross section both along the length and through the thickness of the coupon; metallographic preparation was performed without the use of Al_2O_3 polishing media to prevent contamination errors. Scans were set up to start and

stop immediately adjacent to the internal corrosion product, although in some instances, the first or last few points in the scan entered the inner corrosion product zone. Quantification error in the data was approximately ±1wt%. The probe diameter employed was approximately[7] 200nm and the beam interaction volume was estimated to be 1μm^3 at 20kv. A 20μm interval centerline scan, starting in the thick region and traversing the entire coupon to the wedge tip, indicated no significant deviation from nominal composition for both aluminum and iron, as shown in Figure 17a. The slight increase in aluminum concentration for the last two points in this scan was investigated further with a 5 μm interval line scan through the last 250μm of the coupon tip (Figure 17b); no change in aluminum concentration was observed for this scan.

Corresponding line scans performed through the coupon thickness, perpendicular to the length centerline, are shown in Figure 18. The high aluminum concentrations at the beginning and end of the scan located 250μm from the coupon tip (Figure 18a) were assumed to be due to the beam entering the inner corrosion product. If this deviation from nominal composition was due to alloy depletion, the change would have been much more gradual than observed here. The slight decrease in aluminum and simultaneous increase in iron concentrations at the end of the scan located 100μm from the tip (Figure 18b) are within the experimental error of this technique, and therefore cannot be identified as depletion. From these results, it can be said that the EMPA analysis identified no depletion of aluminum or iron within 1 μm of the inner corrosion product in the region of the sample that was less than 100μm thick.

STEM Annular dark field (ADF) images and EDS maps of cross section samples containing both corrosion products and non-corroded metal are shown in Figure 19 through Figure 24 for all

alloys at both 500 and 5,000 hours of exposure time. Samples in all STEM maps are oriented the same way: non-corroded metal to the left or bottom and corrosion products to the right or top. Regions of platinum (an artifact of the FIB sample preparation process) surrounding external corrosion products are visible in the annular dark field images for some maps; platinum maps were not included in these figures for simplicity.

Measurements of the depth of the inner corrosion layer on all three alloys were taken from the STEM maps and are shown in Table VII. The border between the inner corrosion layer and the external corrosion products was assumed to be the line between the sulfur rich nodules or film, and the oxygen rich layer. This was the most linear boundary observed in the corrosion products. For the Fe-12.5Al-5Cr alloy, the thickness of the entire corrosion layer was measured. This total thickness (oxide plus sulfide) correlates well with the weight gain data for the three alloys.

Figure 19 and Figure 20 are the ADF image and EDS maps of the Fe-10Al-5Cr alloy after 500 and 5,000 hours of exposure, respectively. While most of the 500 hours test coupon exhibited mixed flake corrosion products, the sample analyzed in Figure 19 is from a region of coupon that contained some iron sulfide nodules, such as shown in Figure 8(a) in Part I[6]. A faint outlining of these nodules with aluminum and oxygen, and to a lesser extent, chromium, was also observed on multiple samples. The inner corrosion layer immediately beneath the original metal surface was found to be approximately 0.2μm thick (Table VII) and is rich in aluminum and oxygen, with some chromium and sulfur. Additionally, there are protrusions into the metal that are rich in both aluminum and sulfur. At 5,000 hours, the external iron sulfide nodules have coalesced to

form a continuous film (see Figure 9(b) in Part I[6]), although encapsulation of small regions with aluminum and oxygen is still evident. The inner corrosion product is considerably thicker (08.μm) and the aluminum-sulfur protrusions are further elongated.

After 500 hours of exposure, the binary Fe-12.5Al alloy, Figure 21, developed external iron and sulfur rich blocks or nodules that exhibit the same aluminum-oxygen layer encapsulation as described above. This map is representative of the corrosion morphology presented in Figure 11(c) in Part I[6], with separate sulfide blocks on top of a mixed oxide/sulfide corrosion product. The inner corrosion layer is rich in aluminum and oxygen, with some presence of iron and sulfur. At 5,000 hours, the most significant change in the corrosion product is the coalescence of the individual iron sulfide nodules into a continuous film, Figure 22. The external iron and sulfur rich product in this figure is the sulfide film that was observed using scanning electron microscopy in Figure 13(b) and Figure 14 in Part I[6]. Additionally, an aluminum-oxygen rich layer was observed at the metal – inner scale interface; this layer was observed on multiple samples from this alloy. Sulfur was present at the interface of this layer and the un-corroded metal. Inner corrosion product thickness was found to increase from 0.5μm at 500 hours to almost 2μm at 5,000 hours (Table VII).

EDS maps of the Fe-12.5Al-5Cr alloy after 500 and 5,000 hours of exposure are shown in Figure 23 and Figure 24, respectively (note higher respective magnifications of these maps compared to previous). At 500 hours, a layered structure is observed on the alloy, consisting of a chromium-sulfur rich layer between two aluminum-oxygen rich layers. These layers are approximately 25 to 50nm thick and it is not possible from this analysis to determine if they are internal or external

corrosion products. Somewhat isolated large, blocky corrosion products were observed on this alloy at 5,000 hours, and were shown to be rich in chromium and sulfur, Figure 24. The corrosion products observed on this alloy at both exposure times using scanning electron microscopy (see Figure 7 in Part I[6]) exhibited flake-like in morphology; it is likely that the large, sulfur rich protrusion shown in Figure 24 is one of these flake products. As with the other alloys, a thin (less than 100nm) region of aluminum and oxygen enrichment completely surrounds the chromium-sulfur phase.

To determine the stoichiometry of the sulfur and oxygen rich corrosion products on these alloys, semi-quantification of the STEM EDS maps was attempted using Oxford Instrument's INCA Microanalysis Suite 14 software with standard k-factors. The bulky iron and sulfur rich corrosion products (nodules and film) on all samples were found to have an iron to sulfur concentration ratio (in at%) of between 0.97 and 1.0, indicating that the sulfide phase was FeS, not FeS_2. Similar analysis of the block-like chromium and sulfur rich corrosion product on the Fe-12.5Al-5Cr after 5,000 hours of exposure (Figure 24) had a chromium to sulfur concentration ratio of 0.76, close to the Cr-S ratio for Cr_2S_3 (0.67). Analysis of the other sulfur and oxygen rich regions on the samples could not conclusively identify specific polymorphs of the respective corrosion products.

2.4 Discussion

2.4.1 Electron Probe Microanalysis

The EPMA data shows that there was no loss of aluminum or iron after 5,000 hours of exposure for the Fe-12.5Al alloy. Even in a region of the wedge where the sample thickness was less than

100μm, both aluminum and iron levels were within the experimental error of the nominal concentration. Selection of the binary alloy for the EPMA analysis was based on the considerably greater weight gain for this composition as compared to the other two alloys (Figure 16). It was assumed that depletion effects would be greatest for this particular alloy. However, as shown in Figure 22, the STEM analysis revealed that an aluminum- and oxygen-rich layer developed at the interface of the metal and the inner corrosion product on this alloy sometime between 1,000 and 5,000 hours. It is likely that this layer, which the present work cannot conclusively identify as Al_2O_3, acted as a barrier to slow the diffusion of iron or sulfur and limit the extent of attack. This would explain the lack of any significant increase in sample weight gain between the 1,000 and 5,000 hour tests for this alloy, as reported in Figure 16. If any depletion of aluminum or chromium had occurred prior to the 1,000 hour test, the subsequent exposure for 4,000 additional hours without any significant scale formation may have been enough time for diffusion in the alloy to eliminate the depletion profile that may have developed earlier in this alloy.

2.4.2 Scanning Transmission Electron Microscopy

Interpretation of the STEM-EDS results is aided by evaluating the maps from different alloys in light of their respective changes in aluminum or chromium concentration. Also helpful are the schematic models of the development of the corrosion products, based on the STEM maps, which are shown in Figure 25 through Figure 27. Considering the two alloys with 12.5wt% aluminum (Figure 26 and Figure 27), the major difference in corrosion products is the formation of a chromium sulfide on the Fe-12.5Al-5Cr alloy (at long times) and the formation of an iron sulfide on the Fe-12.5Al alloy. It is proposed that upon initial exposure to the corrosive

environment, aluminum oxide formed on both of these alloy surfaces, Figure 26(a) and Figure 27(a). Of the three base elements in these alloys, aluminum forms the most stable oxide, as evidenced by the magnitude of the free energy of formations ($\Delta G°$) listed in Table VIII[8,9]. The formation of this oxide consumes some amount of aluminum from the alloy beneath the corrosion product and reduces the effective partial pressure of oxygen at the metal / oxide interface. This consumption of oxygen effectively shifts the gas composition from the nominal as shown in Figure 28 to the left, into the chromium sulfide and iron sulfide stability regions and these products then begin to form. On the binary alloy, iron sulfide begins to form both externally and within the existing aluminum and oxygen enriched layer, Figure 26b. Owing to the lower free energy of formation(Table VIII), chromium sulfide forms on Fe-12.5Al-5Cr, Figure 27b. With increased exposure time, the iron sulfide nodules on the binary alloy grow and eventually coalesce to form a thick film, Figure 26c, while some isolated chromium sulfide nodules develop on the ternary alloy, Figure 27c. The development of the aluminum and oxygen coating layer on the sulfur corrosion products of these alloys will be discussed later.

Although aluminum sulfide is more thermodynamically favored over the sulfides of both iron and chromium, it is noteworthy that this phase doesn't form on either alloy. Figure 28 suggests that the shift to sulfide stability for iron and chromium requires a reduction of oxygen pressure by approximately 4 and 11 orders of magnitude, respectively, while aluminum sulfide stability would not be reached until the oxygen pressure decreased by approximately 22 orders of magnitude. Additionally, it should be noted that these diagrams depict only which compounds are in equilibrium with the chosen gas composition; factors such as surface finish, alloy or gas composition and/or reaction kinetics can affect the phase stability[10]. These factors can result in a

"kinetic boundary" where the oxide / sulfide boundary is displaced from the thermodynamic or equilibrium boundary. Stroosnijder et al[11] for example showed that the transition from sulfide formation to oxide formation on both 310 stainless steel and alloy 800 was higher than predicted by the phase stability diagram by up to 3 orders of magnitude due to kinetic effects. If a similar shift is assumed for the present work, the decrease in oxygen partial pressure required to make iron and chromium sulfides stable would be smaller than the values suggested by the equilibrium diagrams.

The development of the different sulfides on the two 12.5wt% aluminum alloys has an important consequence on the corrosion resistance, as iron sulfide typically has a more defective structure than chromium sulfide. In a review of sulfidation of metals and alloys, Mrowec[12] reported that the maximum deviation from stoichiometry for FeS at 800°C is 0.2, while for Cr_2S_3 at 700°C, it is 0.08. While there is a difference in temperature in the present work and the stoichiometry of the sulfides formed here could not be determined, Mrowec's data indicates that the iron sulfide will have a higher defect concentration in the crystal lattice than chromium sulfide. The lower thermodynamic stability (higher ΔG) of the iron sulfides (Table VIII) indicates that less energy is required to remove an atom from it's correct position in the FeS lattice compared to the chromium sulfide lattice; hence, it is expected that FeS would be more highly defective. Diffusion of oxygen or sulfur into the metal or iron out, therefore, will be easier through an iron sulfide than a chromium sulfide, which will result in increased growth of this corrosion product. This is evidenced in both the STEM images and the measurements of inner scale thickness (Table VII). Not only is the thickness much lower overall on the Fe-12.5Al-5Cr alloy, there is also little change in scale thickness for this alloy between 500 and 5,000 hours of exposure.

While the convoluted interface between the metal and the inner scale resulted in a large standard deviation for the average thickness measurement on the binary alloy, it is obvious from the STEM images and the maximum thickness data that the inner scale on Fe-12.5Al increases considerably with increased exposure time. Additionally, this measurement on the binary alloy is for the inner corrosion product only; previous analysis[6] of this sample indicated that the outer iron sulfide corrosion product thickness was on the order of 20μm. Such growth indicates that the corrosion scale at 500 hours is not an effective diffusion barrier. In contrast, the scale that forms on the Fe-12.5Al-5Cr alloy remains thin (on the order of 100nm) up to exposure times of 5,000 hours, indicating that the combination of the initial oxide and chromium sulfide acted as a diffusion barrier to significantly slow the diffusion of metal ions or sulfur through it.

It is important to note that the formation of iron sulfide on the Fe-12.5Al alloy is not indicative of classic breakaway corrosion behavior. The similar weight gain observed for this alloy between the 1,000 and 5,000 hour tests (Figure 16) suggests the corrosion scale after 1,000 hours is preventing further attack by slowing the diffusion of corroding species. Breakaway behavior in sulfidizing environments[10] is usually associated with significant ingress of sulfur through a protective oxide layer and the formation internal sulfides; kinetics rapidly increase with the onset of breakaway corrosion. With the Fe-12.5Al alloy, the corrosion kinetics are parabolic in nature, in that there appears to be a period of rapid growth (up to some time between 500 and 1,000 hours) followed by a period of negligible weight gain (1,000 to 5,000 hours). Given the defective structure and rapid growth kinetics typical of iron sulfide, it is unlikely that this corrosion product is providing the observed protection against further attack at times greater 1,000 hours. Rather, the aluminum and oxygen rich layer that developed at the interface between

the inner scale and metal on this alloy at 5,000 hours (Figure 22) is the most probable origin of the observed protection at longer times. It was not possible in the current study to determine the exact composition of this layer, but it bears resemblance to the oxide "healing layer" observed by other investigators in different alloy systems[13,14,15] At the interface between the corrosion product and the metal, the partial pressures of oxygen and sulfur are controlled by the dissociation pressure of corrosion product. The formation of this oxygen rich layer is most likely due to a decrease in the sulfur pressure at this interface, which would make the oxide phase more stable. Development of this layer is a significant result, as it shows that the formation of a substantial iron sulfide scale on a binary Fe-Al alloy is not necessarily an indicator of complete loss of protection or breakaway corrosion, since the internal aluminum and oxygen rich layer may act as an effective diffusion barrier after an incubation period.

The other informative comparison regarding the corrosion resistance is between the Fe-10Al-5Cr and Fe-12.5Al-5Cr alloys, to determine the effect of changing the aluminum concentration. From the STEM EDS maps (Figure 19 and Figure 20), it is evident that the lower aluminum alloy did not develop a chromium sulfide; rather, iron sulfide formed on this alloy, similar to that observed on the binary alloy. It is hypothesized that upon initial exposure to the corrosive gas, the aluminum concentration in the Fe-10Al-5Cr alloy is not high enough to selectively oxidize only aluminum. In contrast to the Fe-12.5Al-5Cr alloy, oxides of both aluminum and chromium form on the low aluminum alloy (Figure 25a); this is evident in the 500 hour EDS map (Figure 19), where chromium was found alongside the aluminum and oxygen in both the inner corrosion layer and outlining the iron sulfide nodule. Consequentially, the concentration of both of the elements close to the surface is slightly depleted. As with the two alloys previously discussed,

this initial oxide formation also consumes some amount of oxygen from the local atmosphere, making sulfide formation more thermodynamically favored. Iron sulfide, although again the least thermodynamically stable phase, begins to form on this alloy due to the decreased local aluminum and chromium concentrations, Figure 25b. Continued diffusion of sulfur and oxygen into the metal causes the inner corrosion scale to thicken, as iron diffuses out to form more iron sulfide. Coalescence of the sulfide nodules creates regions of sulfide film, and continued ingress of sulfur results in the formation of the aluminum-sulfur rich protrusions observed at the metal-scale interface, Figure 25c.

The growth of the iron sulfide corrosion product may not necessarily result in a complete loss of corrosion resistance for the Fe-10Al-5Cr alloy. As observed with the binary alloy from the 5,000 hour test, the ternary alloy may also eventually develop an aluminum-oxygen rich healing layer at the base of the inner corrosion scale, although at much longer exposure times. The thickness of the inner corrosion product (Table VII) on the Fe-10Al-5Cr alloy is only approximately half as thick as the inner scale on the Fe-12.5Al alloy. The lowering of the partial pressure of sulfur to the critical level at which oxides become thermodynamically favored may not occur until this inner scale develops further into the alloy. Some evidence of this layer is visible in the 5,000 hour sample, Figure 20; however, it was observed on only some of the STEM samples from this alloy at this exposure time, while it was present on nearly all STEM samples for the Fe-12.5Al alloy at 5000 hours.

By combining the schematic diagrams of the corrosion product development from Figure 25 - Figure 27, the difference degree of corrosive attack between the different alloy compositions

becomes apparent. Figure 29 is a re-arrangement of the diagrams for each alloy according to the degree of attack or corrosion product morphology, regardless of exposure time. Stage I represents the initial reaction between the gas and the alloy. At Stage II, the Fe-12.5Al-5Cr alloy has developed the layered corrosion products observed after 500 hours (Figure 23); there is no similar corrosion product morphology for the other alloys. Development of blocky sulfide corrosion products (Stage III) is representative of the Fe-12.5Al-5Cr alloy after 5,000 hours (Figure 24), and the Fe-10Al-5Cr and Fe-12.5Al alloys after 500 hours (Figure 19 and Figure 21 respectively). The aluminum and oxygen rich layers in this stage in Figure 29 are drawn to scale, based on the thickness data presented in Table VII, to indicate the degree of attack on the different alloys. At Stage IV, the Fe-10Al-5Cr and Fe-12.5Al alloys have developed a continuous sulfide film; no similar corrosion product morphology exists for the Fe-12.5Al-5Cr alloy. From this figure, it is evident that the degree of corrosion product development on the Fe-12.5Al-5Cr alloy at 5,000 hours is dramatically less than that of the other two alloys at 500 hours.

The present results suggest that depletion of chromium beneath the initially formed oxide leads to the formation of iron sulfide corrosion products on the Fe-10Al-5Cr alloy. A similar mechanism was cited by Kai et al[16] as being responsible for the formation of iron sulfides on iron aluminum alloys in a sulfidizing environment at 700-900°C. In an oxidizing environment, Lee et al[17] showed that an aluminum- and chromium- depleted region developed beneath an external Al_2O_3 scale on Fe_3Al oxidized at 1,000°C. Shebany and Douglass[18] pre-oxidized several iron, nickel and cobalt alloys to develop a protective oxide scale prior to exposure in sulfur vapor. It was noted that the initial behavior of all these alloys without a pre-oxidation treatment was

relatively the same. When pre-oxidized, however, the protective film on the cobalt alloy broke down after 4 hours and sulfidized much more rapidly than the iron alloy. This discrepancy was attributed to depletion of chromium from the cobalt alloy during the pre-oxidation process that allowed cobalt sulfides to form. A lower critical chromium content required to form Cr_2O_3 in FeCr alloys compared to CoCr alloys prevented a similar depletion region from developing on the iron alloy.

Sub-surface depletion of the less noble metal during oxidation of a binary alloy was first discussed by Wagner[19] and others have since modified or updated that original model[20,21]. In a review of alloy oxidation, Wood[22] summarizes some of this work and states that the formation of a depletion zone beneath an oxide layer depends primarily on three variables: (1) the ratio of the oxidation rate to the interdiffusion coefficient of the oxide former, (2) the ratio of the concentration of oxide former in the alloy to the concentration in the oxide, and (3) the ratio of the molecular volume of the oxide to the atomic volume of the metal (Pilling-Bedworth ratio). Using the data of Akuezue and Whittle[23] and Akuezue and Stringer[24], the interdiffusion coefficients at the temperature of the corrosion tests performed presently, 500°C, can be reasonably estimated to be on the order of 10^{-11} to 10^{-12} cm^2 s^{-1}. Additionally, although α-Al_2O_3 has a relatively slow growth rate at high temperatures, it is likely that at 500°C, transitional aluminas (θ, γ, δ) will form on the alloys studied here, rather than the α-phase; these metastable phases have been shown to exhibit faster growth rates than the slower α-phase[25,26]. Thus in the present work, it is reasonable to assume that the diffusion of aluminum and chromium may be too slow at 500°C to prevent a sub-surface depletion layer from forming in the initial stages of exposure. This is in agreement with the work of Lesage et al[27], who showed that the oxidation of

MA956 resulted in aluminum depletion profiles for temperatures below 1080°C. When oxidation occurred at temperatures above 1080°C, a decrease in the aluminum concentration from the nominal alloy level was noted, but a depletion profile did not develop, since diffusion was fast enough at this temperature to eliminate any depletion that may have been created by oxidation.

The corrosion behavior of the two ternary alloys in this work indicates that the critical concentration of aluminum to form a protective aluminum oxide is somewhere between 9.2wt% and 11.6wt% (the actual composition of the Fe-10Al-5Cr and Fe-12.5Al-5Cr alloys) under the current set of test conditions. Other researchers have noted critical aluminum concentrations for protective behavior in iron aluminum alloys close to these values, although the level varies with both environment and temperature. In a study on the oxidation of iron aluminum alloys at 800°C, Tomaszewicz and Wallwork[28] reported that suppression of iron oxide formation in favor of exclusive Al_2O_3 development was achieved at levels of 7wt% or higher. Below this concentration, scales were a mix of iron and aluminum oxides and the iron aluminum spinel, $FeAl_2O_4$. Similarly, Sadique et al[29] found that aluminum concentrations of 6 to 8wt% were necessary for the formation of Al_2O_3 scales in cyclic oxidation tests at 950°C to 1050°C. At lower temperatures, as phase formation kinetics decrease, higher concentrations of aluminum may be required. At 600°C, 10 to 12wt% has been shown to provide protection of iron aluminum alloys in oxidizing environments[30]. A review by Prescott and Graham[31] on the oxidation of these alloys discusses other investigators' findings.

In environments more closely related to the coal combustion gas employed in the present study, somewhat higher aluminum concentrations have been reported. Natesan and Johnson[32]

conducted a study of Fe-Cr-Al and Fe-Al alloys in several gaseous environments and found that alloys with greater than 10wt% aluminum exhibited protective behavior in sulfur bearing environments at temperature of 650°C to 1000°C. Stott et al[33] showed that alloys containing 8wt% aluminum and 5wt% chromium did not develop Al_2O_3 scales at 500°C in a high sulfur, low oxygen environment, but an alloy with 12wt% aluminum was protective and did not develop significant sulfide corrosion products at 700°C. In a study of several iron aluminum chromium alloys, Klower[34] performed microprobe analysis on a 10wt%Al, 2wt%Cr alloy and found external iron sulfide on top of an internal scale that was a mix of aluminum oxide and chromium sulfide. In a 500°C cyclic sulfidation test of two iron-aluminum alloys with 2wt% chromium, the same study showed that metal loss after 2,000 hours dropped from 120μm for the alloy containing only 10wt% aluminum to 1μm for the 17wt% aluminum alloy. DeVan[5] reported a significant decrease in corrosion kinetics upon increasing the aluminum concentration from 8wt% to 9.5wt% in a H_2-H_2S-H_2O environment at 800°C. In an atmosphere similar to the one employed in the current study, Kai and Huang[16] showed that an iron aluminum alloy with less than 15wt% aluminum formed both sulfides and Al_2O_3, while an alloy with 25wt% aluminum formed only Al_2O_3 at 700°C, though some minor iron sulfide was found on this alloy at higher temperatures. The observation in the present work that an aluminum concentration of between 9.2wt% and 11.6wt% is required for protective behavior is in agreement with the findings of other researchers for similar alloy systems.

Although the difference in aluminum level between the two ternary alloys in this study seems minimal, the 2.5wt% change from 11.5wt% to 9.2wt% represents a 25% decrease in the concentration of this element. Using Thermo-Calc software[35] with the Ternary Alloys Database,

the activities of all elements in the three alloys can be calculated at 500°C, as shown in Table IX. There is an increase in the aluminum activity between the Fe-10Al-5Cr and Fe-12.5Al-5Cr alloys of approximately 11%. Additionally, the ratio of the aluminum activity to the chromium activity increases by 20%, indicating that the Fe-12.5Al-5Cr alloy is thermodynamically more likely to selectively oxidize aluminum.

In addition to the different sulfides that formed on Fe-12.5Al-5Cr compared to the other alloys, another distinguishing feature is the absence of the aluminum and sulfur rich protrusions that were observed at the inner scale-metal interface on the Fe-10Al-5Cr alloy (Figure 30). These platelets were observed in parallel groups and resemble Al_2S_3 platelets observed by others[36,37] at the corrosion-metal interface during the sulfidation of iron aluminum alloys. Patnaik and Smeltzer[36] showed that the inward diffusion of sulfur resulting from the dissociation of external FeS caused Al_2S_3 plates to grow internally on iron aluminum alloys. Przybylski et al[38] observed the plates on an Fe-25wt%Cr-10wt%Al alloy and showed through serial sectioning that they form at select orientations. It is possible that the formation of the chromium sulfide layer and the aluminum oxide layers on the Fe-12.5Al-5Cr alloy slowed inward diffusion of sulfur sufficiently to prevent this phase from forming. The presence of iron sulfide adjacent to the un-corroded metal on the Fe-10Al-5Cr alloy could have acted as a source of sulfur for reaction with the metal to form this phase.

Such aluminum and sulfur rich protrusions were not observed on the binary Fe-12.5Al alloy. Lower magnification images of the metal interface on this alloy however, show that this alloy does form high aspect ratio platelets or needles at this interface (Figure 31a and b). Banovic et

al[39] observed a very similar needle like corrosion product at the metal interface of an iron alloy with 5wt% aluminum exposed to a sulfidizing environment, as shown in Figure 31c. Using electron microprobe analysis, the authors in that study determined that the internal needles were the $FeAl_2S_4$ τ-phase. Considering the similarity in alloy composition and morphology of the platelets observed in this study to the those reported by Banovic, it is likely that they are also the $FeAl_2S_4$ phase. The needles observed on the alloy in the present work appear to be aligned along certain angles, indicating that a crystallographic orientation relationship exists between this phase and the ferrite matrix. Banovic[40] also reported that the $FeAl_2S_4$ phase grew with either 4 or 6 growth directions in ferrite grains, indicating perhaps alignment of the spinel with an easy growth direction in the ferrite.

It is unclear from the present analysis if the platelet features on the Fe-12.5Al and Fe-10Al-5Cr alloys are related, and if so, why the composition changes from sulfur rich on the ternary alloy to oxygen rich on the binary. The platelet formation process may be related to the degree of internal corrosion product growth, such that the Fe-10Al-5Cr alloy, which developed much thinner corrosion products than the binary alloy, may be representative of a much earlier stage of development of these platelets. Patnaik and Smeltzer[36] suggested that the internal Al_2S_3 plates observed iron aluminum alloys sulfidized at 900°C eventually transform into the spinel $FeAl_2S_4$ phase by reaction with the surrounding iron. It is possible then that the protrusions on the Fe-10Al-5Cr alloy are Al_2S_3 and that with increased exposure time they will transform into the $FeAl_2S_4$ phase as inferred on the Fe-12.5Al alloy.

Thermodynamic stability and decomposition of these phases also needs to be considered in this analysis. In the study of the $FeAl_2S_4$ phase, Banovic[40] reported a 5wt% increase in the oxygen concentration (as determined by EPMA) of this spinel corrosion product, with a concurrent decrease in the sulfur concentration of approximately the same amount, over a 6 day period of dessicator storage. A similar degradation of the Al_2S_3 phase upon exposure to water vapor has also been reported by Mrowec and Wedrychowska[41] and it is possible that such decomposition has occurred in the present study as well. Decomposition of the sulfur rich corrosion products could have been accelerated in the STEM work presented here since the electron-transparent samples would have more surface area exposed to oxygen than the bulk samples in the Banovic[40] or Mrowec[41] studies. This could explain the discrepancy of oxygen enrichment in this phase between the work presented here and the findings of Banovic. Both the sulfide decomposition process and the possible sulfide and spinel orientation relationships with the ferrite matrix require further investigation to fully understand the formation mechanism of these corrosion products.

The aluminum and oxygen rich layer observed to be outlining the external sulfur corrosion products in the STEM maps (see in particular Figure 20, Figure 21 and Figure 24) is an interesting aspect of the corrosion of these alloys. It is not possible to determine the mechanisms of formation of this layer from the present analysis; however, this encapsulation bears resemblance to a phenomenon observed in the field of catalysis. The "strong metal support interaction" (SMSI) effect was observed by Tauster et al[42] in a study of hydrogen and carbon monoxide sorption by noble metals supported on TiO_2. To account for an observed decrease in catalytic activity under certain conditions, the authors proposed reactions were occurring

between the catalyst and the substrate. The effect has been observed on other catalyst/substrate systems in conditions similar to those in the corrosion tests of the present work (temperatures around 500°C and reducing environments), but the exact cause of SMSI has yet to be determined. A detailed discussion of the phenomenon is outside the scope of this work, but two general theories[43] are discussed in the pertinent literature to explain the effect. One school of thought describes electronic interactions between the catalyst and support, such as charge transfer, as being responsible for the loss of catalytic activity[44,45,46]. The other theory, generally termed encapsulation, involves migration of the oxide support over the catalyst particle due to surface and interfacial energy considerations[47,48]. Bernal et al have used high resolution electron microscopy to show evidence of encapsulation for the rhodium-ceria[49] and platinum-ceria[50] systems; images of this encapsulation are shown in Figure 32. This morphology is very similar to the outlining of iron sulfide corrosion products with aluminum and oxygen observed in the present work (see for instance aluminum-rich circular feature in Figure 20), and it is possible that a similar mechanism is responsible for both observed structures.

Despite the similarity in morphology, there are significant differences between these two systems, including the size of the features being encapsulated (the catalyst being on the order of a few nanometers, while the iron sulfides can be one micron or larger) and their respective chemistries (a pure metallic particle versus a metal sulfide phase). Other potential mechanisms for the formation of this phase were considered. Diffusion of aluminum ions from the metal from beneath the corrosion products through the sulfide to the scale-gas interface, for instance, would be a longer diffusion path than that of oxide migration. Additionally, if the sulfide phase developed beneath an existing oxide layer, it is likely that growth of the jagged and faceted

sulfide products would have resulted in a fractured, interrupted oxide layer, unlike the continuous layer observed on the samples.

It is possible, however, that the iron sulfide corrosion products contained some amount of aluminum that reacted with the oxygen in the environment to form the encapsulation layer. Such doping of iron sulfide with aluminum has been observed by others[36,51,52]. Strafford and Manifold[51] reported the presence of approximately 1wt% aluminum dissolved in the iron sulfide that formed on an Fe-5wt%Al alloy at 600°C. Similarly, Kai and Douglass[52] found dissolved aluminum in external iron sulfide phases on Fe-Mo-Al ternary alloys in H_2-H_2O-H_2S environments. In both of these studies, oxygen was not measured in the sulfide phase and aluminum was described (through analysis with EPMA traces through the FeS nodules) as being dissolved throughout the sulfide phase, rather than being concentrated in the form of an oxide at the sulfide surface as observed in the present study. It is possible that aluminum doping of the external sulfides occurred in the present study and that it diffused to the sulfide surface to react with oxygen in the gas. The presence of un-oxidized aluminum in the iron sulfide was not detected in the STEM analysis of the 500 and 5,000 hour samples presented here. The lack of any detected aluminum could indicate that all of the dissolved aluminum has moved to the surface and oxidized in less than 500 hours.

Regardless of the mechanism, the presence of the oxide outlining is significant in that it provides a type of secondary corrosion protection. In the event of a breach by a sulfide product through the protective layer, the migration of the oxide over the protruding sulfide will effectively seal off the fast diffusion paths of the sulfide. This is evidenced in Figure 24, where a large

chromium and sulfur rich nodule is seen breaking through the protective aluminum and oxygen rich outer layer. The defect structure of the sulfide, along with it's interface with the oxygen layer, would provide an opening for accelerated diffusion into the alloy. Development of the aluminum and oxygen rich coating over this nodule, however, should limit any attack at this location.

2.5 Conclusions

Three model iron aluminum alloys were exposed to a simulated coal combustion environment for up to 5,000 hours and analysis was performed on the developed corrosion products. From this work, the following conclusions can be drawn:

- The Fe-12.5Al-5Cr alloy exhibited the best corrosion performance of the three alloys in this study; no iron sulfides were observed at any test duration. Corrosion resistance of this alloy was attributed to the formation of aluminum and oxygen rich layers, and the ability of the chromium to form a chromium sulfide, preventing reaction of iron and sulfur and the rapid growth of iron sulfides.

- The binary Fe-12.5Al alloy exhibited the worst corrosion behavior with extensive iron sulfide formation after 1,000 hours. Transport of iron and sulfur through an initially formed aluminum oxide was the cause of iron sulfide formation at this time. Subsequent weight gain for this alloy was limited, however, by the development of an aluminum and oxygen rich layer at the metal / scale interface that acted as a diffusion barrier.

- The Fe-10Al-5Cr alloy began to develop iron sulfides between 1,000 and 5,000 hours of exposure. Chromium was observed to form only oxygen rich corrosion products; in contrast to the Fe-12.5Al-5Cr alloy, chromium sulfides did not form on this lower aluminum alloy.

- The results presented in this work indicate that while chromium additions improve the corrosion resistance of iron aluminum alloys in a simulated coal combustion environment, such improvements are only realized when the aluminum concentration is high enough to form an initial aluminum oxide layer. Additions of chromium to low aluminum iron alloys may be beneficial only for short term exposures. Longer durations result in formation of deleterious iron sulfide.

- Despite the significant weight gain of the binary alloy, no depletion of iron or aluminum was found after 5,000 hours of exposure. Formation of an aluminum and oxygen rich layer internally on this alloy likely resulted in the protective behavior observed after 1,000 hours. Subsequent exposure time would have allowed enough time for diffusion to eliminate any depletion zone.

- Encapsulation of external iron sulfide corrosion products with an aluminum and oxygen rich layer was observed for all three alloys. The mechanism of formation of this oxide layer could not be determined from this work; however, it is possible that oxide migration or encapsulation played a role in it's formation. This layer may serve as a secondary

barrier to diffusion and could effectively reseal any protruding sulfide nodules that develop through an otherwise protective scale.

Table IV - Composition of cast alloys. All values wt %; Al, and Cr averaged for top, middle and bottom samples.

Element	Fe-10Al-5Cr	Fe-12.5Al	Fe-12.5Al-5Cr
Fe	balance	balance	balance
Al	9.21 +/- 0.08	11.56 +/- 0.10	11.47 +/- 0.08
Cr	4.94 +/- 0.01	< 0.01	4.92 +/- 0.03
B	< 0.005	< 0.005	< 0.005
C	< 0.01	< 0.01	< 0.01
Cu	< 0.01	< 0.01	< 0.01
Mn	< 0.01	< 0.01	< 0.01
N	0.002	0.002	0.001
Ni	< 0.01	< 0.01	< 0.01
O	0.008	0.004	0.004
P	< 0.005	< 0.005	< 0.01
S	0.004	0.004	0.003
Si	0.02	0.02	0.02
Ti	< 0.01	< 0.01	< 0.01
Y	< 0.01	< 0.01	< 0.01
Zr	< 0.01	< 0.01	< 0.01

Table V - Composition of gas used in corrosion exposures.
Concentration values in volume percent, partial pressure values in atmospheres.

Component	CO	CO_2	H_2O	H_2S	N_2	Log pO_2	Log pS_2
Concentration	10	5	2	0.12	bal	-19	-8

Table VI - Peak energies (in keV) of Kα lines utilized in STEM EDS analysis.

Element	Fe	Cr	S	Al	O
Peak Energy	6.39	5.39	2.30	1.48	0.50

Table VII - Measured depth (in μm) of internal corrosion layer for 500 and 5000 hour exposures.

Alloy	Average Depth (μm)		Maximum Depth (μm)	
	500 hours	***5,000 hours***	***500 hours***	***5,000 hours***
Fe-10Al-5Cr	0.20 ±0.05	0.79 ±0.12	0.63	1.57
Fe-12.5Al	0.54 ±0.65	1.87 ±0.97	1.64	4.42
Fe-12.5Al-5Cr	0.08 ±0.01	0.10 ±0.02	0.10	0.13

Table VIII - Standard free energies of formation of oxides and sulfides (kcal/mol).

Oxides[8]		Sulfides[9]	
Al_2O_3	-342.6	Al_2S_3	-150.3
Cr_2O_3	-223.3	CrS	-34.7
Fe_3O_4	-206.0	FeS	-26.0
Fe_2O_3	-147.6	$Fe_{0.877}S$	-27.3

Table IX - Calculated elemental activities for the ternary alloys in this study.

Element	Fe-10Al-5Cr		Fe-12.5Al-5Cr		Increase (%)	
	wt%	*activity*	*wt%*	*activity*	*wt%*	*activity*
Aluminum	9.2	0.00215	11.5	0.00239	25.0	11.2
Chromium	4.9	0.00528	4.9	0.00494	0.0	0.0
Iron	85	0.01173	82.5	0.01145	-2.9	-2.4

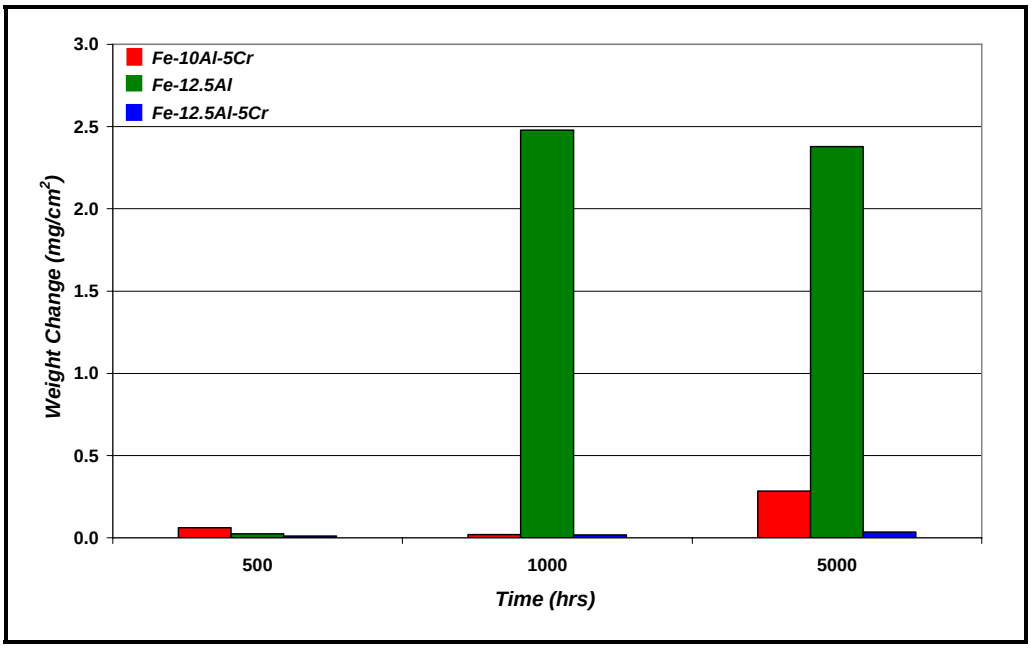

Figure 16 – Weight change for long term corrosion test coupons from [6].

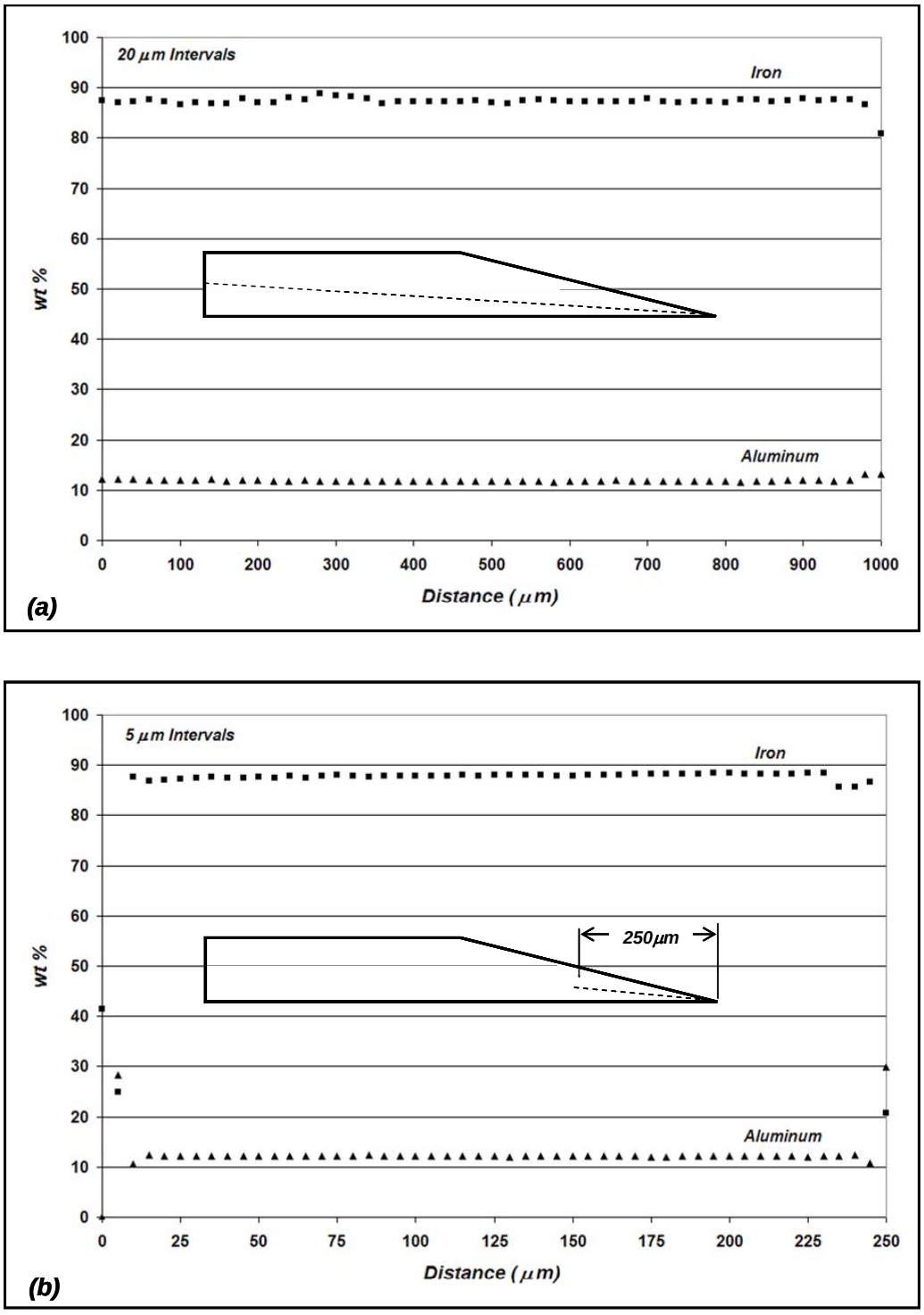

Figure 17 - EPMA data for line scans performed on Fe-12.5Al after 5000 hours of exposure to mixed oxidizing / sulfidizing gas at 500°C along (a) entire coupon centerline and (b) along the centerline in the last 250μm of coupon tip. Inset shows scan location..

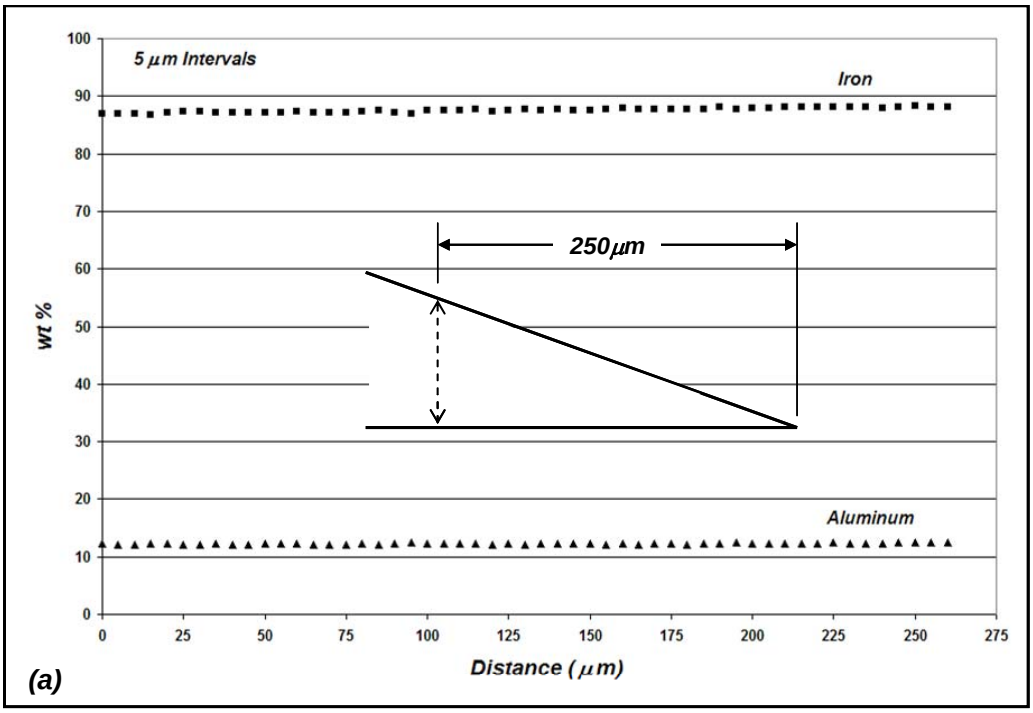

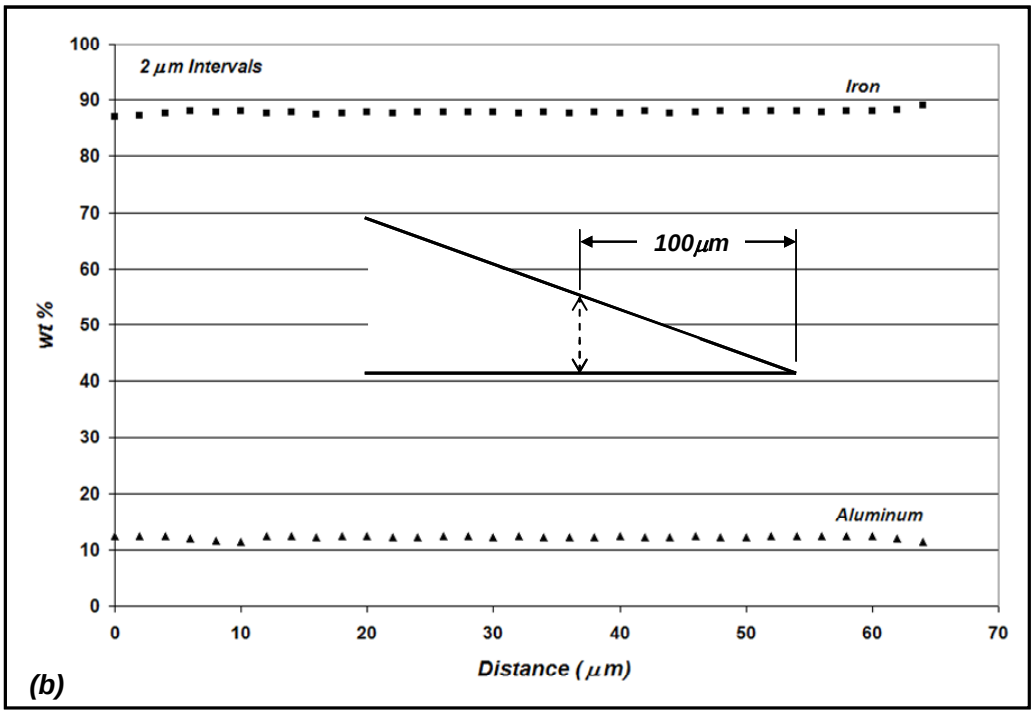

Figure 18 - EPMA data for line scans performed on Fe-12.5Al after 5000 hours of exposure to mixed oxidizing / sulfidizing gas at 500°C through the coupon thickness at (a) 1mm from tip and (b) 100μm from tip. Inset shows scan location.

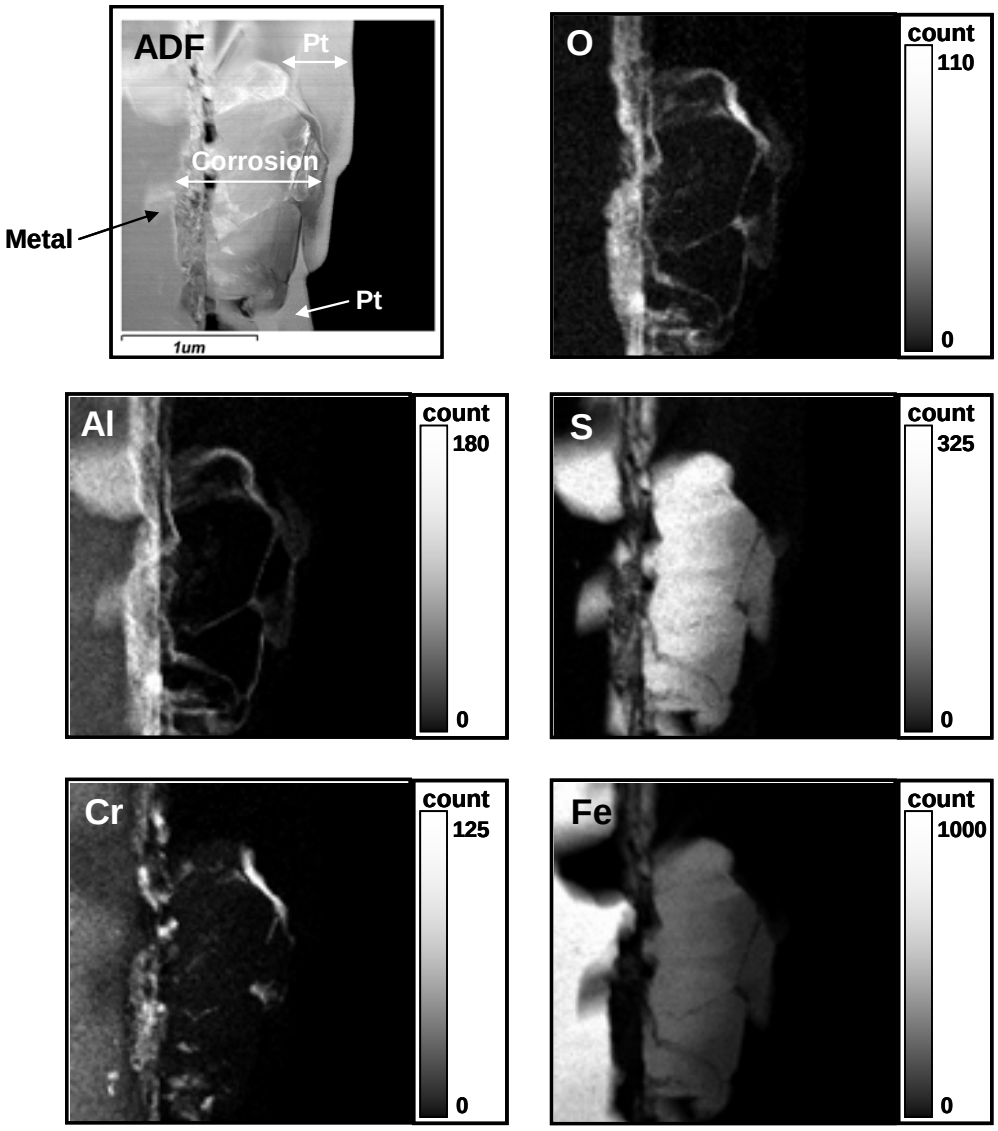

Figure 19 – ADF image and EDS maps (derived from the EDS spectrum image) of Fe-10Al-5Cr alloy exposed for 500 hours to mixed oxidizing / sulfidizing environment at 500°C**.**

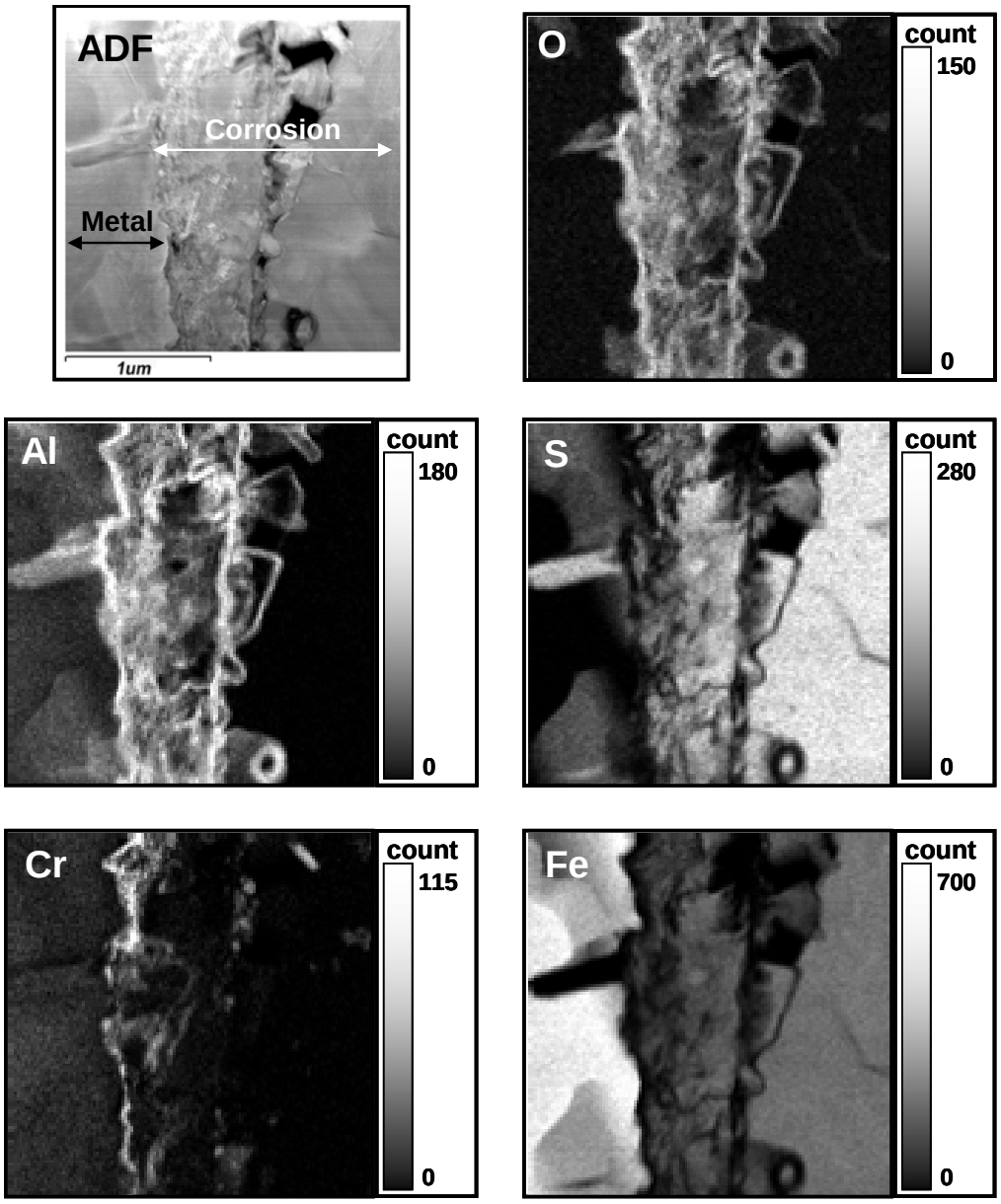

Figure 20 - ADF image and EDS maps (derived from the EDS spectrum image) of Fe-10Al-5Cr alloy exposed for 5,000 hours to mixed oxidizing / sulfidizing environment at 500°C.

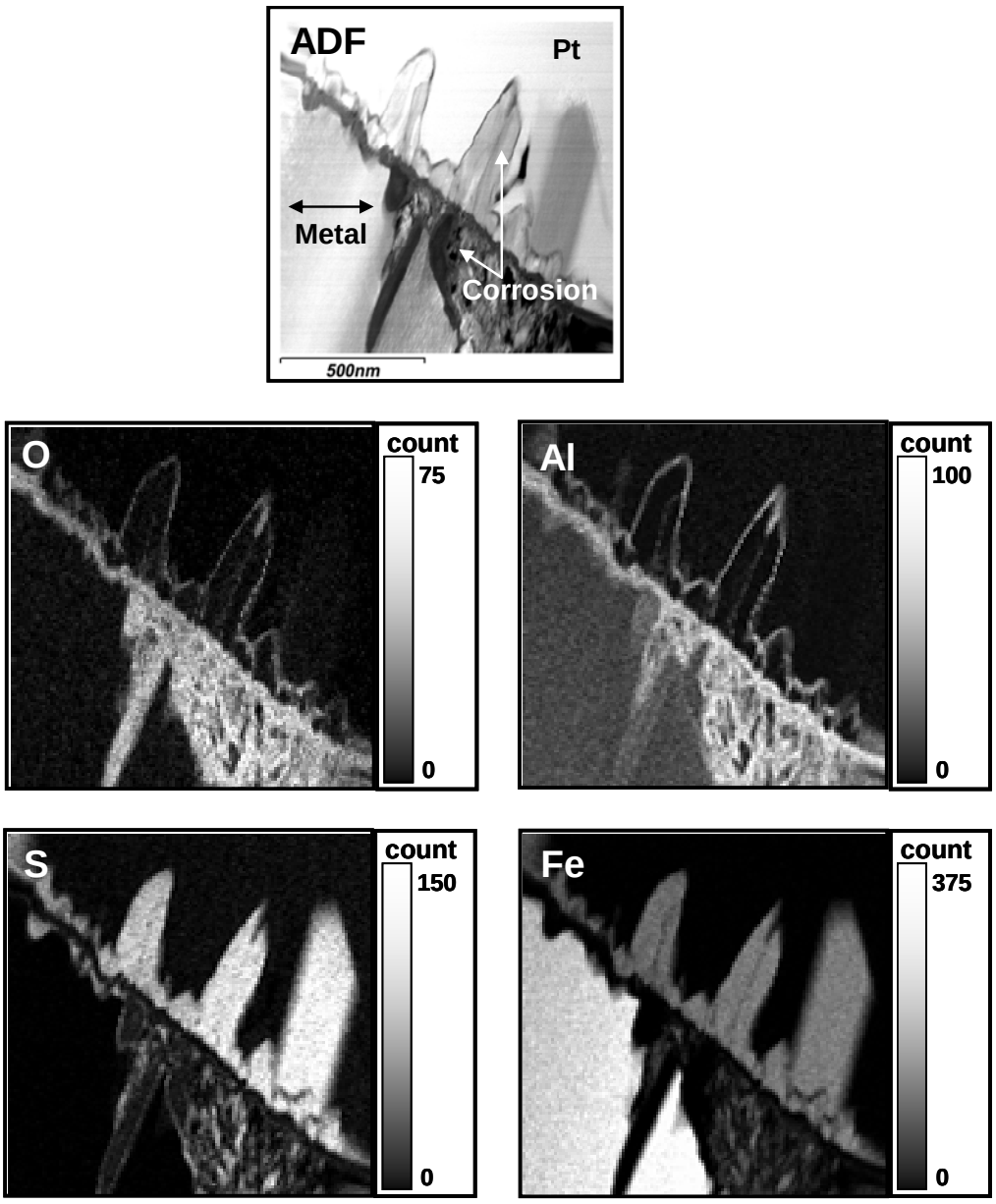

Figure 21 - ADF image and EDS maps (derived from the EDS spectrum image) of Fe-12.5Al alloy exposed for 500 hours to mixed oxidizing / sulfidizing environment at 500°C.

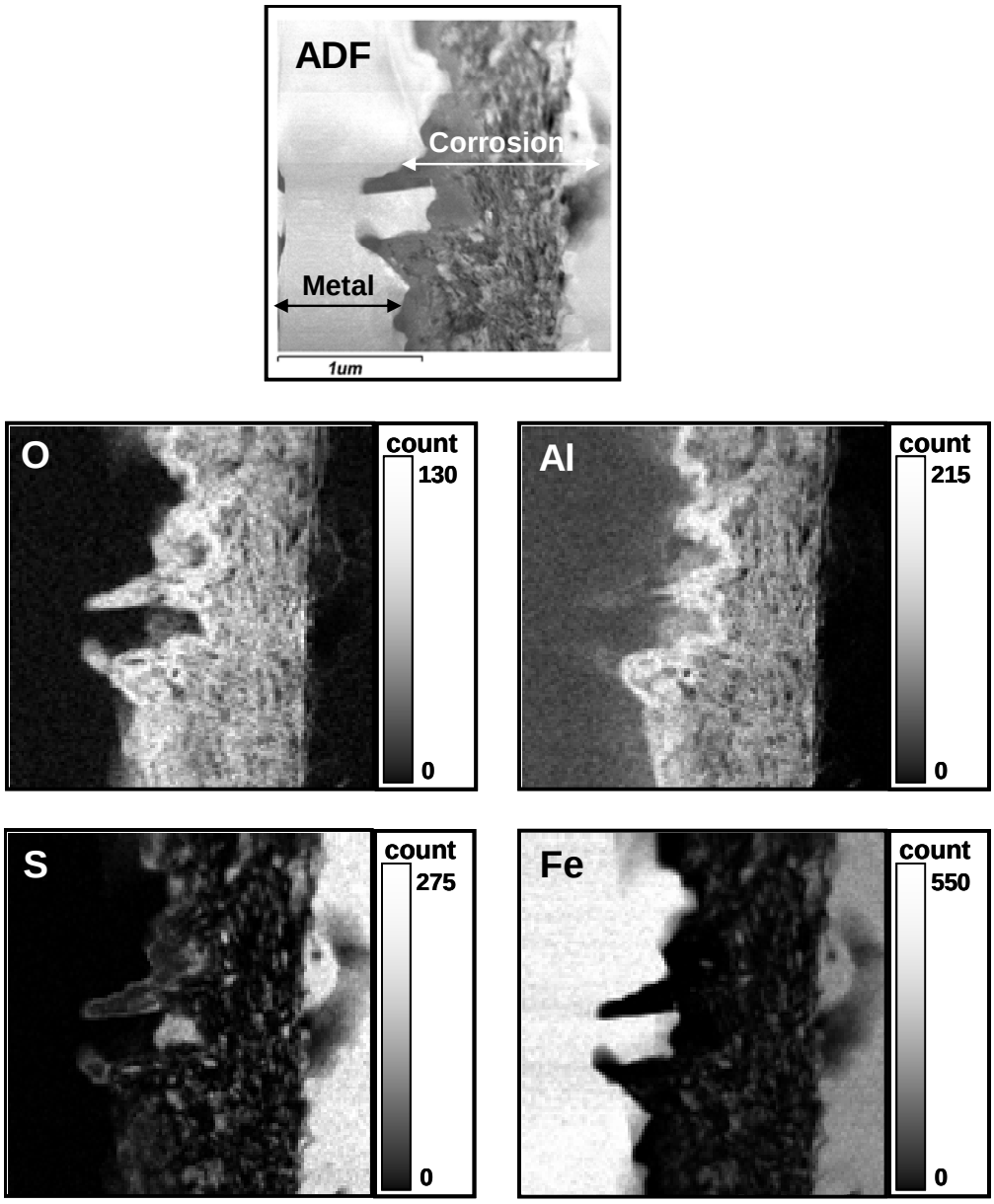

Figure 22 - ADF image and EDS maps (derived from the EDS spectrum image) of Fe-12.5Al alloy exposed for 5,000 hours to mixed oxidizing / sulfidizing environment at 500°C.

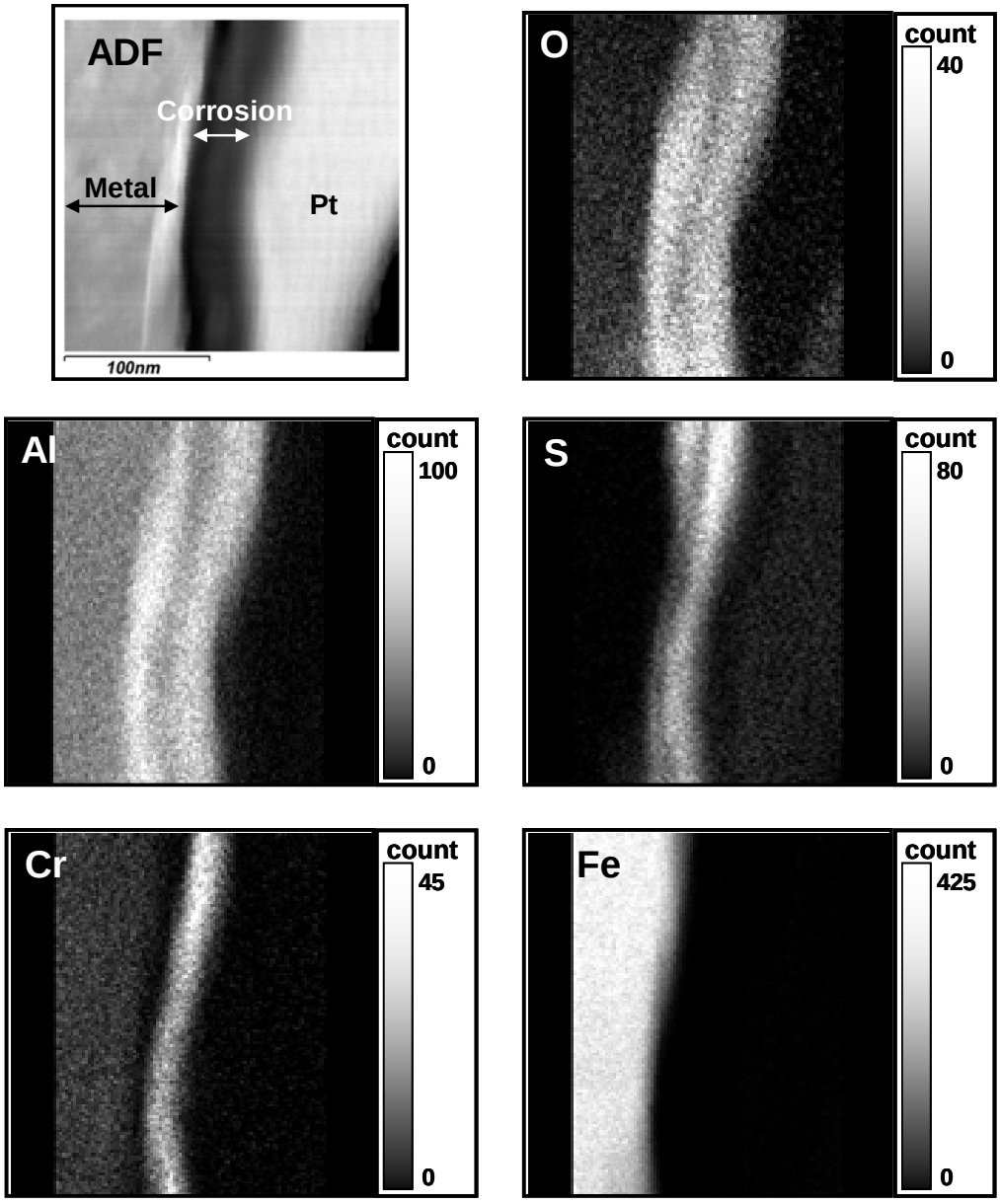

Figure 23 - ADF image and EDS maps (derived from the EDS spectrum image) of Fe-12.5Al-5Cr alloy exposed for 500 hours to mixed oxidizing / sulfidizing environment at 500°C.

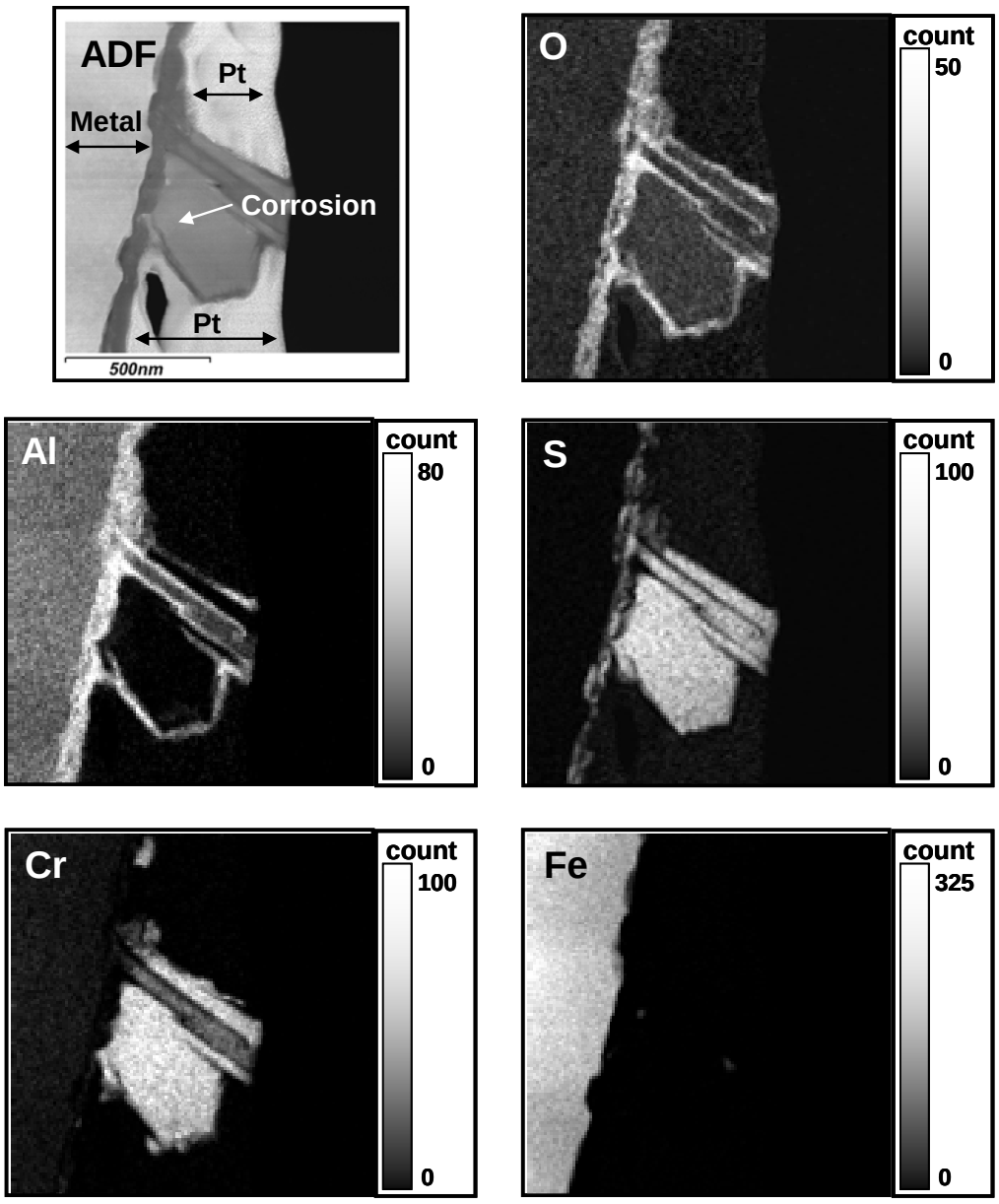

Figure 24 - ADF image and EDS maps (derived from the EDS spectrum image) of Fe-12.5Al-5Cr alloy exposed for 5,000 hours to mixed oxidizing / sulfidizing environment at 500°C.

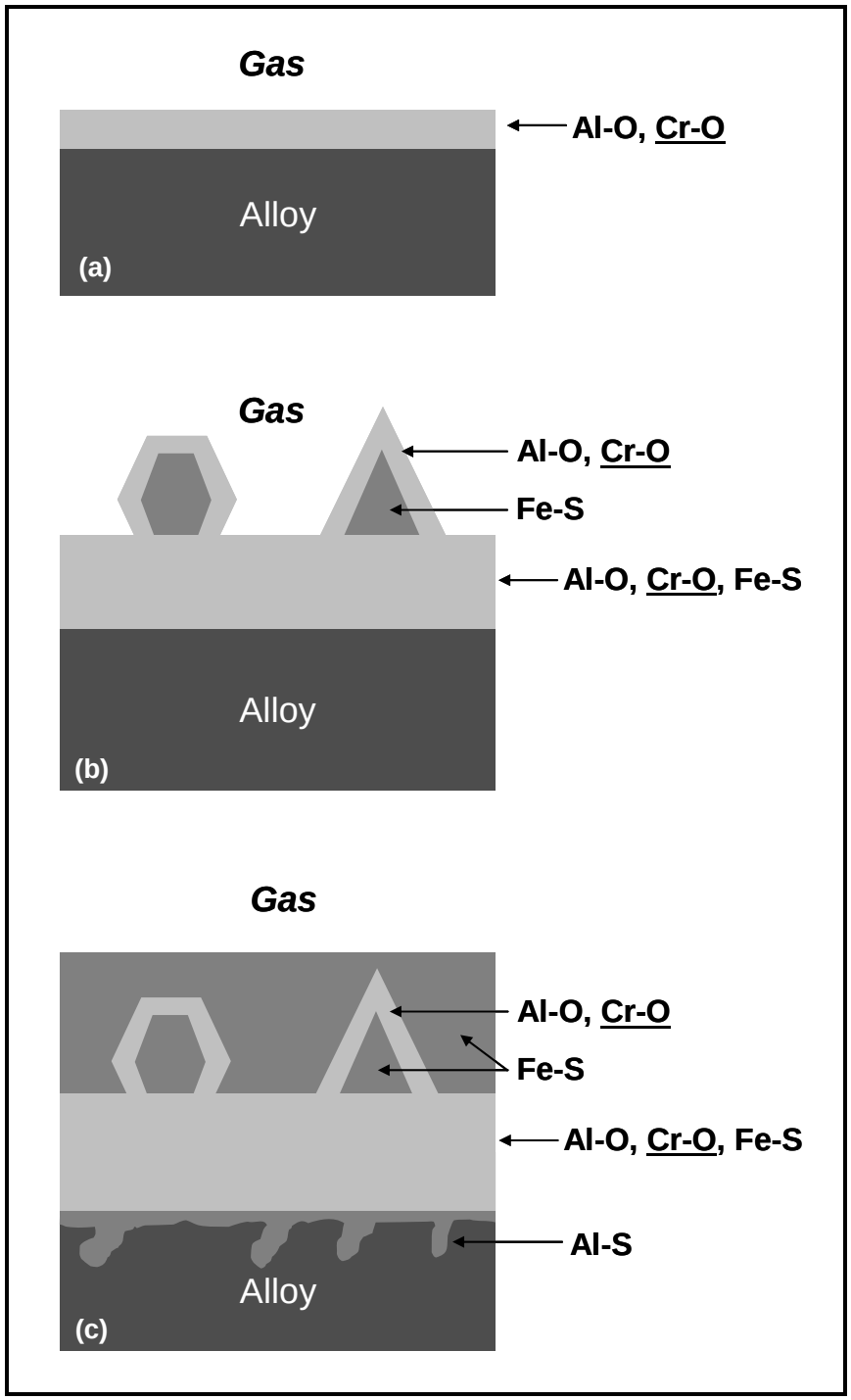

Figure 25 - Schematic representation of corrosion product development on Fe-10Al-5Cr alloy. Initial exposure results in formation of aluminum and chromium rich oxide layer (a). Iron sulfide develops due to diffusion of sulfur and iron through existing oxide layer (b). Continued exposure leads to nodule coalescence and formation of aluminum-sulfur phase at scale-metal interface (c).

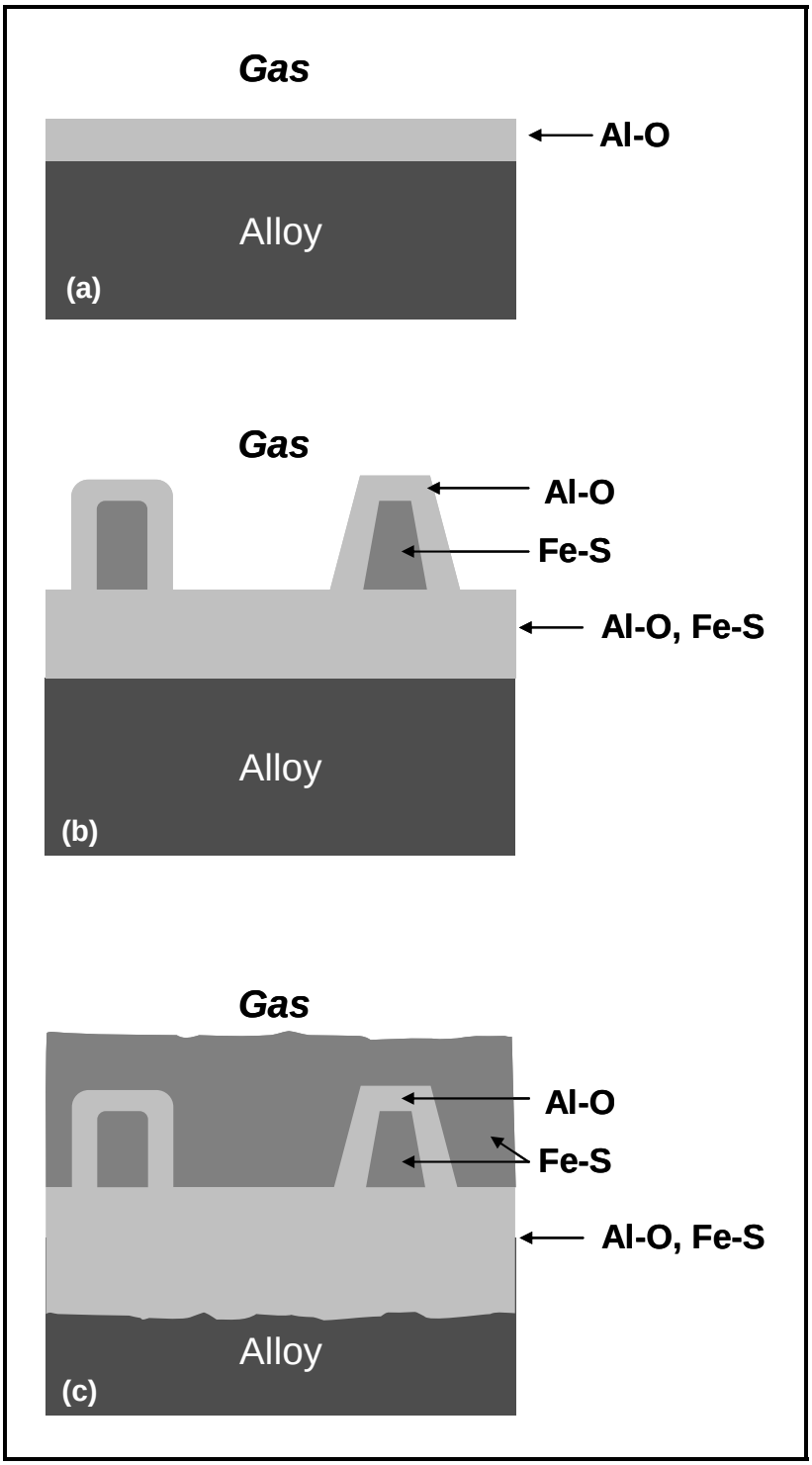

Figure 26 - Schematic representation of corrosion product development on Fe-12.5Al alloy. Initial exposure results in formation of aluminum rich oxide layer (a). Iron sulfide develops due to diffusion of sulfur and iron through the existing oxide layer (b). Coalescence of nodules results in sulfide film formation (c).

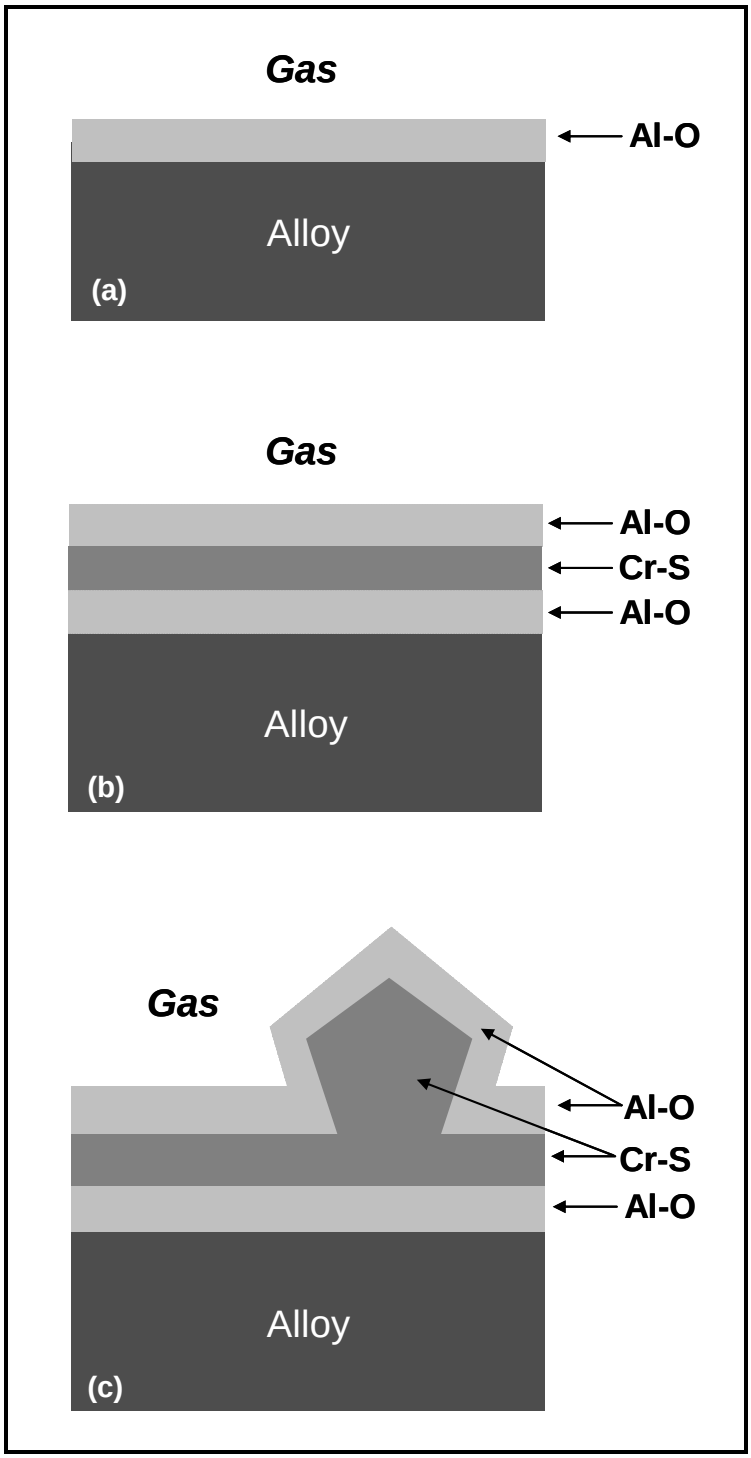

Figure 27 - Schematic representation of corrosion product development on Fe-12.5Al-5Cr alloy. Initial exposure results in formation of aluminum rich oxide layer (a). Chromium-sulfur rich layer forms after penetration of sulfur through existing oxide; with increased exposure time, isolated chromium-sulfur rich protrusion can form (c).

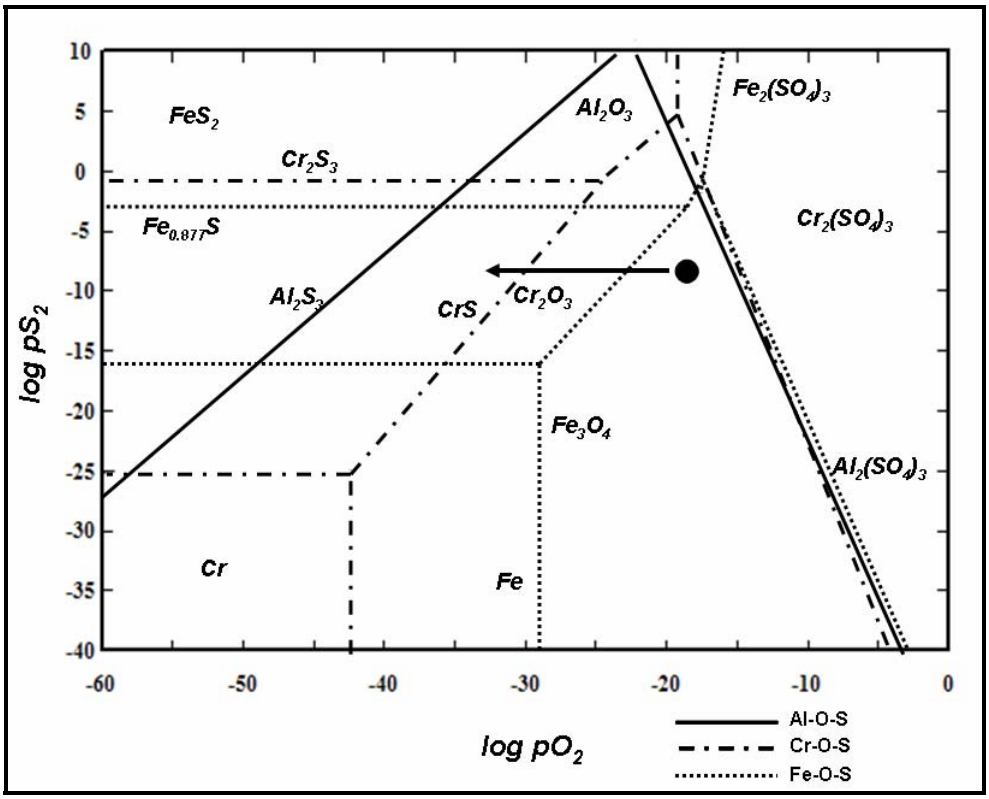

Figure 28 - Phase stability diagram for M-O-S at 500°C, where M=Fe, Al, Cr. Gas composition used in this work marked by circle, arrow indicates direction of gas composition shift after initial reaction with alloy surface.

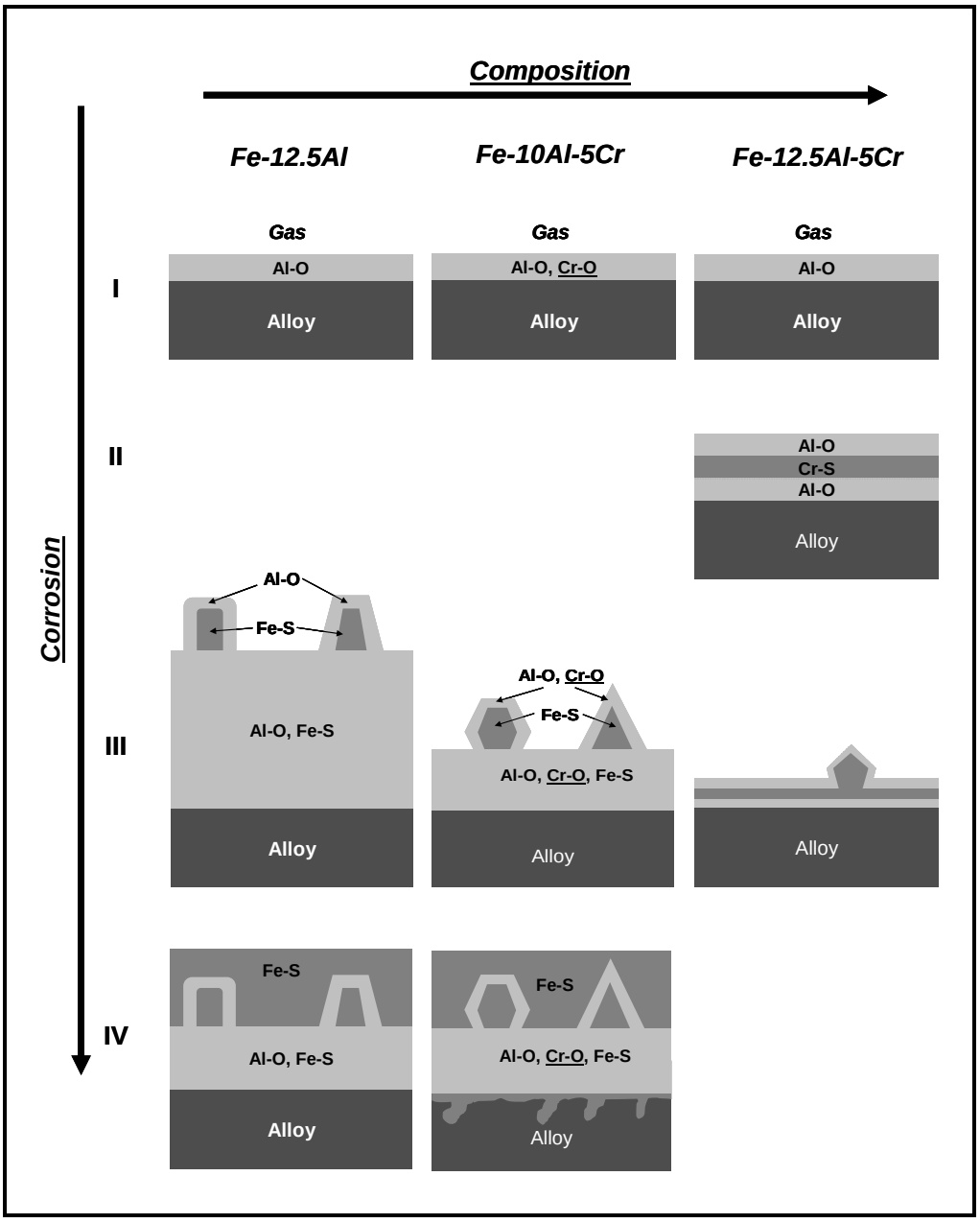

Figure 29 – Arrangement of schematic corrosion diagrams from Figure 25Figure **27**, aligning the diagrams by similar corrosion morphology or degree of attack for the alloys (irrespective of exposure time). Stage III is drawn to scale; other stages magnified to show detail.

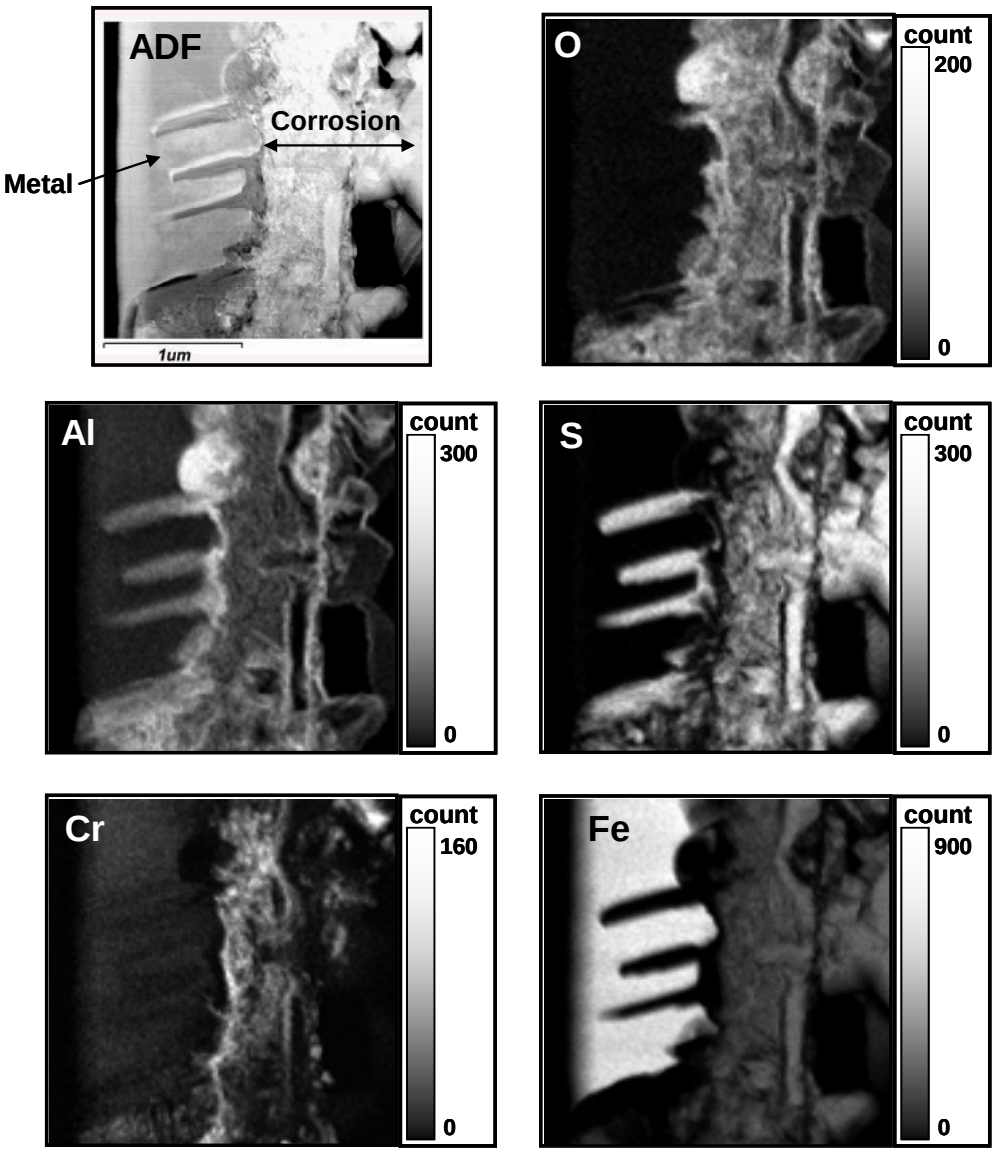

Figure 30 – ADF image and EDS maps (derived from the EDS spectrum image) of Fe-10Al-5Cr alloy after 5000 hours of exposure. Note aluminum and sulfur rich plate-like features at corrosion-product metal interface.

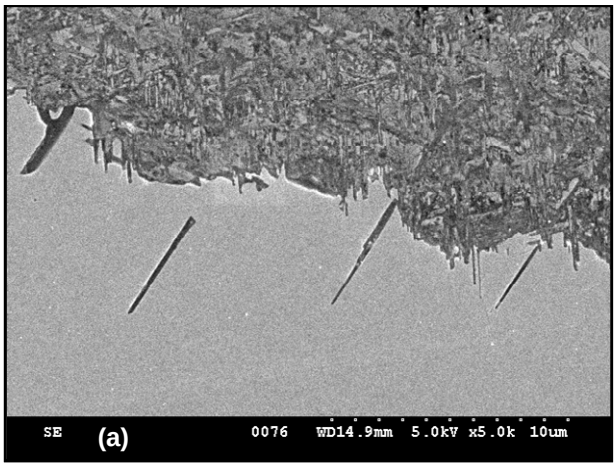

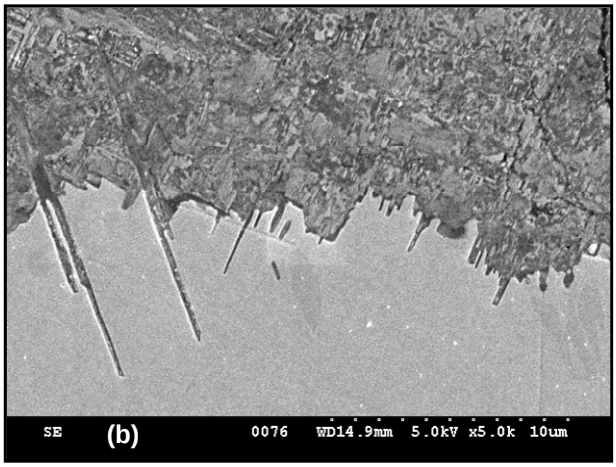

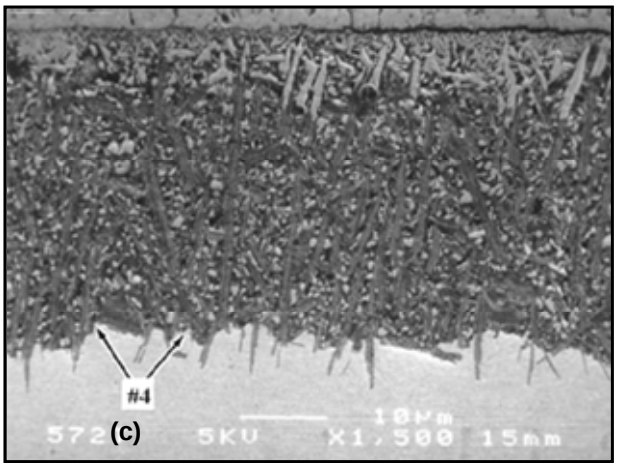

Figure 31 - Inner corrosion and metal interface on the Fe-12.5Al alloy after 5000 hours of exposure(a and b), compared to (c) the same feature observed by Banovic[39] on Fe-5wt%Al alloy.

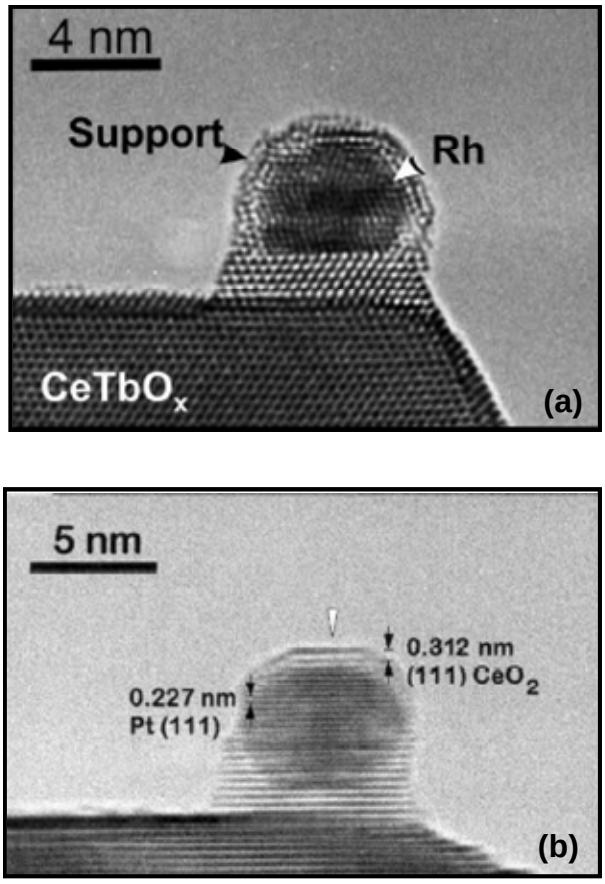

Figure 32 - HREM image of (a) 0.5% $Rh/Ce_{0.8}Tb_{0.2}O_{2-x}$ catalyst reduced at 1173K[49] and (b) 4% Pt/CeO_2 catalyst reduced at 973K[50].

2.6 References

(1) Tomaszewicz, P.; Wallwork, G. R. The Oxidation of High-Purity Iron-Chromium-Aluminum Alloys at 800°C *Oxid. Met.* 1983, *20*, 75-109.

(2) Banovic, S. W.; DuPont, J. N.; Marder, A. R. The Effect of Aluminium Content on the Corrosion Behavior of Fe-Al Alloys in Reducing Environments at 700°C. *Metall. Mater. Trans. A* 2000, *31A*, 1805-1817.

(3) Regina, J. R.; DuPont, J. N.; Marder, A. R. The Effect of Chromium on the Weldability and Microstructure of Fe-Cr-Al Weld Claddings. *Welding Journal (Miami, FL, United States)* 2007, *86*, 170s-178s.

(4) Regina, J. R.; DuPont, J. N.; Marder, A. R. Gaseous Corrosion Resistance of Fe-Al-Based Alloys Containing Cr Additions. Part I - Kinetic Results. *Mater. Sci. Eng. A* 2005, *A404*, 71-78.

(5) DeVan, J. H.; Tortorelli, P. F. The Oxidation-Sulfidation Behavior of Iron Alloys Containing 16-40 at% Aluminum. *Corros. Sci.* 1993, *35*, 1065-1071.

(6) Deacon, R. M.; DuPont, J. N.; Kiely, C. J.; Marder, A. R. *submitted* 2007.

(7) Goldstein, J. I.; Newbury, D. E.; Echlin, P.; Joy, D. C.; Romig, J. A. D.; Lyman, C. E.; Fiori, C.; Lifshin, E. Scanning Electron Microscopy and X-Ray Microanalysis; Plenum Press: New York, 1992.

(8) Pankratz, L. B. Thermodynamic Properties of Elements and Oxides. *Bulletin - United States, Bureau of Mines* 1982, *672*.

(9) Pankratz, L. B.; Mah, A. D.; Watson, S. W. Thermodynamic Properties of Sulfides. *Bulletin - United States, Bureau of Mines* 1987, *689*.

(10) Gleeson, B. Alloy Degradation Under Oxidizing-Sulfidizing Conditions at Elevated Temperatures. *Materials Research (Sao Carlos, Brazil)* 2004, *7*, 61-69.

(11) Stroosnijder, M. F.; Quadakkers, W. J. Review of High Temperature Corrosion of Metals and Alloys in Sulfidizing/Oxidizing Environments. II. Corrosion of Alloys. *High Temp. Technol.* 1986, *4*, 141-151.

(12) Mrowec, S. Mechanism of High-Temperature Sulfide Corrosion of Metals and Alloys. *Werkstoffe und Korrosion* 1980, *31*, 371-386.

(13) Wood, G. C.; Richardson, J. A.; Hobby, M. G.; Boustead, J. Identification of Thin Healing Layers at the Base of Oxide Scales on Iron-Chromium Base Alloys. *Corrosion Science* 1969, *9*, 659-671.

(14) Stott, F. H.; Wood, G. C.; Stringer, J. The Influence of Alloying Elements on the Development and Maintenance of Protective Scales. *Oxid. Met.* 1995, *44*, 113-145.

(15) Zhang, Z. G.; Gesmundo, F.; Hou, P. Y.; Niu, Y. Criteria for the Formation of Protective Al_2O_3 Scales on Fe-Al and Fe-Cr-Al Alloys. *Corrosion Science* 2006, *48*, 741-765.

(16) Kai, W.; Huang, R. T. The Corrosion Behavior of Fe-Al Alloys in $H_2/H_2S/H_2O$ Atmospheres at 700-900°. *Oxidation of Metals* 1997, *48*, 59-86.

(17) Lee, D. B.; Kim, G. Y.; Kim, J. G. The Oxidation of Fe_3Al-(0, 2, 4, 6%)Cr Alloys at 1000°C. *Materials Science & Engineering, A: Structural Materials: Properties, Microstructure and Processing* 2003, *A339*, 109-114.

(18) Sheybany, S.; Douglass, D. L. The Effect of Preoxidation of Some Nickel-, Iron-, and Cobalt-Base Alloys on Subsequent Sulfidation at 982°C in Sulfur Vapor. *Oxidation of Metals* 1988, *30*, 433-463.

(19) Wagner, C. Theoretical Analysis of the Diffusion Processes Determining the Oxidation Rate of Alloys. *J. Electrochem. Soc* 1952, *99*, 369-380.

(20) Whittle, D. P.; Evans, D. J.; Scully, D. B.; Wood, G. C. Compositional Changes in the Underlying Alloy During the Protective Oxidation of Alloys. *Acta Metallurgica* 1967, *15*, 1421-1430.

(21) Bastow, B. D.; Whittle, D. P.; Wood, G. C. Alloy Depletion Profiles Resulting From the Preferential Removal of the Less Noble Metal During Alloy Oxidation. *Oxidation of Metals* 1978, *12*, 413-438.

(22) Wood, G. C. High-Temperature Oxidation of Alloys. *Oxid. Metals* 1970, *2*, 11-57.

(23) Akuezue, H. C.; Whittle, D. P. Interdiffusion in Iron-Aluminum System: Aluminizing. *Metal Science* 1983, *17*, 27-31.

(24) Akuezue, H. C.; Stringer, J. Interdiffusion in Ternary Iron-Chromium-Aluminum Alloys. *Metallurgical Transactions A: Physical Metallurgy and Materials Science* 1989, *20A*, 2767-2781.

(25) Brumm, M. W.; Grabke, H. J. The Oxidation Behavior of Nickel Aluminide (NiAl). I. Phase Transformations in the Alumina Scale During Oxidation of NiAl and NiAl-Chromium Alloys. *Corros. Sci.* 1992, *33*, 1677-1690.

(26) Prasanna, K. M. N.; Khanna, A. S.; Chandra, R.; Quadakkers, W. J. Effect of Q-Alumina Formation on the Growth Kinetics of Alumina-Forming Superalloys. *Oxidation of Metals* 1996, *46*, 465-480.

(27) Lesage, B.; Marechal, L.; Huntz, A. M.; Molins, R. Aluminum Depletion in FeCrAl Alloys During Oxidation. *Diffusion and Defect Data--Solid State Data, Pt. A: Defect and Diffusion Forum* 2001, *194-199*, 1707-1712.

(28) Tomaszewicz, P.; Wallwork, G. R. Observations of Nodule Growth During the Oxidation of Pure Binary Iron-Aluminum Alloys. *Oxid. Met.* 1983, *19,* 165-185.

(29) Sadique, S. E.; Mollah, A. H.; Islam, M. S.; Ali, M. M.; Megat, M. H. H.; Basri, S. High-Temperature Oxidation Behavior of Iron-Chromium-Aluminum Alloys. *Oxidation of Metals* 2000, *54,* 385-400.

(30) Tomaszewicz, P.; Wallwork, G. R. Iron-Aluminum Alloys: a Review of Their Oxidation Behavior. *Rev. High-Temp. Mater.* 1978, *4,* 75-105.

(31) Prescott, R.; Graham, M. J. The Oxidation of Iron-Aluminum Alloys. *Oxid. Met.* 1992, *38,* 73-87.

(32) Natesan, K.; Johnson, R. N. Corrosion performance of Fe-Cr-Al and Fe aluminide alloys in complex gas environments. Heat-Resistant Materials II, Conference Proceedings of the International Conference on Heat-Resistant Materials, 2nd, Gatlinburg, Tenn., Sept. 11-14, 1995.

(33) Stott, F. H.; Chuah, K. T.; Bradley, L. B. Oxidation-Sulfidation of Iron Aluminides at High Temperature. *Materials and Corrosion* 1996, *47,* 695-700.

(34) Klower, J. High temperature corrosion behavior of iron aluminides and iron-aluminum-chromium alloys. *Materials and Corrosion* 1996, *47,* 685-694.

(35) Sundmann, B. Thermo-Calc. Department of Materials Science and Engineering, KTH, S-100 44. 2001. Stockholm, Sweden.

(36) Patnaik, P. C.; Smeltzer, W. W. Sulfidation Properties of Iron-Aluminum Alloys at 1173 K in Hydrogen Sulfide-Hydrogen Atmospheres. *Oxidation of Metals* 1985, *23,* 53-75.

(37) Smith, P. J.; Jackson, P. R. S.; Smeltzer, W. W. The Sulfidation Behavior of an Iron-10 Atomic Percent Aluminum Alloy in Argon-Sulfur and Hydrogen-Hydrogen Sulfide Atmospheres at 1023 K. *J. Electrochem. Soc.* 1987, *134,* 1424-1431.

(38) Przybylski, K.; Narita, T.; Smeltzer, W. W. Kinetics and Mechanism of High-Temperature Sulfidation of an Fe-23.4Cr-18.6Al Alloy in Hydrogen Sulfide-Hydrogen Atmospheres. *Oxidation of Metals* 1992, *38,* 1-32.

(39) Banovic, S. W.; DuPont, J. N.; Marder, A. R. The Use of Ternary Phase Diagrams in the Study of High Temperature Corrosion Products Formed on Fe-5 Wt% Al Alloys in Reducing and Oxidizing Environments. *Acta Mater.* 2000, *48,* 2815-2822.

(40) Banovic, S. W.; DuPont, J. N.; Marder, A. R. Metallographic Preparation and Degradation of the Tau-Phase ($FeAl_2S_4$) Formed After High-Temperature Oxidation-Sulfidation of Fe-Al Alloys. *Mater. Charact.* 2000, *45,* 241-249.

(41) Mrowec, S.; Wedrychowska, M. Kinetics and Mechanism of High-Temperature Sulfur Corrosion of Iron-Chromium-Aluminum Alloys. *Oxid. Met.* 1979, *13,* 481-504.

(42) Tauster, S. J.; Fung, S. C.; Garten, R. L. Strong Metal-Support Interactions. Group 8 Noble Metals Supported on Titanium Dioxide. *Journal of the American Chemical Society* 1978, *100,* 170-175.

(43) Haller, G. L.; Resasco, D. E. Metal-Support Interaction: Group VIII Metals and Reducible Oxides. *Advances in Catalysis* 1989, *36,* 173-235.

(44) Ioannides, T.; Verykios, X. E. Charge Transfer in Metal Catalysts Supported on Doped TiO_2: a Theoretical Approach Based on Metal-Semiconductor Contact Theory. *Journal of Catalysis* 1996, *161,* 560-569.

(45) Nicole, J.; Tsiplakides, D.; Pliangos, C.; Verykios, X. E.; Comninellis, C.; Vayenas, C. G. Electrochemical Promotion and Metal-Support Interactions. *Journal of Catalysis* 2001, *204,* 23-34.

(46) Vayenas, C. G.; Brosda, S.; Pliangos, C. The Double-Layer Approach to Promotion, Electrocatalysis, Electrochemical Promotion, and Metal-Support Interactions. *Journal of Catalysis* 2003, *216,* 487-504.

(47) Pan, J. M.; Madey, T. E. The Encapsulation of Iron on Titania(110). *Catalysis Letters* 1993, *20,* 269-274.

(48) Fu, Q.; Wagner, T. Metal/Oxide Interfacial Reactions: Oxidation of Metals on $SrTiO_3$ (100) and TiO_2 (110). *Journal of Physical Chemistry B* 2005, *109,* 11697-11705.

(49) Bernal, S.; Calvino, J. J.; Cauqui, M. A.; Gatica, J. M.; Lopez Cartes, C.; Perez Omil, J. A.; Pintado, J. M. Some Contributions of Electron Microscopy to the Characterisation of the Strong Metal-Support Interaction Effect. *Catalysis Today* 2003, *77,* 385-406.

(50) Bernal, S.; Calvino, J. J.; Gatica, J. M.; Larese, C.; Lopez-Cartes, C.; Perez-Omil, J. A. Nanostructural Evolution of a Pt/CeO2 Catalyst Reduced at Increasing Temperatures (473-1223 K): a HREM Study. *Journal of Catalysis* 1997, *169,* 510-515.

(51) Strafford, K. N.; Manifold, R. Scaling Behavior of an Iron-5% Aluminum Alloy in Sulfur Vapor. *Oxid. Metals* 1969, *1,* 221-240.

(52) Kai, W.; Douglass, D. L. The High-Temperature Corrosion Behavior of Iron-Molybdenum-Aluminum Alloys in Hydrogen/Water Vapor/Hydrogen Sulfide Mixed-Gas Environments. *Oxid. Met.* 1993, *39,* 281-316.

3 IN-SITU X-RAY PHOTOELECTRON SPECTROSCOPY OXIDATION OF TWO IRON ALUMINUM ALLOYS

3.1 Introduction

Analysis of as-corroded coupons by electron microscopy is an extremely useful technique for understanding the role of alloy composition on corrosion resistance. One drawback of such analysis, however, is that information about the very early stages of corrosion often can not be ascertained, since transformation at later times may change the initial corrosion products. Examining the preliminary stages of corrosion product development is made difficult by the small size of the products and their transient nature. One technique that is especially suited for this type of investigation is x-ray photoelectron spectroscopy (XPS). Since the measured signal is electrons ejected from the sample surface, XPS is extremely sensitive to surface chemistry and can detect the very beginning of alloy corrosion when only a few nuclei or atomic layers of oxides or sulfides have formed. Further details on XPS and its applications can be found in one of several texts on the subject[1,2,3].

In order to effectively examine initial corrosion products, care must be taken to minimize sample contamination between the processes of corrosion and analysis. When exposed to a sufficient quantity of oxygen, some metals (such as aluminum and chromium) will form oxides at ambient temperatures, potentially skewing analysis of the corrosion products. Additionally, it has been shown[4,5] that some sulfur bearing corrosion products, such as $FeAl_2S_4$, degrade when exposed to moisture at room temperature. One way to avoid such problems is to perform the corrosion exposures *in-situ*, within the equipment used for analysis, in order to eliminate exposure to ambient conditions and minimize time between corrosion and examination.

In-situ corrosion of metal coupons in the simulated low NO_x gases at 500°C was not possible in the present study, due to the potential for damage to the XPS equipment by the corrosive gases. It was possible, however, to permit oxygen at low pressures into the analysis chamber and thus perform in-situ oxidation, rather than oxidation / sulfidation, experiments at 500°C. While the results from these tests will not correlate directly with the data from corrosion exposures in the sulfur bearing gases, such experiments will none the less provide valuable information regarding the effect of alloy composition on oxidation.

3.2 Experimental

In-situ oxidation of Fe-12.5Al and Fe-12.5Al-5Cr was performed in a Scienta ESCA 300 instrument with a monochromatic Al K_α source. Coupons for the XPS experiments were prepared using the same method employed for the low NO_x corrosion tests: after grinding to 600 grit SiC, samples were polished on 6μm diamond and 0.3μm alumina, followed by cleaning ultrasonically in acetone. After sample insertion, the analysis chamber was evacuated to approximately $5x10^{-9}$ torr and the samples were resistively heated to 500°C. For one set of experiments, argon sputtering was performed in the analysis chamber prior to oxidation for short times (less than 2 minutes) to remove surface contamination, hopefully leaving the native surface oxide largely intact. Other samples were sputtered for much longer times (>60 minutes) to remove as much surface oxide as possible. After the sputtering treatment, all samples were oxidized at 500°C in the analysis chamber with O_2 at a pressure of approximately $3x10^{-7}$ torr for times up to 45 minutes.

3.3 Results and Discussion

Samples that were sputtered for less than two minutes are referred to as "as polished" since the native oxide layer that developed after polishing was not completely removed by the short sputtering treatment, while samples that received the longer sputtering procedure, and thus had the majority of oxide removed, are referred to as "as sputtered". Figure 33 shows the aluminum and Al^{3+} spectra for both the Fe-12.5Al and Fe-12.5Al-5Cr alloys in the as polished condition after several oxidation times. From this figure, it is evident that the area underneath the Al^{3+} peak at approximately 75-76eV binding energy increases with exposure time, due to the increased formation of aluminum oxide (Al_2O_3). Measurements were taken of the area underneath both the oxide and metallic curves for each exposure time and the results are presented as a ratio of peak areas in Figure 34. The area underneath the curve is an approximate measurement of how much of the oxide has developed, and it is clear from this figure that the addition of chromium to the Fe-12.5 wt% Al alloy significantly slows the formation of aluminum oxide.

This effect was even more dramatic for the sputtered alloys. As shown in Figure 35, the oxide peak for the binary alloy is much larger at all oxidation times than the Al^{3+} peak for the ternary alloy. Measurements of area under the curve, presented in Figure 36, further demonstrates the effect of chromium on slowing the formation of aluminum oxide in the as sputtered condition.

Analysis of the chromium peak 2p peaks ($Cr2p^{3/2}$ = 574.5eV, $Cr2p^{1/2}$ = 583.5eV) for this ternary alloy in the as sputtered condition, however, does not provide any significant information on the mechanism of chromium oxidation in these experiments. As shown in Figure 37a, there is only a

minimal change in the shape of the chromium $2p^{3/2}$ peak for the as polished condition after 45 minutes of oxidation. The shoulder on the low binding energy side of the $2p^{3/2}$ peak is likely due to Cr^{3+} from the initial stages of Cr_2O_3 formation. It is also noted that there was no observed change in the chromium peak position at any oxidation time for the as sputtered state; in this condition, the chromium peak remained symmetrical and feature free for all oxidation times (Figure 37b).

Another interesting feature was observed on the as sputtered alloys: a change in the shape of the iron 2p peaks ($Fe2p^{3/2}$ = 707eV, $Fe2p^{1/2}$ = 720eV) occurred on the binary alloy at the 45 minute oxidation time (Figure 38). No change in these peaks occurred for the chromium containing alloy. Additionally, a concomitant shift in the oxygen peak 1s peak at 532eV for the same exposure time for Fe-12.5Al is shown in Figure 39a; again there is no change for the Fe-12.5Al-5Cr alloy, Figure 39b. Although it is not possible to determine quantitative compositions from the present work, the changes observed on the binary alloy are an indication that iron oxide type compounds are forming after 45 minutes of oxidation. The shoulder on the $Fe2p^{3/2}$ peak for the binary alloy in Figure 38 is evidence of a change in bonding state for this element. This, along with the shift of the O 1s peak in Figure 39(a) to a lower binding energy, is evidence for the formation of iron oxide for the Fe-12.5Al alloy. From these results alone, it would appear that the chromium addition is preventing the formation of iron oxide compounds at long oxidation times. However, if adding chromium would have effected the iron oxide formation, the Fe-oxides would have been observed on the binary alloy in the *as polished* condition as well. This did not occur; only aluminum oxides were observed on the as polished alloys after the oxidation treatments and the $Fe2p^{1/2}$ and $Fe2p^{3/2}$ peaks show no sign of a chemical shift due to oxide

formation (Figure 40). Since the only difference between these experiments is the sputtering time, it is likely that the native oxide promotes the formation of a more protective oxide layer that is able to suppress the formation of iron oxides at long oxidation times.

Analysis of the native oxide on the 'as-polished' binary coupon, prior to any sputtering treatment, revealed the presence of both iron and aluminum oxides on the binary alloy. After 10 seconds of oxidation, however, evidence of the iron oxide disappears, and the aluminum oxide remains and grows with increasing exposure time. This is evidenced by the change in the shape of the Fe 2p peaks (Figure 41a) and the chemical shift to higher binding energies of the O 1s peak (Figure 41b). The disappearance of the secondary shoulder on the high energy side of the $Fe2p^{1/2}$ and $Fe2p^{3/2}$ peaks indicates that after only 10 seconds of oxidation, iron is present at the surface only in the metallic state. The shift of the oxygen peak to higher energies at the same exposure time also means the surface oxide is mostly alumina after 10 seconds. This observation is echoed in the slight chemical shift for the Al^{3+} peak between the as-polished and oxidized conditions (Figure 33). All subsequent oxidation times showed only the presence of aluminum oxide on this alloy.

The presence of the iron oxide type product on the as-polished sample most likely has only a minimal effect on the subsequent oxidation of the Fe-12.5Al alloy. Additionally, it is possible that this product is not an oxide of iron, but rather an iron oxy-hydroxide, such as FeOOH. The fact that this phase disappears after only 10 seconds of oxidation is an indication that it does not play a significant role in effecting the later oxidation. More important, however, is the presence of aluminum oxide on the alloy prior to the oxidation treatments. It is likely that the native

aluminum oxide acts as a template for the formation of more aluminum oxide when the coupon is exposed to the oxygen. Existing aluminum oxide on the surface may promote the development of aluminum oxide rather than iron oxides during the oxidation treatments. Additionally, the presence of the native oxide on the as polished alloy may provide this alloy with an advantage over the as sputtered alloy in that some amount of the coupon is already protected by the alumina. The as sputtered coupon would require more oxidation time to completely cover the coupon with alumina, since it begins in the bare metal condition. In this case, the aluminum oxide may not grow quickly enough to cover the coupon before some amount of iron oxide can form.

It should be noted that the iron oxide compound in the native oxide was only observed on the binary alloy. For the Fe-12.5Al-5Cr alloy, no iron products were observed at any exposure time; only aluminum oxide as found in the as polished condition. The chromium addition appears to prevent the formation of iron oxide at room temperature.

3.4 Conclusions

Oxidation of Fe-12.5Al and Fe-12.5Al-Cr was performed in pure oxygen at 500°C in an XPS analysis chamber. From this work, the following can be concluded:

- Addition of 5wt% chromium to the Fe-12.5Al alloy slowed the formation of aluminum oxide during the oxidation treatment.

- The chromium addition was also shown to change the nature of the native oxide on the as polished alloys by eliminating the iron oxide type phases in lieu of aluminum oxide.

- The presence of a native oxide on the surface of the coupon prior to any oxidation at 500°C seems to prevent the formation of iron oxide type products at long exposure times, possibly by acting as a template for aluminum oxide formation.

3.5 References

(1) Briggs, D.; Seah, M. P. Practical Surface Analysis; John Wiley and Sons: New York, 1983.

(2) Riviere, J. C. Surface Analysis Techniques; Claredon Press: Oxford, 1990.

(3) Barr, T. L. Modern ESCA; CRC Press: Boca Raton, FL, 1994.

(4) Mrowec, S.; Wedrychowska, M. Kinetics and Mechanism of High-Temperature Sulfur Corrosion of Iron-Chromium-Aluminum Alloys. *Oxid. Met.* 1979, *13,* 481-504.

(5) Banovic, S. W.; DuPont, J. N.; Marder, A. R. Metallographic Preparation and Degradation of the Tau-Phase ($FeAl_2S_4$) Formed After High-Temperature Oxidation-Sulfidation of Fe-Al Alloys. *Mater. Charact.* 2000, *45,* 241-249.

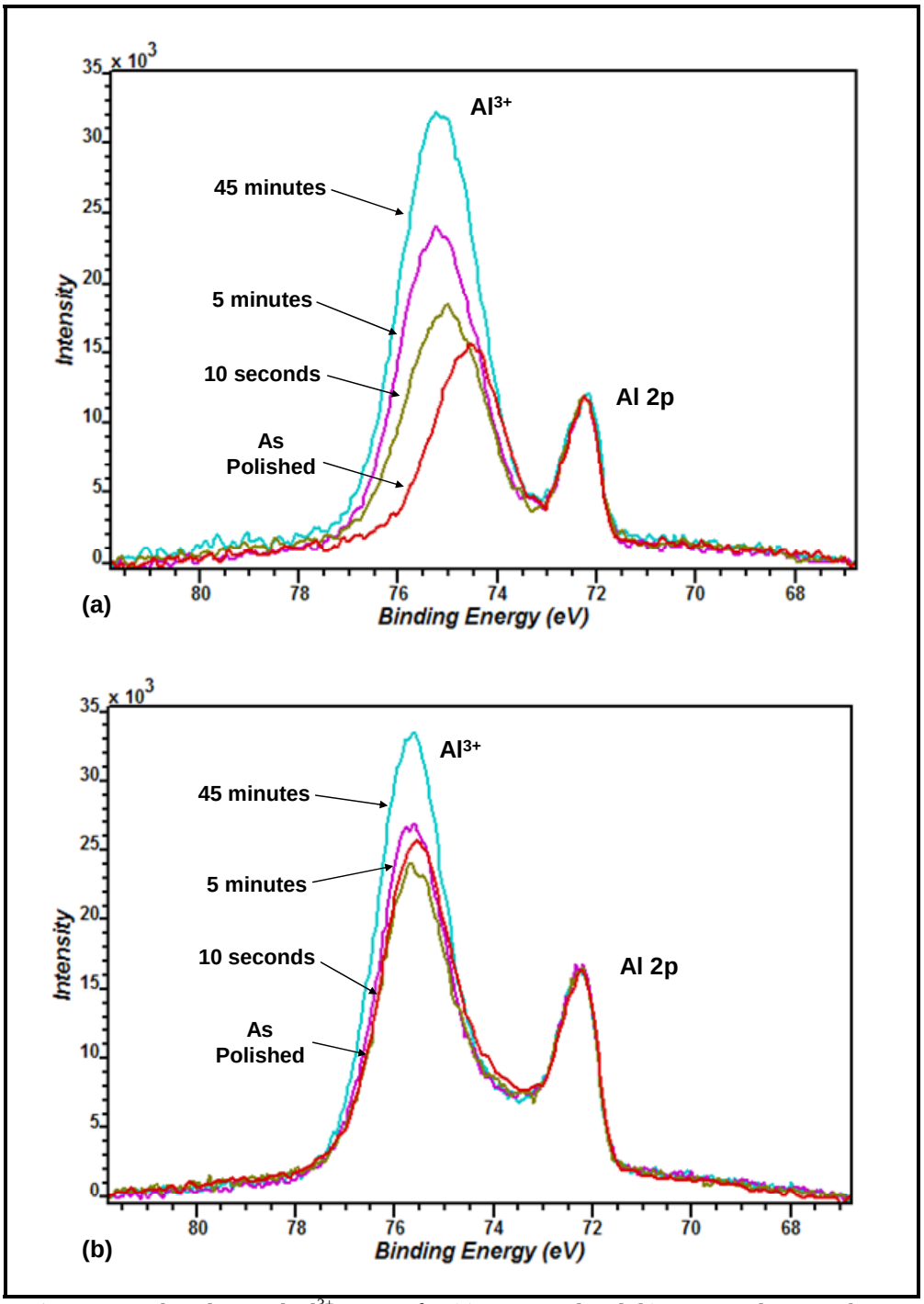

Figure 33 - The Al 2p and Al^{3+} spectra for (a) Fe-12.5Al and (b) Fe-12.5Al-5Cr in the as polished condition after in situ oxidation.

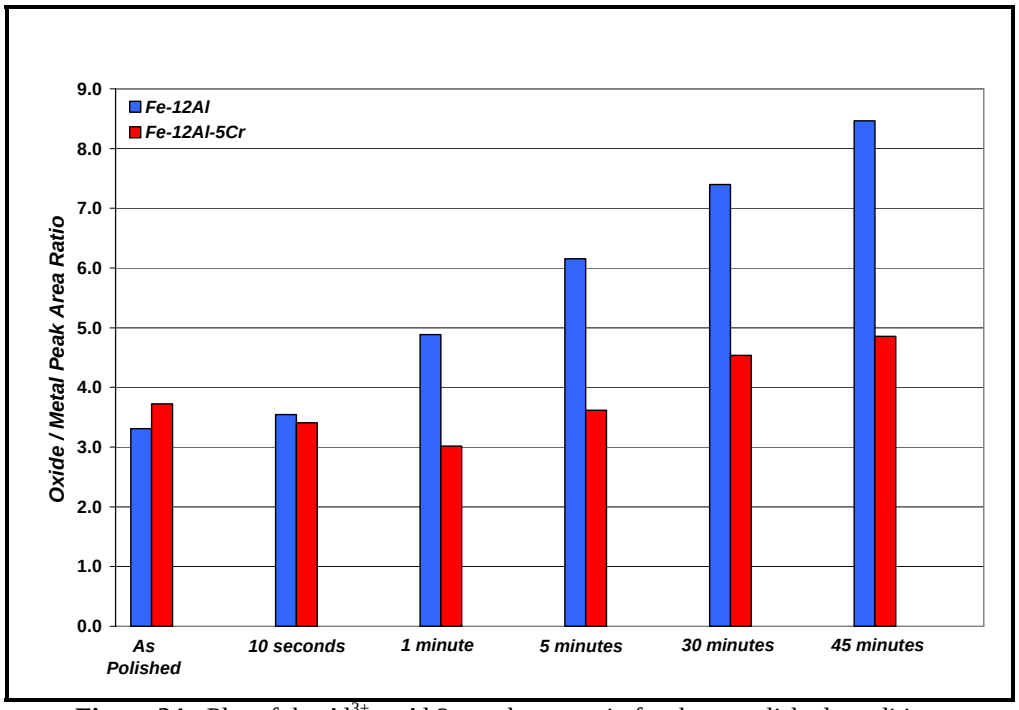

Figure 34 - Plot of the Al^{3+} to Al 2p peak area ratio for the as polished condition.

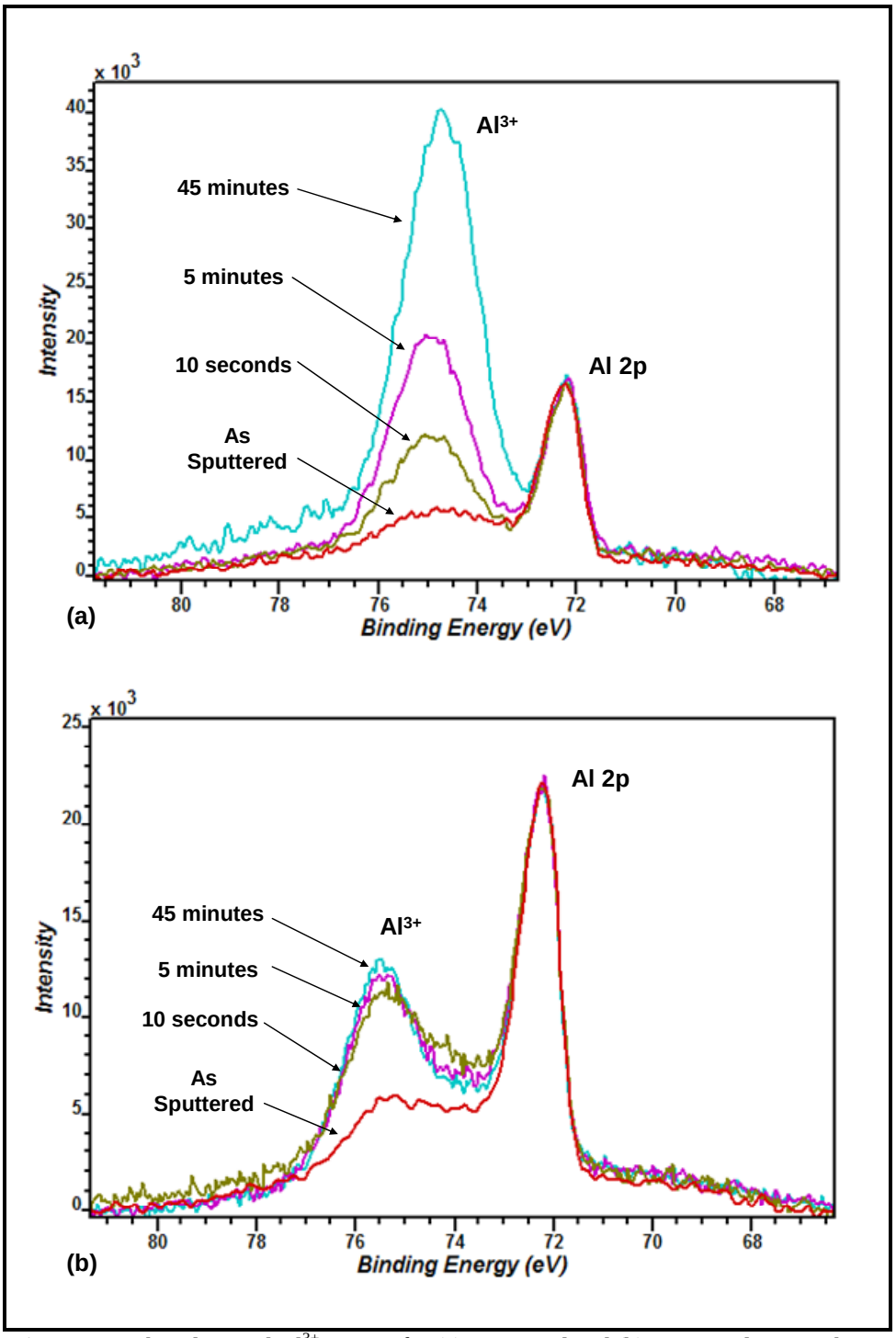

Figure 35 - The Al 2p and Al^{3+} spectra for (a) Fe-12.5Al and (b) Fe-12.5Al-5Cr in the as sputtered condition after in situ oxidation.

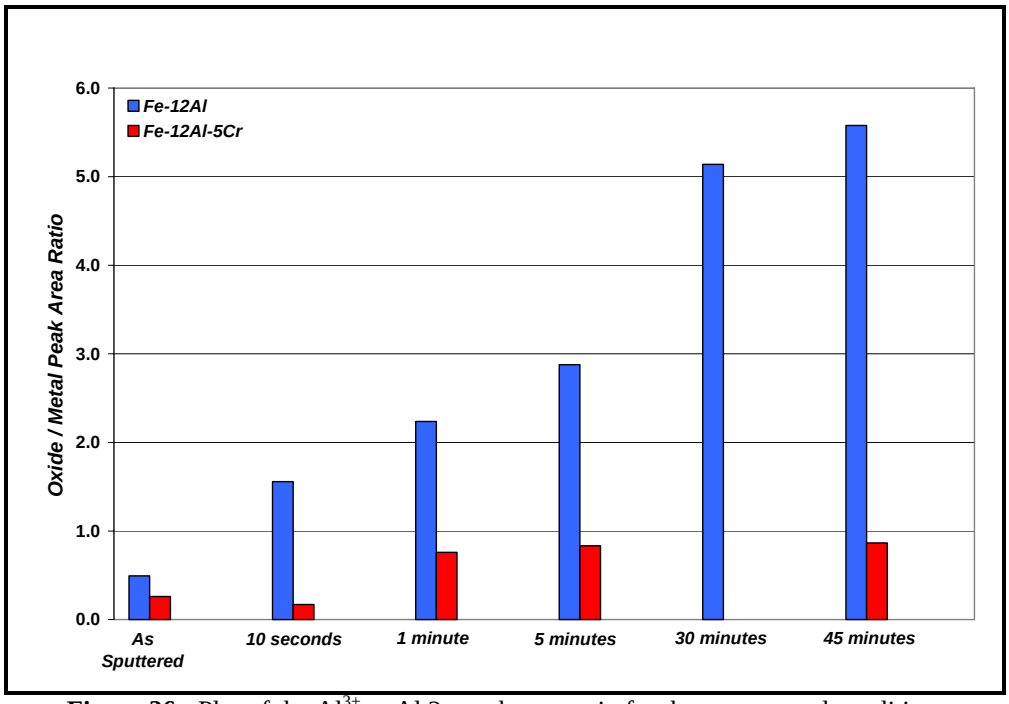

Figure 36 - Plot of the Al^{3+} to Al 2p peak area ratio for the as sputtered condition.

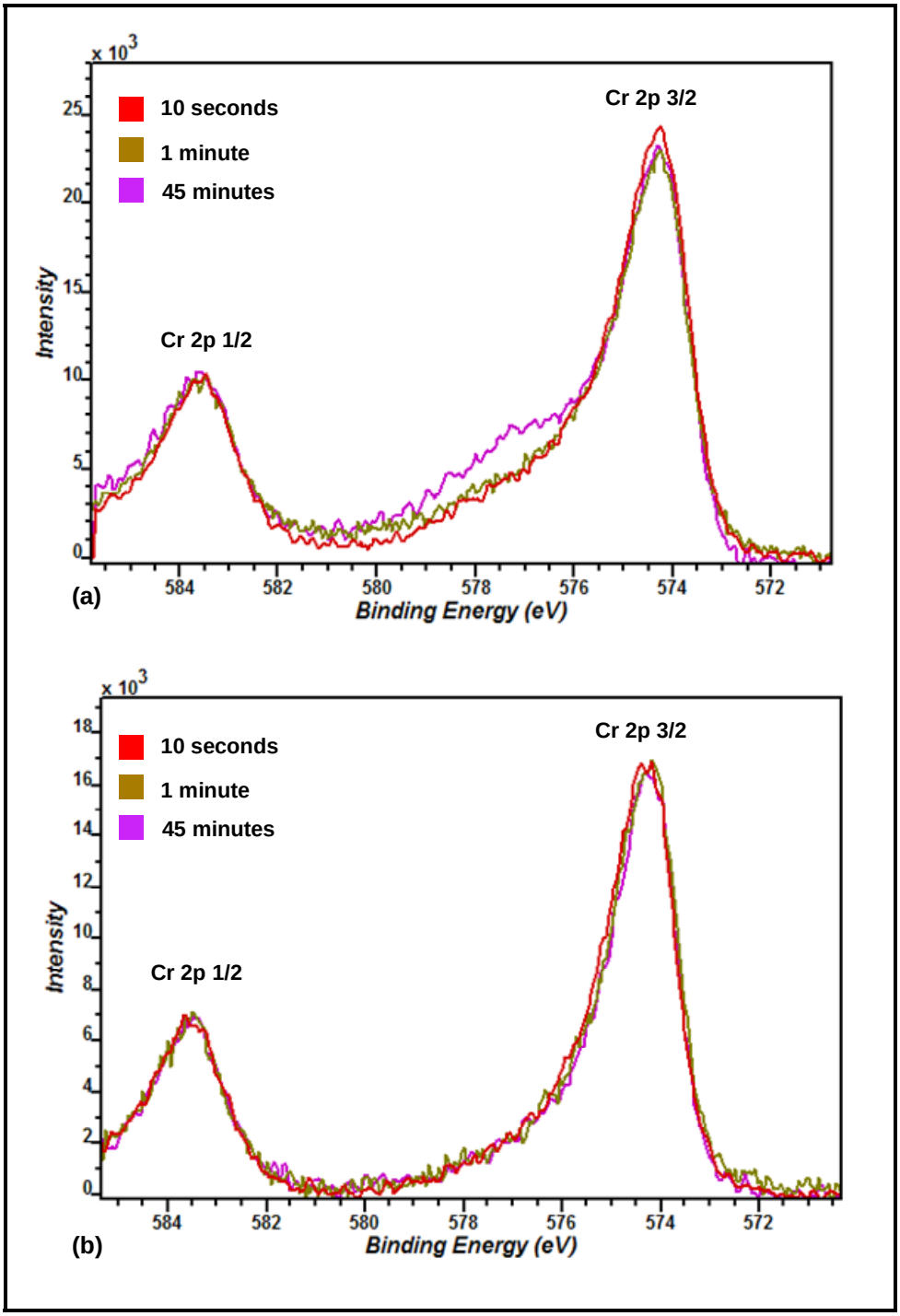

Figure 37 - The Cr 2p spectra for Fe-12.5Al-5Cr in the (a) as polished and (b) as sputtered conditions after 10 seconds, 1 minute and 45 minutes of oxidation at 500°C

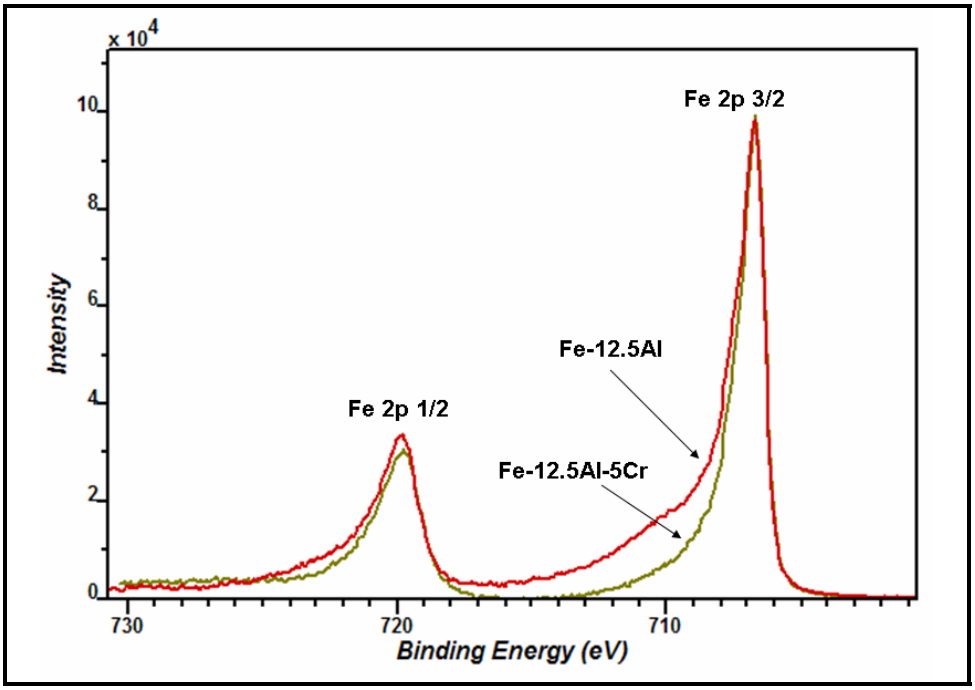

Figure 38 – The Fe 2p spectra for Fe-12.5Al and Fe-12.5Al-5Cr in the as sputtered condition after 45 minutes of oxidation at 500°C.

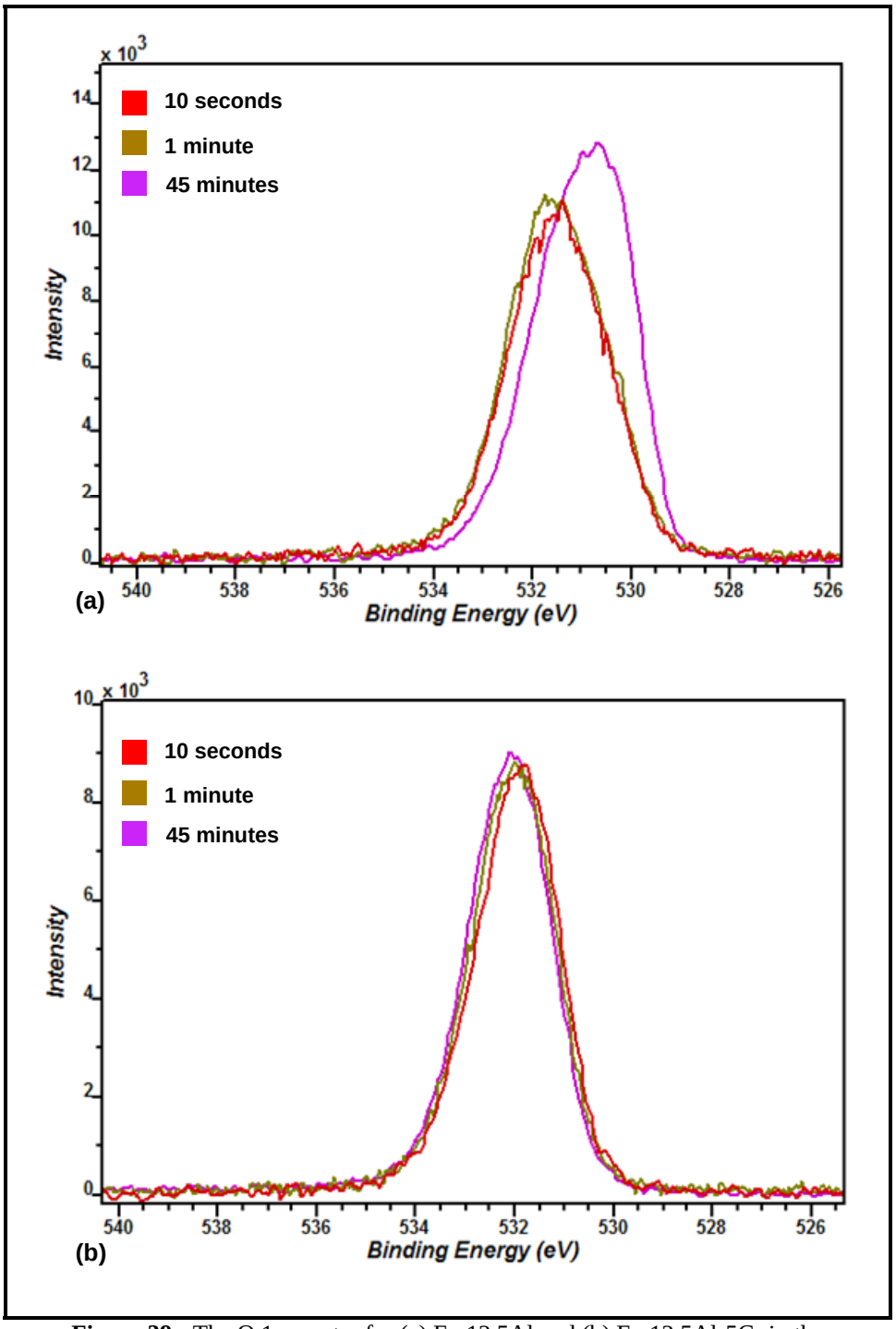

Figure 39 - The O 1s spectra for (a) Fe-12.5Al and (b) Fe-12.5Al-5Cr in the as sputtered condition after 10 seconds, 1 minute and 45 minutes of oxidation at 500°C.

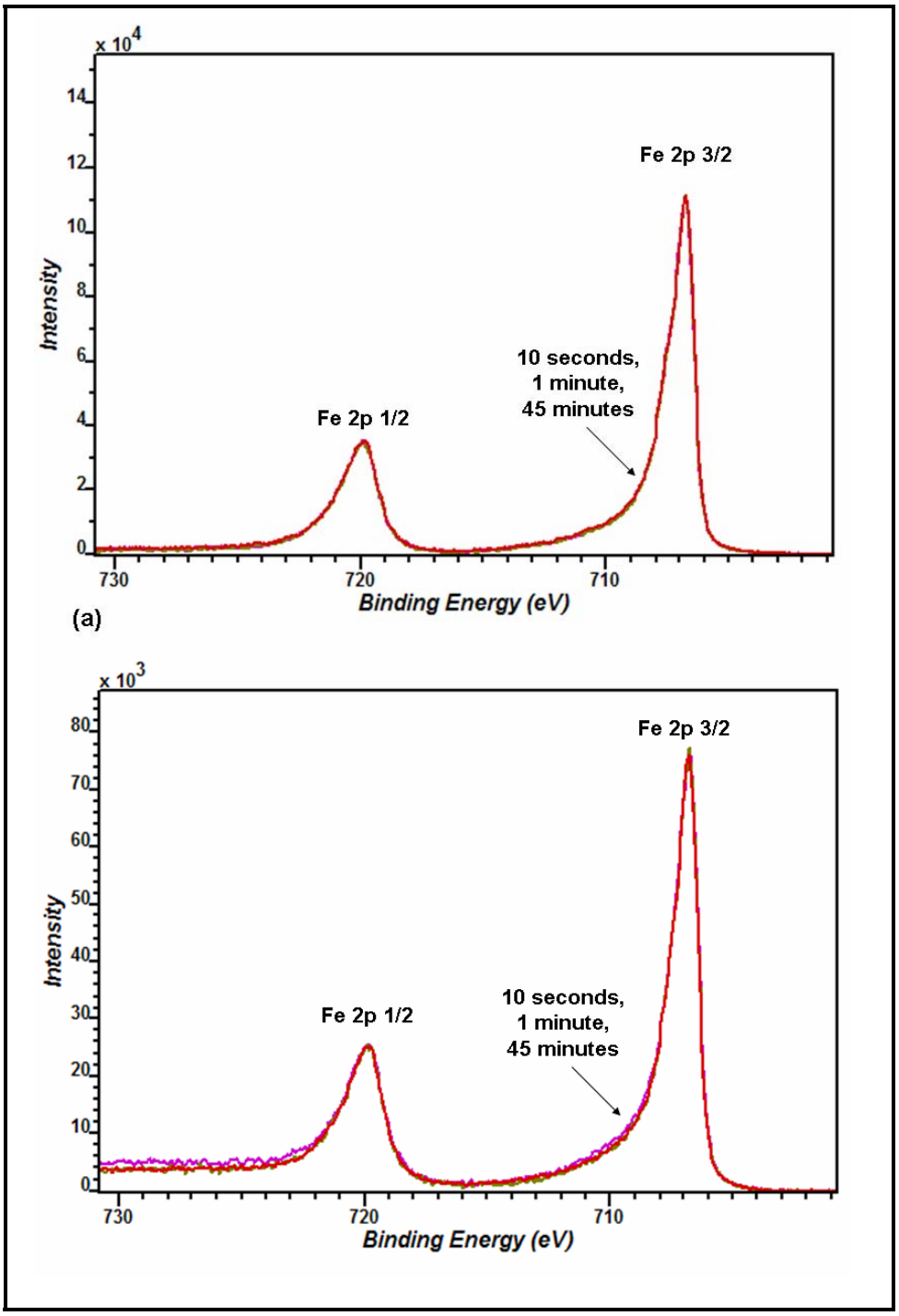

Figure 40 - The Fe 2p spectra for (a) Fe-12.5Al and (b) Fe-12.5Al-5Cr in the as polished condition after 45 minutes of oxidation at 500°C.

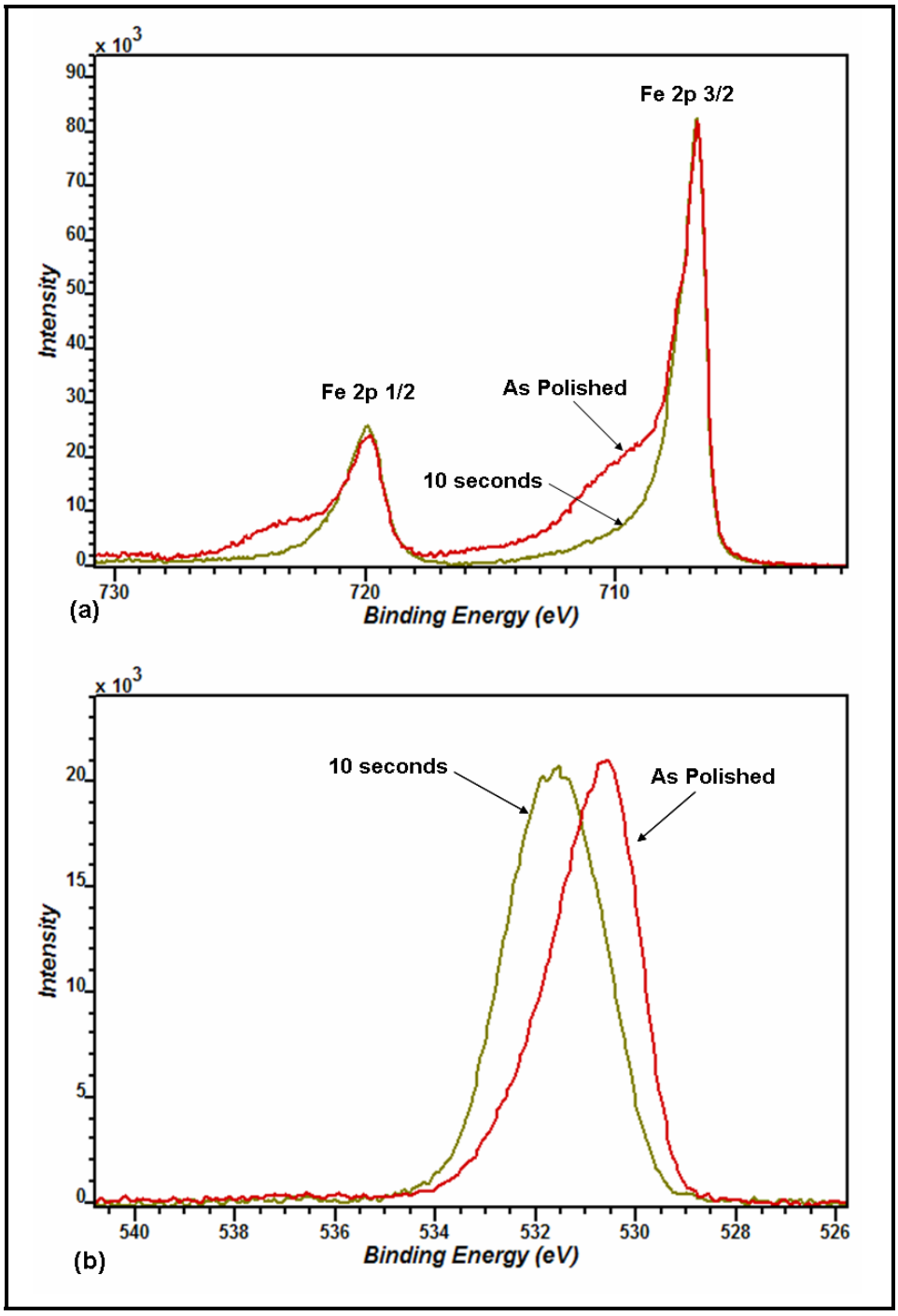

Figure 41 – Comparison of the as polished and 10 second oxidation spectra for (a) Fe $2p^{1/2}$ and $Fe2p^{3/2}$ and (b) oxygen 1s for the Fe-12.5Al alloy.